

IMPERIAL COLLEGE LONDON

DEPARTMENT OF COMPUTING

# **Model based Expression Transfer**

by

Martin Papanek

Submitted in partial fulfilment of the requirements for the MSc Degree in Advanced Computing  
of Imperial College London

September 16, 2010

---

## Abstract

---

## Acknowledgments

# Contents

<b>1</b>	<b>Introduction</b>	<b>6</b>
1.1	Motivation . . . . .	6
1.2	Contributions . . . . .	7
<b>2</b>	<b>Background</b>	<b>8</b>
2.1	Deformable Models . . . . .	8
2.1.1	Physics Based Models . . . . .	9
2.1.1.1	Finite Element Method (FEM) . . . . .	9
2.1.1.2	Modal Analysis . . . . .	10
2.1.1.3	Recovering shape with FEM . . . . .	11
2.1.2	Statistical Models . . . . .	12
2.1.2.1	PCA and Eigenfaces . . . . .	12
2.1.2.2	Morphable Model . . . . .	13
2.1.2.3	Combined Models of Shape and Appearance . . . . .	14
2.1.3	Tensor Models . . . . .	17
2.1.3.1	Multilinear Algebra . . . . .	18
2.1.3.2	Tensor-Based Model . . . . .	21
2.1.3.3	Tensor-based Statistical Discriminant Method . . . . .	22
2.2	3D Pose Estimation . . . . .	23
2.2.1	Camera Model . . . . .	23
2.2.1.1	Perspective Camera Model . . . . .	23
2.2.1.2	Orthogonal Camera Model . . . . .	24
2.2.1.3	Weak Perspective Camera Model . . . . .	25
2.2.2	Rotation and Translation . . . . .	25
2.2.3	Pose estimation with the POSIT algorithm . . . . .	28
2.3	Feature Point Tracking . . . . .	29
2.3.1	Kanade-Lucas-Tomasi Feature Tracker . . . . .	29
2.4	Optimization . . . . .	31
2.4.1	Least Squares and Non Negative Least Squares . . . . .	31
2.4.2	Nelder Mead Downhill Simplex . . . . .	32
2.4.2.1	The Downhill Simplex Algorithm . . . . .	33
<b>3</b>	<b>Design</b>	<b>35</b>
3.1	Design Challenges . . . . .	35
3.2	Frameworks and APIs . . . . .	36
3.2.1	OpenCV . . . . .	37
3.2.2	OpenGL . . . . .	37
3.2.3	Qt . . . . .	37
3.3	Pre-processing . . . . .	37
3.3.1	Correspondence . . . . .	37
3.3.2	Database . . . . .	38
3.4	Model Construction . . . . .	39
3.4.1	Data Tensor . . . . .	39

3.4.2	Computing the HOSVD . . . . .	40
3.4.3	Generating new faces . . . . .	42
3.5	Model Parameter Estimation . . . . .	43
3.5.1	Locating Feature Points . . . . .	44
3.5.2	Tracking Feature Points . . . . .	45
3.5.3	Camera Parameters . . . . .	46
3.5.4	Minimizing the Error Function . . . . .	47
3.5.5	Overfitting . . . . .	53
3.5.6	Fitting Algorithm . . . . .	55
3.6	Expression Transfer . . . . .	57
3.7	System Architecture . . . . .	59
3.7.1	View Layer . . . . .	59
3.7.2	Model Layer . . . . .	61
3.7.3	Controller Layer . . . . .	63
<b>4</b>	<b>Results and Evaluation</b> . . . . .	<b>64</b>
4.1	Face Generation . . . . .	64
4.2	Tracking Results . . . . .	67
4.3	Fitting Algorithm Results . . . . .	69
4.4	Expression Transfer Results . . . . .	73
4.5	Performance . . . . .	76
<b>5</b>	<b>Conclusion</b> . . . . .	<b>77</b>
5.1	Future Work . . . . .	77

# Chapter 1

## Introduction

### 1.1 Motivation

Allowing computers to understand the world around them is one of the most intriguing goals of computer science. In order to aid humans in day-to-day tasks, the ideal computer should be able to perceive its surroundings, correctly identify the objects and beings around it and act based on this information. Achieving this level of sophisticated, environment-aware behavior is the focus of popular computer science fields such as machine learning, computer vision and logic.

The problem of understanding the surrounding world can be broken down into a number of sub-problems. First the machine must obtain and process the information on its sensors. Then it has to process this data in order to find objects in the sensory input. Finally, the machine has to assign meaning to the scene it perceived based on the configuration and the properties of the objects it found. This allows the machine to understand what state the environment is in and it may then utilize this information using simple if-then rules.

For humans, all of the aforementioned sub-problems seem simple. However, programming machines to perform these tasks has proven to be quite difficult. Computers often do possess better sensors than most humans and thus are readily able to obtain data from sensors. Yet, they are sorely lacking when it comes to locating objects in this sensory input and correctly assessing the properties and configuration of these objects. While it is possible to locate circles and lines, joining these to locate a face or a tree can only be done if the machine knows what a face or a tree should look like. Thus, the machine needs to have prior information about the objects it can expect. This prior information can be encoded in a *model*. The model describes the structure of the object. This, in turn, allows the machine to explain aspects of its sensory input as the an instance of this model.

Certain objects may also change their shape or appearance. For example a face may transition from a closed eyed state to an open eyed state. An even better example is the body of a human, which is also highly dynamic. These deformable objects are often of special interest to us in our everyday life. A machine should therefore be able to recognize an arbitrarily deformed object and also correctly identify the the degree of deformation, since the amount of deformation may be crucial for the understanding of the scene. The challenge thus lies in constructing an appropriate *deformable model*.

Given a deformable model, the machine then has to process the sensor input and locate instances of the model by adjusting the model parameters. This task is known as *model-based recognition*. The parameters of the model allow the machine to interpret the scene.

In addition to locating an instance of the model in a single sensory input the machine should also be able to track movement of this instance given a sequence of snapshots of the environment. The task of identifying and tracking an instance of a model from one sensory snapshot to another, in spite of deformations of shape and changes in position, is known as *model-based tracking*.

This paper will describe convenient deformable shape and appearance models and effective algorithms for locating these models. Sensory snapshots will be limited exclusively to images of the environment. As we will be dealing with images we will investigate motion tracking algorithms.

These are necessary to follow optical cues in our input image which makes it possible to track the movements of the model through successive images.

## 1.2 Contributions

The area where deformable models are applicable is quite large. We will focus on one very interesting application of dynamical models and model extraction which is *expression transfer*. The purpose of expression transfer is to capture the expressions from a video recording of one individual and generate a video of another individual mimicking these expressions. The alternative to transferring these expressions would be to construct a physical model of the face and simulate the observed expressions from scratch by manipulating the parameters of the model. The advantage of transferring the dynamics of a subjects face to that of another is that it enables us to create very realistic animations without too much user intervention.

This paper describes the developement of an expression transfer application, which combines motion tracking and a deformable model to gain understanding of the face deformations present in the input video recording.

We made the following contributions

- Developed an expression transfer application complete with a graphical user interface.
- Formalized an algorithm for expression transfer using a deformable model of face shapes (Section 3.6).
- Derived a fitting algorithm for finding the deformable model parameters from an image (Sections 3.5.4 and 3.5.6).
- Elucidated a multilinear deformable model desgined for expression transfer (Section 3.4.2).

# Chapter 2

## Background

Considerable amount of research has been done on using models to characterize a deformable object as well as on model-based object recognition and tracking. In this chapter we will present an overview of various modeling techniques. Likewise, we will discuss computer vision algorithms which will allow us to locate and track features of interest in the image. These features are necessary to fit an instance of the model to the image.

### 2.1 Deformable Models

Models give the computer prior information about the structure of a class of objects. Most real world objects have a dynamic structure. To allow the computer to locate such dynamic objects it is necessary to account for this variability by giving the computer prior information about the possible variations. A deformable model describes the expected structure of a class of objects while at the same time allowing for variations from the expected structure. Thus, if a somewhat deformed instance of this class of objects is present in the image, the deformable model will be able to explain this as a deformation from the expected shape.

The quality of a deformable model can be assessed based on two important characteristics. First, the model should be *general* enough so that it is capable of representing any realistic deformation of the object. On the other hand, the computer should only be able to find an instance of this model in its surroundings if and only if this object is present. The deformable model therefore has to be *specific* so that it does not locate non-existent instances of a model in the input. Clearly, a model that is too general will inadvertently fit objects from a different class and, vice versa, a model that is too specific will not be able to explain all the variations of the object structure and will thus fail to locate instances of the correct class. The optimal deformable model must balance generality and specificity.

The variance in shape or appearance of a model may be due to combination of the following factors:

- Variations of shape due to deformations of the object.
- Arbitrary scaling of the object, possibly due to distance from the observer.
- Arbitrary rotations of the object which may cause occlusions.
- Some measure of Gaussian input noise.
- Differences in color or intensity caused by a change in lighting conditions.

Some of these sources of variation may be explained away using standard machine vision techniques. Noisy input can be explained by means of Gaussian filtering. However, other sources of variation such as those due to deformations of the object need to be represented by appropriate parameters of the model. This is where a deformable model becomes necessary. The deformable model simulates deformations based on the parameter values. Thus, to construct the model, the mapping from

parameters to deformations must be learned. The two most prevalent approaches to discovering this mapping are using either *physical models* or *statistical models*.

Physical models construct deformable models which mimic the elastic deformations of the class of object they model. The parameters of a physical model control the amount of actual physical deformation.

Statistical deformable models are trained on a set of examples of a class of objects. With this group of models, a basis for the deformations observed in this set of examples is constructed through statistical analysis. This basis then allows the model to predict probable instances of the objects of this class.

An important subgroup of statistical models are the *tensor models*. The tensor models are obtained using a mathematical generalization of statistical analysis techniques in higher dimensions.

Finally, given that a deformable model is uniquely defined by its parameters, the goal of model-based object recognition is then to fit an instance of a model to an appropriate object in the image. The problem of fitting the model to the image is essentially an optimization problem. In order to fit the model we need to correctly adjust parameters that control the model. In addition to determining the intrinsic parameters of the model it is necessary to also find how the object is rotated, moved and scaled to explain the variation in structure which is not caused by the deformations. The recognition algorithm also needs to be robust enough to be able to deal with variations caused by noise.

### 2.1.1 Physics Based Models

Natural objects all obey physical laws. Human and animal bodies change shape when their muscles contract and loosen, which in turn alters the shape of the elastic soft tissues which surround the muscles. Movement is further constrained by the skeleton and gravity. Due to the dynamic nature of such objects it is quite impractical to model the structure of these objects as consisting of only rigid components. To cope with such highly dynamic bodies researchers have turned to physics to describe the rules governing these dynamics in form of a set of equations. Pentland and Sclaroff in [25] give a closed form solution for extracting a physical model from images. Terzopoulos and Metaxas combine physics-based deformable models with Kalman filtering theory in [22].

As the name suggests, physical models emulate the physical laws that govern deformations. Physical models are predominantly formulated using the finite element analysis. An in depth discussion of finite element analysis can be found in [1].

#### 2.1.1.1 Finite Element Method (FEM)

The FEM method is a numerical engineering technique for the simulation of dynamic behavior of solids and structures. With the finite element method the assumption is made that the object alters shape as if it were made of a clay-like material. In physics, *strain* is the measure of deformation or displacement from a rigid body state. The stiffness of the material determines responses to strain and stress and thus describes the degrees of freedom of the material.

The underlying idea behind FEM is that the object is approximated as an assemblage of elements of finite size. These elements are interconnected with each other by nodal points throughout the object. The structure of an object is thus discretized into a mesh of  $N$  finite elements. The elements are placed next to each other so that no gaps remain in between. When the object undergoes a deformation, this in turn propagates through the mesh of finite elements which themselves deform accordingly. The displacements within these elements are assumed to be a function of the displacements measured at the nodal points. This assumption is fundamental for the FEM and can be formalized as

$$u^{(m)}(x, y, z) = \mathbf{H}^{(m)}(x, y, z) * \mathbf{U} \quad (2.1)$$

where  $u^{(m)}$  is the displacement at  $x$ ,  $y$ , and  $z$  coordinate within the element  $m$ ,  $\mathbf{H}^{(m)}$  the displacement interpolation matrix and  $\mathbf{U}$  the global displacement measured at every nodal point. With equation 2.1 the displacements at any point in the object can be calculated. The values of the

displacement interpolation matrix  $\mathbf{H}^{(m)}$  depend on the shape of the finite elements that make up the mesh.

From the displacement  $u^{(m)}(x, y, z)$ , the strain can be calculated as the derivative of the displacement with respect to  $x$ ,  $y$ , and  $z$ . Thus, the strain  $\epsilon^{(m)}(x, y, z)$  at the element  $m$  is given by

$$\epsilon^{(m)}(x, y, z) = \mathbf{B}^{(m)}(x, y, z) * \mathbf{U} \quad (2.2)$$

where  $\mathbf{B}^{(m)}(x, y, z)$  is the strain-displacement matrix. This matrix can be calculated by differentiating the displacement interpolation matrix  $\mathbf{H}^{(m)}$ . With equations 2.1 and 2.2 the behavior of the object structure given a global nodal point displacement  $\mathbf{U}$  is defined.

The goal of displacement-based finite element analysis is to calculate unknown nodal point displacements from a known force or load acting on the object. When a load is applied to the structure of the object it will cause a deformation of the mesh. The nodal points in the mesh will bounce and move until they reach a state of equilibrium. It is important to stress that in this equilibrium the shape of the object is still deformed due the applied force. However, the nodal points may have assumed new stable positions and hence we refer to it as an equilibrium. The equation governing the equilibrium is derived using equations 2.1, 2.2 and the Principle of Virtual Work [1]. It relates the stiffness matrix  $\mathbf{K}$  and the unknown nodal displacements  $\mathbf{U}$  to the loads  $\mathbf{R}$  as follows

$$\mathbf{K}\mathbf{U} = \mathbf{R} \quad (2.3)$$

The stiffness matrix  $\mathbf{K}$  is calculated as the sum of the stiffness matrices  $\mathbf{K}^{(m)}$  of the individual finite elements. The  $\mathbf{K}^{(m)}$  are computed from the strain-displacement matrices  $\mathbf{B}^{(m)}$  and the elasticity matrix  $\mathbf{E}^{(m)}$  as

$$\mathbf{K} = \sum_m \mathbf{K}^{(m)} = \sum_m \int_{V^{(m)}} \mathbf{B}^{(m)T} \mathbf{E}^{(m)} \mathbf{B}^{(m)} dV^{(m)} \quad (2.4)$$

where the integral goes over the volume  $V^{(m)}$  of the element  $m$ . This approach to computing the stiffness matrix is known as the *direct stiffness method*. The displacement interpolation matrix and strain-displacement interpolation matrix are constructed for each finite element. Their calculation depends on the displacement interpolation function seen in equation 2.1. Fortunately, these functions have a well defined formulation which depends on the degrees of freedom (nodal point connections) of the element. This formulation, along with numerical integration techniques for calculating the stiffness matrix can be found in chapter 5 of [1]. The elasticity matrix relates stress and strain in the material. Its form depends on the dimensionality of the element. In a one dimensional element the elasticity matrix is a scalar known as *Young's Modulus*. The value of Young's Modulus describes the elastic properties of materials and is computed as the constant ratio between stress and strain in the material.

Equation 2.3 describes a static equilibrium at a specific point in time. If the loads are applied rapidly then inertial and energy damping forces must be taken into account. Equation 2.5 gives the dynamic form of the FEM equilibrium equation where  $\dot{\mathbf{U}}$ ,  $\ddot{\mathbf{U}}$  are the first and second time derivative of  $\mathbf{U}$  respectively.

$$\mathbf{M}\ddot{\mathbf{U}} + \mathbf{C}\dot{\mathbf{U}} + \mathbf{K}\mathbf{U} = \mathbf{R} \quad (2.5)$$

Here  $\mathbf{M}$  is the mass matrix and  $\mathbf{C}$  the damping matrix. This differential equation is often referred to as the FEM governing equation. To solve for the unknown nodal displacements  $\mathbf{U}$ , standard numerical techniques for solving differential equations can be used.

### 2.1.1.2 Modal Analysis

Solving the dynamic equilibrium equation 2.5 by direct integration is very costly as shown in [1]. However, it is possible to diagonalize the system of equations by changing the finite element displacement basis to a generalized displacement basis  $\Phi$  as

$$\mathbf{U} = \Phi\tilde{\mathbf{U}} \quad (2.6)$$

The advantage of the new generalized basis can be seen when equation 2.5 is pre-multiplied from the left by  $\Phi^T$  to give

$$\Phi^T \mathbf{M} \Phi \ddot{\mathbf{U}} + \Phi^T \mathbf{C} \Phi \dot{\mathbf{U}} + \Phi^T \mathbf{K} \Phi^T \tilde{\mathbf{U}} = \Phi^T \mathbf{R} \quad (2.7)$$

The above equation can be diagonalized if  $\Phi$  is chosen as consisting of the  $n$  eigenvectors of the eigensolutions  $(\omega_1^2, \phi_1), \dots, (\omega_n^2, \phi_n)$  which solve the eigenproblem

$$\mathbf{K}\Phi = \Omega^2 \mathbf{M}\Phi \quad (2.8)$$

so that

$$\Phi^T \mathbf{K} \Phi = \Omega^2 \quad (2.9)$$

$$\Phi^T \mathbf{M} \Phi = \mathbf{I} \quad (2.10)$$

These eigenvectors are the free vibrational modes of the equilibrium equation. Choosing  $\Phi$  in this manner transforms equation 2.7 into

$$\ddot{\tilde{\mathbf{U}}} + \tilde{\mathbf{C}} \dot{\tilde{\mathbf{U}}} + \Omega^2 \tilde{\mathbf{U}} = \tilde{\mathbf{R}} \quad (2.11)$$

Under the assumption that the transformed damping matrix  $\tilde{\mathbf{C}}$  is also diagonal, above equation 2.11 is diagonalized form of equation 2.5 since  $\Omega^2$  is a diagonal matrix. Diagonalizing decouples the individual components of  $\mathbf{U}$ . This means that we obtain a separate differential equation for each component of  $\mathbf{U}$  and as such it is not necessary to compute the inverse of the  $\mathbf{K}$ . Computing this inverse is costly and may not always be possible if  $\mathbf{U}$  is singular. Thus, the diagonalized equation 2.11 can be solved for the displacements  $\tilde{\mathbf{U}}$  either in closed form or integrated numerically in fewer steps.

### 2.1.1.3 Recovering shape with FEM

Through Modal analysis it is possible to easily generate displacements of an arbitrary object given its stiffness matrix  $\mathbf{K}$ . These displacements deform the object. Since the matrix  $\Phi$  encodes the free vibration modes, it is possible to generate a new face by taking a vector of weights  $\mathbf{u}$  and calculating a deformed instance of the object class by adding the displacements to the mean shape  $\bar{\mathbf{x}}$  using

$$\mathbf{x} = \bar{\mathbf{x}} + \Phi \mathbf{u} \quad (2.12)$$

Equation 2.12 synthesizes a new object from a vector of parameters  $\mathbf{u}$ . It is therefore possible to fit a model of a class of objects with a known stiffness function to a candidate object in an image by solving an optimization problem which locates the parameters  $\mathbf{u}$ .

Alternatively, it is also possible to use the equilibrium equation 2.3 to recover the shape of the candidate object. Assuming that the positions of the nodal points are found in the image and that their 3D position is recovered, then the load vector  $\mathbf{R}$  can be calculated as

$$[R_{3k}, R_{3k+1}, R_{3k+2}] = [x_k^w, y_k^w, z_k^w] - [x_k, y_k, z_k] \quad (2.13)$$

where  $x_k^w$ ,  $y_k^w$  and  $z_k^w$  is the position of the nodal point with index  $k$  which is obtained from the image. The rest position of this nodal point in the model is given by  $x_k$ ,  $y_k$  and  $z_k$ . This approach to constructing the load vector  $\mathbf{R}$  is analogous to attaching springs between the nodal point measurements and the corresponding points in the model. Given the load vector the goal is now to solve the previously seen equilibrium equation

$$\mathbf{K}\mathbf{U} = \mathbf{R} \quad (2.14)$$

To solve for the displacements  $\mathbf{U}$  the stiffness matrix  $\mathbf{K}$  needs to be inverted. This is often a very costly operation which can be avoided by diagonalizing the equilibrium equation. This is done using modal analysis with the generalized basis from given in equation 2.8.

## 2.1.2 Statistical Models

Statistical models attempt to understand and model the variation inherent in the deformable object through statistical analysis. In statistical analysis a data set is examined and characterized so that predictions and judgments based on the underlying data distributions can be made. In order to use the techniques of statistical analysis to build a deformable model, it is necessary to have a dataset to analyze. This dataset should be made up of many instances of the class of objects we want to model. These instances are usually given as a set of vertices (either 2D or 3D) which define the object.

The less sophisticated *shape models* attempt to model the variation of the data that defines the shape of an object. The shape model describes the boundaries of an object. For instance, a shape model of a face will denote the location and measures of the defining contours of a face.

The more sophisticated *appearance models* perform statistical analysis on the entire appearance of the object – which includes variance coming from the texture, lighting etc. This appearance model describes the location and color of the pixels that define the object.

### 2.1.2.1 PCA and Eigenfaces

In 1991, Turk and Pentland [35] pioneered a 2D model-based face recognition approach based on the statistical technique called *principal component analysis* (PCA). The PCA is an orthogonal projection of the data onto a lower dimensional linear space such that the variance of the projected data is maximized. The PCA therefore identifies the primary directions in which data varies, since these are the vector directions which maximize variance. These vectors span the *principal subspace*. The formula to compute the principal directions is derived from maximizing the variance of a projection of the data [3]. By solving this maximization problem we find that variance in the  $M$ -dimensional principal subspace, spanned by the vectors  $\mathbf{u}_i$ , is given by

$$\mathbf{S}\mathbf{u}_i = \lambda_i \mathbf{u}_i \quad (2.15)$$

where  $\mathbf{S}$  is the  $D \times D$  covariance matrix of the  $D$ -dimensional data set. From 2.15 we see that the vectors  $\mathbf{u}_i$  are the eigenvectors, and that the  $\lambda_i$  are the eigenvalues of the covariance matrix of data set. In order to maximize the variance of the  $M$ -dimensional principal subspace, given by this equation, we pick the  $M$  eigenvectors which correspond to the largest eigenvalues. These  $M$  eigenvectors are the principal directions which span the  $M$ -dimensional principal subspace. If  $D = M$ , then there is no dimensionality reduction and the PCA reduces to just a rotation of the coordinate axes which aligns them with the axes of the principal subspace. To express PCA as a linear transformation we combine the  $M$  eigenvectors into a matrix  $\Phi_{pca} = [\mathbf{u}_1 \dots \mathbf{u}_m]$  to get

$$\mathbf{S}\Phi_{pca} = \Phi_{pca}\Lambda \quad (2.16)$$

Given the  $D$ -dimensional data set represented as a matrix  $\mathbf{D}$ , then the PCA transformation matrix  $\Phi_{pca}$  may be calculated in two equivalent ways. Either we compute the covariance matrix  $\mathbf{S} = \mathbf{U}^T\mathbf{U}/(D-1)$ , where  $\mathbf{U}$  is the mean centered data set matrix. Or the PCA transformation matrix is obtained from the singular value decomposition of the the mean centered data set as  $\mathbf{U} = \Phi_{pca}\Sigma\mathbf{V}$ .

Turk and Pentland's face recognition scheme uses a data set of images to learn what they call *eigenfaces*. Expressed in mathematical terms – the eigenfaces are eigenvectors of the 2D image space. As seen from the PCA analysis, these eigenvectors represent the axes of a space spanning the 2D face data set, which are responsible for any significant variation. To obtain the eigenfaces Turk and Pentland compute the SVD decomposition of this covariance matrix. Any individual face from the training data set can then be exactly represented as a linear combination all the eigenfaces.

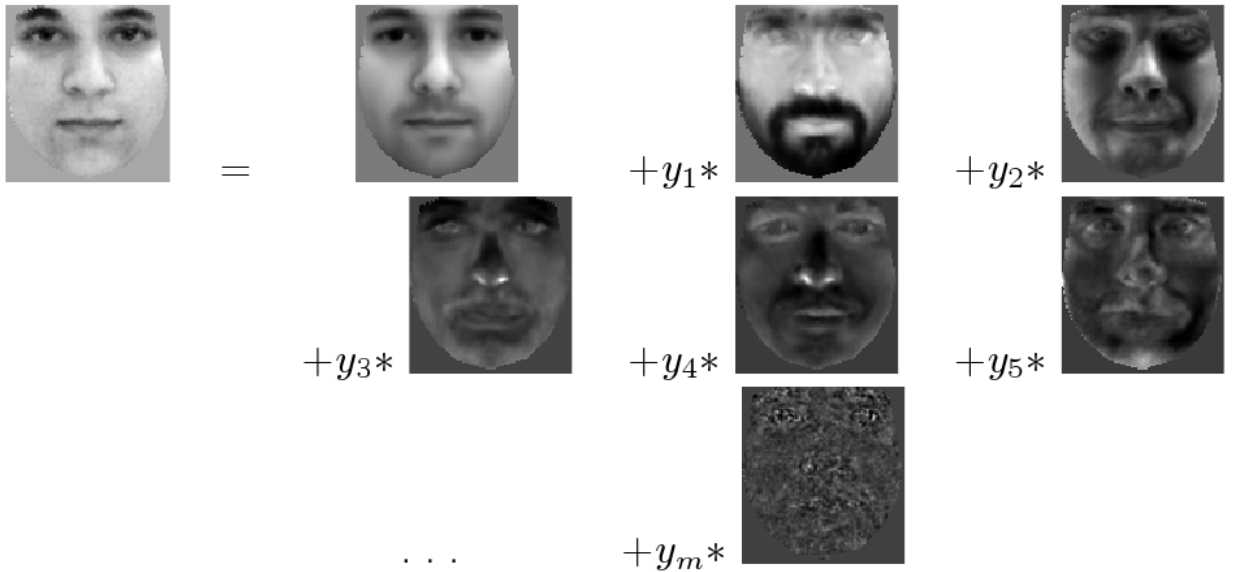


Figure 2.1: Using the eigenfaces we can represent an image as a linear combination of the eigenfaces. Taken from [28].

The weight of each eigenface in the linear combination is computed from the projection of the face image onto this eigenface. To recognize a face we first calculate these weights. Then we calculate the Euclidean distance of the vector of weights to the weights of faces from our training data set. The face from the data set with weights which are closest to the new image's weights is chosen as a match.

In an image of 256 by 256 we have a 65,536 dimensional vector that represents the face image. This means we would require 65,536 eigenfaces to be able to exactly represent every face. However, images of faces are very similar in their configuration which means that the underlying principal subspace of faces has a lower dimension than 65,536. To reduce the dimensionality, PCA is performed to identify the subset of eigenfaces which span a lower dimensional principal subspace. Using this subset of eigenfaces, which are called the principal eigenfaces, we can effectively encode a 65,536 dimensional face image vector using a vector of much smaller dimensions.

The drawback of a PCA based model is that the recognition rate drops significantly once independent sources of variation are introduced. Turk and Pentland noted that the eigenfaces approach has issues with variations in lighting, head size, head orientation or faces exhibiting expressions [35]. Likewise, when faces are partially occluded in images it causes difficulties to the technique.

The eigenfaces approach is based heavily on information and coding theory. As explained, the PCA makes it possible to encode a face image using low dimensional vector. As such PCA is often used to reduce dimensionality in more sophisticated modeling approaches.

### 2.1.2.2 Morphable Model

Blanz et al use PCA to construct a statistical model of 3D face shape and texture [4], [5]. The orthogonal matrix of basis vectors is extracted from a database of 3D faces with texture. This basis spans a vector space which Blanz refers to as the *Morphable Model*.

The faces in the database are encoded as shape vectors with  $S_i$  to being the vector representing the 3D shape of a human face, stored as the  $x, y, z$ -coordinates of all the vertices of that face. So

$$\mathbf{S}_i = (x_1, y_1, z_1, x_2, \dots, x_n, y_n, z_n)^T \quad (2.17)$$

Similarly, the texture vectors are defined as

$$\mathbf{T}_i = (R_1, G_1, B_1, R_2, \dots, R_n, G_n, B_n)^T \quad (2.18)$$

The idea behind the morphable model is that a linear combination of the  $\mathbf{S}_i$  and  $\mathbf{T}_i$ , which is within  $\pm 3$  standard deviations from the mean, constitutes a realistic face. The full morphable model is given by the formula

$$\mathbf{S} = \sum_{i=1}^N a_i \mathbf{S}_i \quad \mathbf{T} = \sum_{i=1}^N b_i \mathbf{T}_i \quad (2.19)$$

Blanz et al also performed a Principal Component Analysis (PCA) on the dataset of examples to produce orthogonal basis vectors that can be used in the morphable model instead of the examples directly. This reduces the dimensionality of the model. The eigenvectors denoted as  $\mathbf{s}_i$  and  $\mathbf{t}_i$  can be used to generate new faces as follows

$$\mathbf{S} = \bar{\mathbf{s}} + \sum_{i=1}^m \alpha_i \mathbf{s}_i \quad \mathbf{T} = \bar{\mathbf{t}} + \sum_{i=1}^m \beta_i \mathbf{t}_i \quad (2.20)$$

where  $\bar{\mathbf{s}}$ ,  $\bar{\mathbf{t}}$  are the means of the shape and texture data and  $m < N$ . The parameters  $\alpha_i$  and  $\beta_i$  are the shape and texture parameters controlling the deformable model.

The PCA process identifies vectors which represent the most variance in the examples and as such contain the most information about the images. This means any image can now be represented by the linear combination of a smaller number of these components than would be required of the original examples. The linear combination is controlled by the parameters of the deformable model. This is, in essence, the eigenfaces modeling approach only now applied to 3D shapes and textures.

The shape vector and texture vector encode the location and texture values at specific feature (landmark) points. Therefore, to allow the morphable model to fit to the source image, a point-to-point correspondence must be ensured on the example images, so that important features such as the tip of the nose are correctly matched up in the examples. During the recognition process the features in the source image are matched to those in the examples, in order to calculate the correct combinations of the basis vectors. According to Blanz, to fit the Morphable Model of 3D faces to an image, the user has to manually select about 7 feature points.

### 2.1.2.3 Combined Models of Shape and Appearance

Texture variations and shape variations are correlated. Clearly, with any source of lighting it is the shape of an object which influences what parts of the object will appear darker or lighter. Cootes and Taylor [11] describe modeling approaches which account for the correlations between the two sources of variation. The models they introduce are well suited for highly variable structures such as faces or internal organs. Using PCA based shape and texture models, Cootes and Taylor construct Active Shape and Active Appearance Models which, despite the name, are model fitting algorithms that find the parameters of statistical models to fit instances of objects in images.

The shape model is constructed by annotating feature points in images, collecting these into a data matrix and then performing PCA on the covariance matrix of this data to generate a lower dimensional basis  $\mathbf{P}_s$ . The shape model then makes it possible to synthesize new shapes as follows

$$\mathbf{S} = \bar{\mathbf{s}} + \mathbf{P}_s \mathbf{b}_s \quad (2.21)$$

To construct the texture model, the image is first warped into the mean shape  $\bar{\mathbf{s}}$  to obtain a “shape-free” image. The gray-scale values at points in the shape-free image, which correspond to feature points in the mean shape are then measured and combined into a texture data matrix. Then PCA is used to find eigenvector matrix  $\mathbf{P}_t$ . This matrix of eigenvectors gives the linear model for texture as

$$\mathbf{T} = \bar{\mathbf{t}} + \mathbf{P}_t \mathbf{b}_t \quad (2.22)$$

In an approach similar to that of Blanz seen in formula 2.20, Cootes and Taylor separate the shape and the information of a target image into two distinct vectors – the shape parameter vector

$\mathbf{b}_s$  and the texture represented by the grey-level vector  $\mathbf{b}_t$  (here the image is gray-scaled). To obtain a model which addresses both shape and texture, these parameter vectors are combined into one vector  $\mathbf{b} = [\mathbf{b}_s \mathbf{b}_t]^T$ . Then PCA is applied to this combined vector to get an eigenvector basis  $\mathbf{P}_c = \begin{pmatrix} P_{cs} \\ P_{ct} \end{pmatrix}$  for the parameters  $\mathbf{b}_s$  and  $\mathbf{b}_t$ . This new basis encapsulates the correlation between shape and texture, thus making it possible to express the other parameters as functions of a parameter vector  $\mathbf{c}$  as follows

$$\mathbf{S} = \bar{\mathbf{s}} + \mathbf{P}_s \mathbf{W}_s^{-1} \mathbf{P}_{cs} c \quad (2.23)$$

$$\mathbf{T} = \bar{\mathbf{t}} + \mathbf{P}_t \mathbf{P}_{ct} \mathbf{c} \quad (2.24)$$

where  $\mathbf{W}_s$  is a diagonal matrix of weights which allows the shape and texture models to have different units. To reconstruct a new face using this model we first determine the  $\mathbf{b}_s$  and  $\mathbf{b}_g$  parameters from the new face image. These parameters are then used to calculate the  $c$  using by projecting them using the eigenvector basis as  $\mathbf{c} = \mathbf{P}_c^T \mathbf{b}$ .

**Active Shape Model.** The Active Shape model (ASM) proposed by Cootes and Taylor is a model fitting algorithm based on the statistical models of shape and texture. The ASM enables us to locate a shape in an image using an iterative procedure as shown in figure 2.2. To search for objects in an image using the ASM, we first place the shape model, which we obtained from the training data, into the center of the image. In the next iterations, a texture profile of  $k$  neighboring points around each point of the shape model is taken and compared with the texture profile of this point obtained when training the model. Then the shape model point is moved to make the difference between the two profiles smaller. This process is repeated until convergence is reached.



Figure 2.2: Active Shape Model iterations shown on finding the shape of a previously unseen face. Taken from [10].

The ASM moves the point only based on the texture profile of a local neighborhood of this point. The obvious problem with this approach is that it is a local search technique and thus it depends too much on the choice of the starting point. If the target image is not centered on the face and the algorithm begins in the center of the image, then it can possibly converge on incorrect shapes such as the nose, as can be seen in figure 2.3. This is due to the fact that as a local search method, the ASM cannot escape a local minimum.

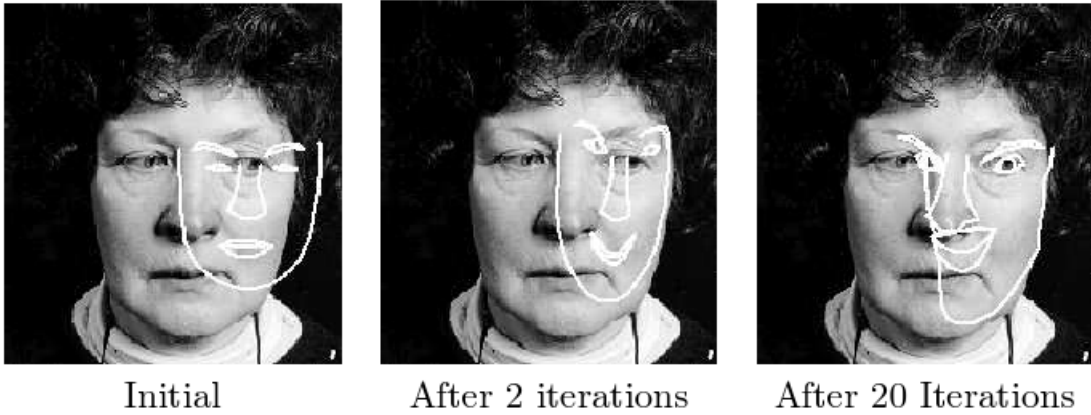


Figure 2.3: Incorrect convergence of the ASM when the search is initialized incorrectly. This can happen when the face is not centered in the image or when the search does not begin in the center of the image. Taken from [10].

To improve the efficiency and the robustness of ASM, Cootes suggests performing several searches at different resolution. First a coarse search is performed on the image with a low resolution until the search converges. The resulting configuration of the shape model points from this coarse search then serves as the starting point for a search in the same image with a better resolution. The advantage of adopting this coarse to fine search approach is that it makes the search less susceptible to converging on incorrect shapes. When searching at a lower resolutions it will be easier to find the outlines of the face. Once the search is restarted with a higher resolution, shapes like the mouth and the nose can be identified.

**Active Appearance Model.** The Active Appearance Model (AAM) is a model fitting technique based on a combined shape and texture model defined by equations 2.23 and 2.24. The AAM enhances the Active Shape model search by also considering the texture information in the entire object.

The AAM search attempts to minimize the difference between the texture (the grey-levels) of the image we are processing and the grey-levels of the image generated with the current model parameters. The difference vector which is minimized every iteration is defined as:

$$\delta\mathbf{I} = \mathbf{I}_i - \mathbf{I}_m \quad (2.25)$$

where  $\mathbf{I}_m$  is the vector of the grey-levels generated with the current model parameters and  $\mathbf{I}_i$  is a vector containing the grey-levels of the image. The goal of AAM is to minimize the difference  $\delta\mathbf{I}$  between the synthesized and observed grey-levels.

To simplify this optimization problem, Cootes and Taylor propose to allow the computer to learn the relationship between the difference vector  $\delta\mathbf{I}$  and the error in the model parameters. Learning this relationship makes it possible to correctly improve the model for a given measured error in an iterative procedure.

The AAM iterations are depicted in figure 2.4. The process attempts to change model parameters to fit it to an unseen face. This fitting is done by minimizing the differences between pixels at the landmark points.

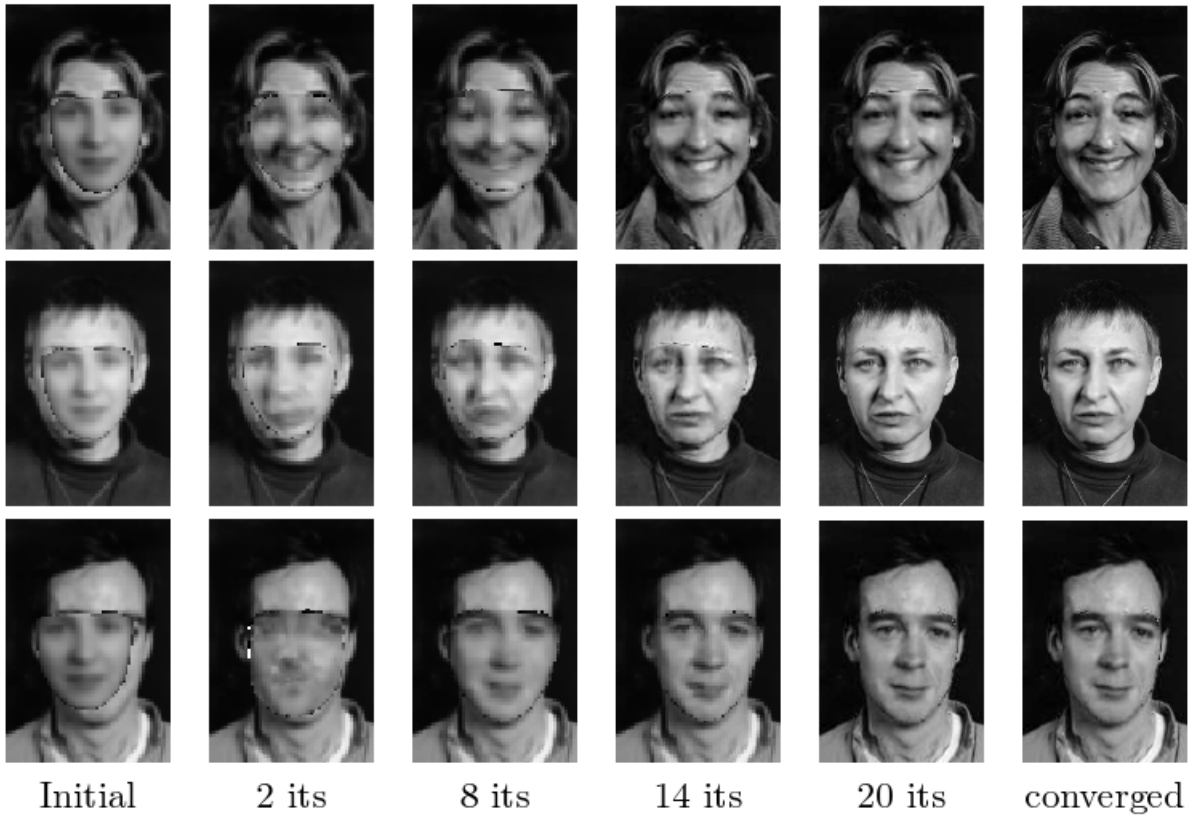


Figure 2.4: Active Appearance Model iterations shown when searching for previously unseen faces. Taken from [11].

The drawback of both the ASM and AAM search is that it is required of the user to specify landmark points on the target image. This means the technique is not well suited for applications where the model would have to be matched to a large number of faces. To combat this problem, a number of automatic 2D and 3D landmark location solutions can be used [11].

Another problem of both the ASM and the AAM lies in the fact that they do not distinguish or model the individual factors responsible for shape or texture variation. They only acknowledge two sources of variation in the image. In the case of face models, this means that variation caused by identity and the variation caused by expression are not perceived as two fundamentally different sources. Thus, it is impossible to only alter one variational source while leaving the other source constant. This makes the models unsuitable for expression transfer.

### 2.1.3 Tensor Models

Vasilescu and Terzopoulos [36], [38], [37] defined a generalization of statistical methods using multilinear algebra. Statistical analysis of images using PCA identifies the variation directions of the training dataset. The drawback of the PCA is that it only addresses one factor – one source of variance in the images. All variation is explained using the orthogonal eigenvectors and the eigenvalues. With images of faces, the PCA approach works well when only the identity or only the expression varies. Using methods of multilinear analysis it is possible to model the interaction of several sources of variation.

The multilinear approach has mostly replaced the PCA method and will be also used in the expression transfer application we develop. Here we will go over an overview of multilinear algebra to elucidate the advantages of multilinear models. Details concerning design and implementation specifics of the tensor based model will be covered in chapter 3. A comprehensive discussion of multilinear algebra and its application was compiled by De Lathauwer in [19]. Detailed discussion of matrix calculations and matrix calculus can be found in [13], [18], [32].

### 2.1.3.1 Multilinear Algebra

Multilinear algebra is based on the generalization of matrix operations. Matrices are linear operators and can be seen as linear functions defined over vector spaces. In multilinear algebra the operators are *tensors*.

**Tensors.** In multilinear algebra tensors define multilinear operators over a set of vector spaces. Tensors are organized into mode spaces. The  $N$ -mode tensor contains  $N$  mode spaces and each item of data contained in the tensor is indexed by  $N$  values. The number of modes determines the order of a tensor, so an  $N$ -mode tensor has order  $N$ . If  $\mathcal{A}$  is a tensor of order  $N$ , then  $\mathcal{A} \in \mathbb{R}^{I_1 \times I_2 \times \dots \times I_N}$  where  $I_i$  are the mode space sizes. Vectors are  $1^{st}$  order tensors, matrices are  $2^{nd}$  order tensors. In a matrix the first mode space is the row space, the 2-mode space is the column space.

**Tensor Flattening.** Any tensor can be flattened into a matrix. Tensor flattening (or matrix unfolding) is defined as follows; given an  $N$ th-order tensor  $\mathcal{A} \in \mathbb{R}^{I_1 \times I_2 \times \dots \times I_N}$ , this tensor can be flattened along mode  $i \in \{1, 2, \dots, N\}$  to give  $\mathbf{A}_{(i)} \in \mathbb{R}^{I_i \times I_1 I_2 \dots I_{i-1} I_{i+1} \dots I_N}$ .

The flattening corresponds to aligning the vectors from the mode space  $i$  into a matrix. To illustrate tensor flattening lets define the  $3^{rd}$  order tensor  $\mathcal{B} \in \mathbb{R}^{3 \times 2 \times 3}$  by  $b_{111} = b_{112} = b_{113} = b_{211} = b_{213} = -b_{212} = -b_{313} = 1$ ,  $b_{311} = b_{122} = b_{322} = b_{323} = -b_{213} = -b_{222} = 2$ ,  $b_{312} = 0$ ,  $b_{121} = b_{221} = 4$  and  $b_{223} = -5$ . Then tensor flattening along mode 1 is given by

$$\mathbf{B}_{(1)} = \left( \begin{array}{ccc|ccc} 1 & 1 & 1 & 4 & 2 & 1 \\ 1 & -1 & -2 & 4 & -2 & -5 \\ 2 & 0 & -1 & 2 & 2 & 2 \end{array} \right)$$

The flattening along mode 2 are the vectors along the second mode space

$$\mathbf{B}_{(2)} = \left( \begin{array}{ccc|ccc} 1 & 1 & 2 & 1 & -1 & 0 & 1 & -2 & -1 \\ 4 & 4 & 2 & 2 & -2 & 2 & 1 & -5 & 2 \end{array} \right)$$

Tensor flattening is useful since it makes it possible to express tensor operations using matrices. The schema for flattening a  $3^{rd}$  order tensor is shown in figure 2.5

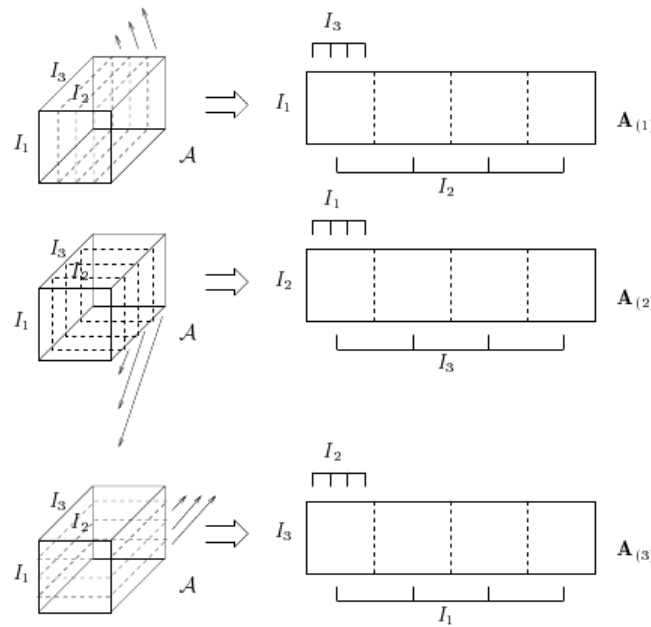


Figure 2.5: Flattening of the  $(I_1 \times I_2 \times I_3)$ -tensor  $\mathcal{A}$  into three matrices; the  $(I_1 \times I_2 I_3)$ -matrix  $\mathbf{A}_{(1)}$ , the  $(I_2 \times I_3 I_1)$ -matrix  $\mathbf{A}_{(2)}$  and the  $(I_3 \times I_1 I_2)$ -matrix  $\mathbf{A}_{(3)}$ . Taken from [19].

**Kronecker product.** The Kronecker Product between a  $m \times n$  matrix  $A$  and a  $p \times q$  matrix  $B$  is a  $(mp) \times (nq)$  matrix defined as

$$A \otimes B = \begin{pmatrix} a_{11}B & a_{12}B & \dots & a_{1n}B \\ a_{21}B & a_{22}B & \dots & a_{2n}B \\ \vdots & & & \\ a_{m1}B & a_{m2}B & \dots & a_{mn}B \end{pmatrix} \quad (2.26)$$

**Properties.** The Kronecker product possesses a number of useful properties. First the connection between matrix product and kronecker product is given by

$$(A \otimes B)(C \otimes D) = (AC \otimes BD) \quad (2.27)$$

where  $A$  is a  $m \times n$  matrix,  $B$  a  $p \times q$  matrix,  $C$  a  $n \times r$  matrix and  $D$  a  $q \times s$  matrix.

**Proof.** The proof comes from block multiplication of the two Kronecker products as follows

$$\begin{aligned} (A \otimes B)(C \otimes D) &= \begin{pmatrix} a_{11}B & a_{12}B & \dots & a_{1n}B \\ a_{21}B & a_{22}B & \dots & a_{2n}B \\ \vdots & & & \\ a_{m1}B & a_{m2}B & \dots & a_{mn}B \end{pmatrix} \begin{pmatrix} c_{11}D & c_{12}D & \dots & c_{1r}D \\ c_{21}D & c_{22}D & \dots & c_{2r}D \\ \vdots & & & \\ c_{n1}D & c_{n2}D & \dots & c_{nr}D \end{pmatrix} \\ &= \begin{pmatrix} (\sum_{j=1}^n a_{1j}c_{j1})DB & (\sum_{j=1}^n a_{1j}c_{j2})DB & \dots & (\sum_{j=1}^n a_{1j}c_{jr})DB \\ (\sum_{j=1}^n a_{2j}c_{j1})DB & (\sum_{j=1}^n a_{2j}c_{j2})DB & \dots & (\sum_{j=1}^n a_{2j}c_{jr})DB \\ \vdots & & & \\ (\sum_{j=1}^n a_{mj}c_{j1})DB & (\sum_{j=1}^n a_{mj}c_{j2})DB & \dots & (\sum_{j=1}^n a_{mj}c_{jr})DB \end{pmatrix} \\ &= (AC \otimes BD) \end{aligned}$$

The transpose of the Kronecker product is the transpose of the component matrices.

$$(A \otimes B)^T = A^T \otimes B^T \quad (2.28)$$

**Proof.** The proof can be seen from block transposing the Kronecker product.

$$(A \otimes B)^T = \begin{pmatrix} a_{11}B & \dots & a_{1n}B \\ a_{21}B & \dots & a_{2n}B \\ \vdots & & \\ a_{m1}B & \dots & a_{mn}B \end{pmatrix}^T = \begin{pmatrix} a_{11}B^T & \dots & a_{m1}B^T \\ a_{12}B^T & \dots & a_{m2}B^T \\ \vdots & & \\ a_{1n}B^T & \dots & a_{mn}B^T \end{pmatrix} = A^T \otimes B^T$$

If the matrices  $A$  and  $B$  are invertible then the Kronecker product is invertible as well. The inverse of the Kronecker product is given by

$$(A \otimes B)^{-1} = A^{-1} \otimes B^{-1} \quad (2.29)$$

**Proof.** The inverse formula is derived from property 2.27.

$$(AA^{-1} \otimes BB^{-1}) = (A \otimes B)(A^{-1} \otimes B^{-1}) = I$$

thus  $(A^{-1} \otimes B^{-1})$  is the inverse of the Kronecker product.

From 2.27 and 2.28 we can see that the Kronecker product of two orthogonal matrices is again orthogonal.

$$(A \otimes B)^T(A \otimes B) = (A^T \otimes B^T)(A \otimes B) = (A^T A \otimes B^T B) = (I \otimes I) = I \quad (2.30)$$

and similarly to show for  $(A \otimes B)(A \otimes B)^T = I$ .

**Frobenius Norm.** The Frobenius-norm of a tensor is a measure of the size of the tensor. It is defined as

$$\|\mathcal{A}\| = \sqrt{\sum_{i_1} \sum_{i_2} \dots \sum_{i_N} a_{i_1 i_2 \dots i_N}^2} \quad (2.31)$$

Thus the Frobenius norm is merely the sum over the square of all elements. For matrices the Frobenius norm simplifies to a square root of the trace of the squared matrix.

**Mode- $n$  product.** The mode spaces of a tensor can be altered independently of the other mode spaces by a linear transformations called *mode- $n$  product*. The mode- $n$  product is defined between a matrix  $\mathbf{M}$  and a tensor  $\mathcal{A}$  with the result being another tensor  $\mathcal{B}$ . The product is written as  $\mathcal{B} = \mathcal{A} \times_n \mathbf{M}$ . The mode- $n$  product by the matrix  $\mathbf{M}$  transforms all the vectors  $\mathbf{v}$  in the  $n$ -th mode of the tensor into vectors  $\mathbf{Mv}$ . It is therefore possible to separately transform the vectors in mode-3 and the vectors in mode-2. The mode- $n$  product can also be expressed in terms of flattened matrices as  $\mathbf{B}_{(n)} = \mathbf{MA}_{(n)}$ . We can therefore rewrite the singular value decomposition (SVD) of a matrix  $\mathbf{D} = \mathbf{U}\Sigma\mathbf{V}^T$  using the mode- $n$  product as  $\mathbf{D} = \mathbf{\Sigma} \times_1 \mathbf{U} \times_2 \mathbf{V}$ .

The successive application of  $N$  mode- $n$  products to a tensor can be represented using flattened tensors, matrix products and Kronecker products as follows

$$\mathcal{B} = \mathcal{A} \times_1 \mathbf{M}_1 \times_2 \mathbf{M}_2 \dots \times_n \mathbf{M}_n \dots \times_N \mathbf{M}_N \quad (2.32)$$

$$\mathbf{B}_{(n)} = \mathbf{M}_n \mathbf{A}_{(n)} (\mathbf{M}_{n-1} \otimes \mathbf{M}_{n-2} \otimes \dots \mathbf{M}_1 \otimes \mathbf{M}_N \otimes \dots \mathbf{M}_n + 1)^T \quad (2.33)$$

Equation 2.32 shows the application of  $N$  mode- $n$  products. In equation 2.33 the equivalent formulation is given using matrices instead of tensors. Note that the transpose can be brought into the parentheses in the second term of 2.33, due to the transpose property of the Kronecker product 2.28. The order of the matrices inside of the parentheses is important. If this order is changed, then the resulting matrix has the same columns but in a different order.

**High Order Singular Value Decomposition (HOSVD).** The *N-Mode singular value decomposition* (or high order SVD) is a linear transformation of a tensor. An  $N$ -order tensor has  $N$  mode spaces. The high order SVD orthogonalizes the mode spaces by finding the  $N$  sets of orthonormal basis vectors which span the column space along the respective mode space. The HOSVD decomposition is as follows [19]

$$\mathcal{A} = \mathcal{S} \times_1 \mathbf{U}_1 \times_2 \mathbf{U}_2 \times_3 \mathbf{U}_3 \dots \times_N \mathbf{U}_N \quad (2.34)$$

Equation 2.34 decomposes the tensor into a *core tensor*  $\mathcal{S}$  and orthonormal mode matrices  $\mathbf{U}_1 \dots \mathbf{U}_N$ . The mode matrix  $\mathbf{U}_i$  contains the orthonormal vectors  $u_{ij}$  which form the orthogonal basis of the column space of the flattened tensor  $\mathbf{A}_{(n)}$ . The core tensor governs the interaction between these mode matrices and is as such analogous to a diagonal matrix of eigenvalues used in PCA. Eigenvalues can be seen as measures of the variance along the corresponding eigenvector directions. However, the core tensor does not have a diagonal structure. Rather it has the property of all-orthogonality whereby all subtensors of  $\mathcal{S}$ , obtained by fixing one index, are orthogonal. The Frobenius norms of these subtensors decrease, which makes it possible to reduce the dimensionality of the data set by truncating the core tensor. It is therefore possible to approximate the original tensor using a reduced core tensor. The approximation of a tensor  $\mathcal{A}$  using a reduced core tensor  $\mathcal{S}_{reduced}$  is derived from the mode- $n$  SVD and is defined as:

$$\mathcal{A} \approx \mathcal{S}_{reduced} \times_1 \hat{\mathbf{U}}_1 \times_2 \hat{\mathbf{U}}_2 \times_3 \hat{\mathbf{U}}_3 \dots \times_N \hat{\mathbf{U}}_N \quad (2.35)$$

The matrices  $\hat{\mathbf{U}}_i$  are truncated versions of the eigenvector matrices for the corresponding mode space. Figure 2.6 depicts the approximate HOSVD using the truncated core tensor and mode matrices.

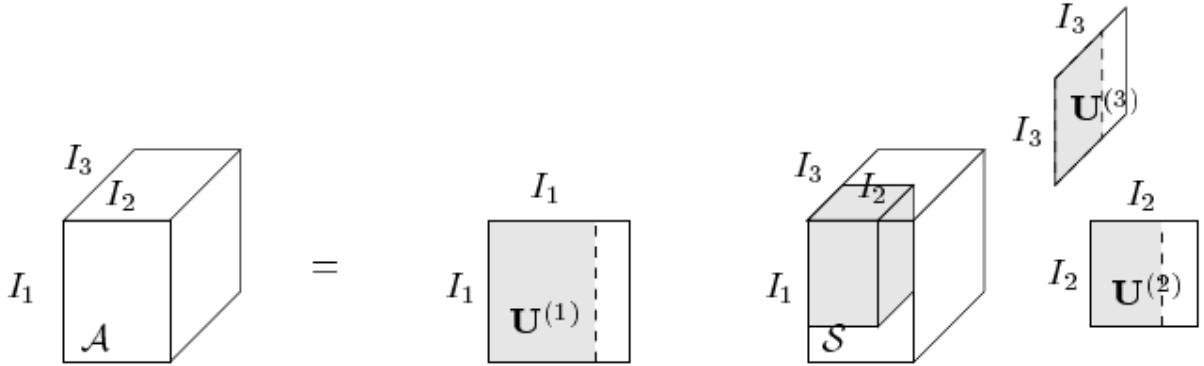


Figure 2.6: The HOSVD decomposition of 3<sup>rd</sup> order tensor  $\mathcal{A}$  into three mode matrices  $\mathbf{U}^{(1)}$ ,  $\mathbf{U}^{(2)}$ ,  $\mathbf{U}^{(3)}$  and the core tensor  $\mathcal{S}$ . The shaded part of the core tensor and the mode matrices represents a the truncated versions of these multilinear operators. The composition of the truncated mode matrices and the truncated tensor approximates the tensor  $\mathcal{A}$ . Taken from [19].

**HOSVD Algorithm.** The HOSVD decomposition of a tensor  $\mathcal{A}$  of order  $N$  is computed as follows:

- **Step 1.** For  $i = 1, \dots, N$  compute the mode matrix  $\mathbf{U}_i$  by calculating the SVD of the flattened matrix  $\mathbf{D}_{(i)} = \mathbf{U}_i \Sigma_i \mathbf{V}_i^T$ . The left singular matrix of  $\mathbf{D}_{(i)}$  is the mode matrix for mode  $i$ .
- **Step 2.** Compute the core tensor by reversing equation 2.34 to get the core tensor as

$$\mathcal{S} = \mathcal{A} \times_1 \mathbf{U}_1^T \times_2 \mathbf{U}_2^T \times_3 \mathbf{U}_3^T \cdots \times_N \mathbf{U}_N^T \quad (2.36)$$

### 2.1.3.2 Tensor-Based Model

The possibility of using a multilinear approach to construct face models was explored by numerous researchers. Vasilescu and Terzopoulos [36] build a tensor from a database of face images and construct *tensorfaces* by performing HOSVD on the data tensor. Tensorfaces are contained as vector the mode matrices  $\mathbf{U}_i$ . Vlasic, Brand, Pfister and Popovic [40] build a tensor model of 3D faces and utilize it to recognize faces in video sequences for the purpose of expression transfer. The group successfully managed to implemented a face transfer application based on a multilinear face model which allowed for expressions and even for speech related movements to be transferred between video-recordings of two different subjects. The multilinear model was estimated from geometric variations in 3D face scans that Vlasic and his group collected. Two tensor models with different dimensionality were utilized. Their first model was a lower dimensional bilinear model that organized the data into three groups of vertices, identity and expression. Their higher dimensional model organized faces into groups of expressions, vertices, identities and visemes. The parameters for the multilinear face model, which were used to synthesize new expressions, were extracted from the video input using an optical flow algorithm.

To construct a bilinear face model it is necessary to separate the faces from the database into groups of expressions and identities in order to organize them into the tensor. The tensor based approach allows us to organize the data in a way that makes for easier manipulation with a transformation matrix. The groups are aligned in the tensor along the modes as shown in figure 2.7. In this example the vertices change along the mode-1 space, the identity changes along the mode-2 space and the expressions change along the mode-3 space.

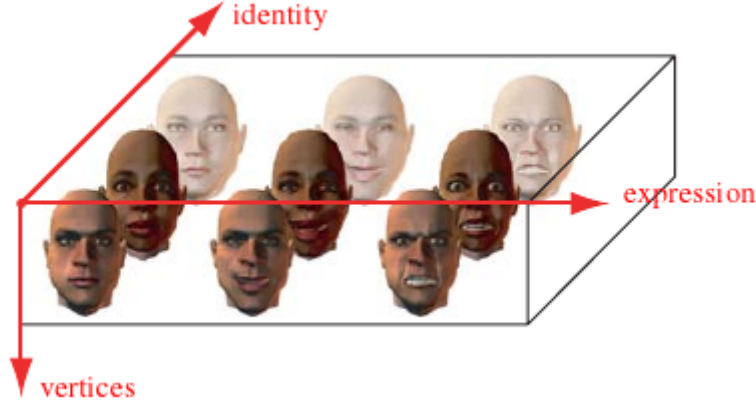


Figure 2.7: Multilinear face model showing how different attributes change along the modes. Taken from [40].

Vlasic et al constructed a multilinear face model using mode-n SVD by decomposing the organized tensor into mode matrices. A generative model can be constructed when the core tensor and the mode-1 matrix are combined together using the mode- $n$  product. This is because the first mode space holds the vertices, which the model should be capable of generating. Using equation 2.35 the data tensor  $\mathcal{D}$  is decomposed as

$$\mathcal{D} \approx \mathcal{M} \times_2 \hat{\mathbf{U}}_2 \times_3 \hat{\mathbf{U}}_3 \cdots \times_N \hat{\mathbf{U}}_N \quad (2.37)$$

where tensor  $\mathcal{M}$  is called the *multilinear model*. The multilinear model can then be used to synthesize new faces. Mode multiplying the multilinear model with one row from each mode matrix we recover exactly one of the original faces. Mode multiplying the model  $\mathcal{M}$  with a linear combination of rows from the truncated mode matrices synthesizes a new face  $\mathbf{f}$  giving us the generative tensor model as

$$\mathbf{f} = \mathcal{M} \times_2 \mathbf{w}_2^T \times_3 \mathbf{w}_3^T \cdots \times_N \mathbf{w}_N^T \quad (2.38)$$

The weight vectors  $\mathbf{w}_2, \dots, \mathbf{w}_N$  are column vectors which encode the attribute of the corresponding mode space.

The tensor-based model is similar to what we saw in the eigenfaces PCA approach in figure 2.1. However, the tensor-based approach has the advantage that we can manipulate the different sources of variance (i.e. in the case of a face model the identity, the expressions) separately. This advantage outweighs the additional computational complexity carried by the high order SVD and makes this model suitable for the task of expression transfer.

The drawback of the method described by Vlasic et al is that it requires the tensor to be fully populated. This means that we require all expressions to be performed by all subjects to have a full tensor. This raises issues when some data is corrupted or lost during data gathering. There are two ways of coping with this problem. The first approach is to use a statistical method to model the data. Alternatively the missing data can be estimated from the current data.

### 2.1.3.3 Tensor-based Statistical Discriminant Method

The tensor-based statistical discriminant method (SDM) was successfully used by Minoi and Gillies [24, 23] to synthesize expressions and to neutralize faces displaying an expression. The SDM is based on Fischer's linear discriminant analysis (LDA) [16]. The LDA differs from the standard PCA eigenfaces approach in that it seeks to separate data into distinct classes. The way this is done is by projecting the data into a lower dimensional subspace that maximizes the between class separability and minimizes the within class variance.

In LDA we first separate the training data set into a number of groups. Then we look for the between class scatter matrix  $S_b$  and the within class scatter matrix  $S_w$ . The matrix  $\Phi_{lda}$  that

defines the projection onto the desired low dimensional space is defined as:

$$\Phi_{lda} = \arg \max_{\Phi} \frac{|\Phi^T S_b \Phi|}{|\Phi^T S_w \Phi|} \quad (2.39)$$

In equation 2.39 the ratio of the determinant of the between class separability and the determinant of the within class variability is maximized. The maximum of this equation is the optimal projection.

However, the LDA approach has difficulties when the training data set is small in comparison to the dimensions of the image. This is called the *small sample size problem* and it causes the scatter matrices to be singular when the number of data items is less than the number of variables. To overcome the small size problem the statistical discriminant method can be used.

The SDM approach consists of two stages. In the first stage the PCA and LDA are used to reduce the dimensionality and find the discriminant directions of the classes. The PCA helps to overcome the small size problem common to stand-alone LDA. In the second stage the most discriminant vectors of our classes are projected back into the original high dimensional space. This back projection will give us a vector for every class in the high dimensional space. These vectors allow us to synthesize an expression for a new face image by moving the the surface points of this new image in the direction of one of the vectors.

The SDM technique can be extended to tensor models by expanding the mode responsible for expressions into a number of modes representing individual expression classes, thereby effectively increasing the dimension of the tensor. The expanded tensor model still retains the quality of independence along the modes of variance. However, due to the expansion, the SDM can be applied to the tensor if we flatten the sub-tensors into matrices.

## 2.2 3D Pose Estimation

The goal of 3D pose estimation is to determine the position and orientation of an object from a 2D image of this object. A special case of 3D pose estimation is the *Perspective-n-Point* (PnP) problem. This class of problems is specified as follows - given are the exact locations of a set of feature points on the object and the positions of points in the 2D image. The points in the 2D image correspond to the 3D feature points. The goal is to find how the object must be moved, rotated, scaled so that when the 3D feature points are projected using a camera model, the result will approximate the input set of corresponding 2D points.

### 2.2.1 Camera Model

The camera model describes a *projective transformation*. This transformation maps a 3D point  $\mathbf{X} = (X, Y, Z)^T$  to a 2D image point  $\mathbf{x} = (x, y)^T$ . The three most important camera models are the perspective model, the orthogonal model and the weak perspective model.

#### 2.2.1.1 Perspective Camera Model

In perspective projection rays coming from points in the scene all enter the *center of projection*. These points are then “projected” onto an imaging surface, the *image plane*. The size of the image relative to the distant object is given by the parameter *focal length*. The focal length is the distance between the center of projection and the image plane. If the image plane is behind the center of projection, then the image of the object on the image plane is inverted. If the image plane is placed in front of the center of projection, then the image and the object have the same orientation. The center of projection essentially corresponds to an ideal pinhole camera. The perspective projection is therefore known as the pinhole camera model.

The normal vector to the pinhole plane, which goes through the pinhole itself is called the *optical axis*. The optical axis is usually chosen as either the negative or positive  $z$  axis and the pinhole is chosen to lie at the origin. The intersection of the optical axis and the image plane is known as the *principal point*. The configuration of the pinhole camera model is shown in figure 2.8.

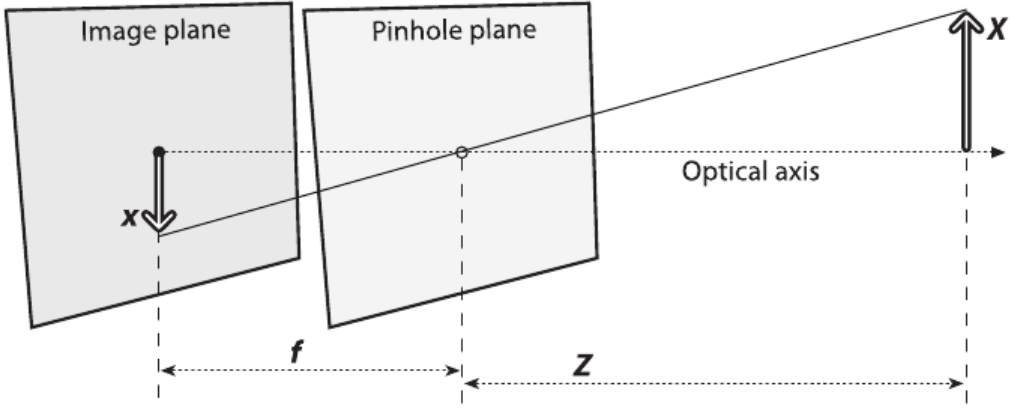


Figure 2.8: Perspective projection camera model with the image plane behind the camera. Taken from [7].

From figure 2.8, we can see that the image plane is located at  $Z = f$  where  $f$  is the focal length. The coordinates of the projection of  $X$  can therefore be calculated using similar triangles to obtain  $-x/f = X/Z$ . If the image plane were to be placed in front of the camera then the ratio given by the similar triangles will stay the same but the new coordinate will no longer be negative.

Hence, assuming that the principal point is given by  $(c_x, c_y)^T$  and the focal length is  $f$ , then the projection  $(x, y)^T$  of the point  $\mathbf{X} = (X, Y, Z)^T$  is given by

$$\begin{pmatrix} x \\ y \end{pmatrix} = \frac{f}{Z} \begin{pmatrix} X \\ Y \end{pmatrix} + \begin{pmatrix} c_x \\ c_y \end{pmatrix} \quad (2.40)$$

The perspective projection is a non-linear transformation which cannot be written as a multiplication of a 3D points in Cartesian coordinates with a matrix. To obtain a matrix formulation, we must use homogeneous coordinates. The homogeneous coordinates of a point are  $P_h = [p_x, p_y, p_z, s]^T$ . The fourth coordinate component  $s$  is called *scale*. We transform a point in homogeneous coordinates into Cartesian coordinates by dividing the first three components by the scale to get the point  $P_c = [p_x/s, p_y/s, p_z/s]^T$ . Using homogeneous coordinates the pin hole camera model has the form

$$\gamma \begin{pmatrix} x \\ y \\ 1 \end{pmatrix} = \begin{pmatrix} f_x & 0 & c_x & 0 \\ 0 & f_y & c_y & 0 \\ 0 & 0 & 1 & 0 \end{pmatrix} \begin{pmatrix} X \\ Y \\ Z \\ 1 \end{pmatrix} \quad (2.41)$$

where  $\gamma = 1/s$  is responsible for converting the homogeneous result of the multiplication to Cartesian coordinates. In equation 3.22 two different focal lengths have been used. This is due to the fact that with any camera equipment the image plane will have dimensions in millimeters. The values  $f_x$  and  $f_y$  therefore incorporate the focal length as well as the conversion from units of the imaging equipment to pixels.

### 2.2.1.2 Orthogonal Camera Model

In the orthogonal camera model the image of an object is obtained by casting rays parallel to the optical axis from points  $(X, Y, Z)$  on the object and intersecting these rays with the image plane. The  $Z$  component is thereby dropped entirely. The projected point is thus given by  $x = X$  and  $y = Y$ . The geometry of the orthogonal projection is shown in figure 2.9. Orthographic projection is sometimes called parallel projection, since unlike in perspective projection, parallel lines remain after being projected into the image plane.

### 2.2.1.3 Weak Perspective Camera Model

The weak perspective camera model is in essence just a scaled orthographic projection. With this camera model it is possible to approximate a perspective transformation under the following conditions.

- The object lies close to the optical axis.
- The object's depth (the difference between the maximum and minimum  $z$  value of the object) is small in comparison to the object's average distance from the center of projection.

Since the depths of the different points on the object are close to each other, we make the assumption all these depths are equal. Then a perspective projection of any object point  $(X, Y, Z)$  can be approximated as

$$\begin{pmatrix} x \\ y \end{pmatrix} = \frac{f}{Z_{avg}} \begin{pmatrix} X \\ Y \end{pmatrix} + \begin{pmatrix} c_x \\ c_y \end{pmatrix} \quad (2.42)$$

where  $Z_{avg}$  is the average distance of the object's point from the camera. Geometrically, we place a plane parallel to the image plane at a distance  $Z_{avg}$  from the center of projection. Then the object points orthogonally projected onto this new plane. Finally, we perspectively project these projected points onto the image plane. The geometry of the weak perspective projection is shown in figure 2.9.

Moreover, the weak perspective transformation is a linear transformation unlike the strong perspective transformation, since we are dividing by a constant  $Z_{avg}$  and not the  $Z$  component of the point.

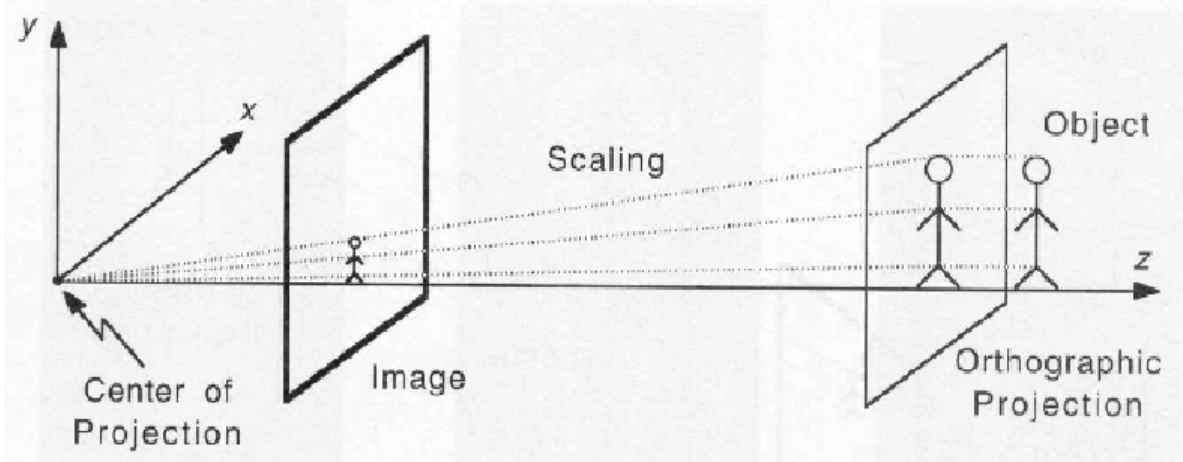


Figure 2.9: Weak perspective projection is a scaled orthographic projection. The image obtained by orthographic projection is scaled by the constant  $f/Z_{avg}$ . Taken from [8].

### 2.2.2 Rotation and Translation

It is usual in most 3D rendering frameworks to define two coordinate systems. One coordinate system for the camera and one for the object. This makes it possible to apply transformations to objects independently since the points that make up each object are defined in each object's separate coordinate system. A transformation translates the points from the object coordinate system into the camera coordinate system. In case of  $n$  objects there are  $n$  independent object coordinate systems thereby making it possible to apply a different transformation to each of the  $n$  object coordinate systems and move the objects independently which is a crucial task for 3D rendering frameworks.

The transformations of the objects are based on the degrees of freedom for movement in 3D space. The two classes of transformations are rotation and translation. The origin of the object coordinate system is moved to the origin of the camera coordinate system during translation.

Rotation aligns the viewing direction of the camera coordinate system with the viewing direction of the object coordinate system. The mapping from object coordinate space to camera coordinate space is shown in figure 2.10.

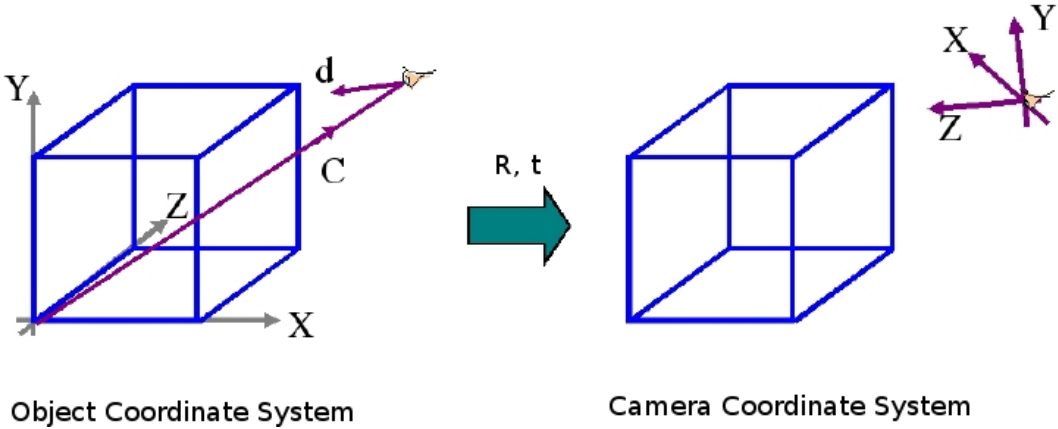


Figure 2.10: Mapping points from object coordinates to camera coordinates using rotation and translation. The displacement of the origin of the camera system from the origin of the object system is  $\mathbf{C}$ . The camera is viewing in the direction of the vector  $d$ . Taken from [17].

The rotation of the object in  $n$  dimensions can be described using *Givens rotations* [18]. A Givens rotation has the form

$$G(i, k, \theta) = \begin{pmatrix} & & i & & k & & \\ & & 0 & & 0 & & 0 \\ & & \ddots & & \vdots & & \vdots \\ & & 0 & \dots & c_\theta & \dots & s_\theta & \dots & 0 \\ i & & \vdots & & \vdots & & \ddots & & \vdots \\ & & 0 & \dots & -s_\theta & \dots & c_\theta & \dots & 0 \\ & & \vdots & & \vdots & & \vdots & & \vdots \\ & & 0 & \dots & 0 & \dots & 0 & \dots & 1 \end{pmatrix} \quad (2.43)$$

where  $c_\theta = \cos(\theta)$  and  $s_\theta = \sin(\theta)$ . Pre-multiplying with the Givens rotation  $G(i, k, \theta)^T$  corresponds to a counterclockwise rotation by  $\theta$  radians in the  $(i, k)$  coordinate plane, pre-multiplying with  $G(i, k, \theta)$  rotates the  $(i, k)$  plane by  $\theta$  radians in clockwise direction.

From the Pythagorean theorem  $\cos(\theta)^2 + \sin(\theta)^2 = 1$  and the symmetries of the sine and cosine function  $\cos(-\theta) = \cos(\theta)$ ,  $\sin(-\theta) = -\sin(\theta)$ , it is obvious that Givens rotations are orthogonal.

$$G(i, k, \theta)^T G(i, k, \theta) = G(i, k, \theta) G(i, k, \theta)^T = \mathbf{I} \quad (2.44)$$

The transposed Givens rotation amounts to a rotation in the opposite direction by the same angle thus the two rotations cancel out.

To describe the rotation of the object in three dimensional space we use the following Givens rotations

$$R_x(\phi) = \begin{pmatrix} 1 & 0 & 0 \\ 0 & c_\phi & s_\phi \\ 0 & -s_\phi & c_\phi \end{pmatrix} \quad R_y(\psi) = \begin{pmatrix} c_\psi & 0 & -s_\psi \\ 0 & 1 & 0 \\ s_\psi & 0 & c_\psi \end{pmatrix} \quad R_z(\theta) = \begin{pmatrix} c_\theta & s_\theta & 0 \\ -s_\theta & c_\theta & 0 \\ 0 & 0 & 1 \end{pmatrix} \quad (2.45)$$

Note that the matrix  $R_y(\psi)$  is in fact the transposed Givens rotation. This is due to the fact that we are interested in describing a left handed coordinate<sup>1</sup> system with the positive  $X$  axis pointing up, the positive  $Y$  axis pointing to the right and the  $Z$  axis pointing into the page. As such the

<sup>1</sup>Some authors prefer to instead use the right handed coordinate system to describe an arbitrary 3D rotation.

rotation around the  $(X, Z)$  plane needs to be described by the Given a point  $\mathbf{x} = (x, y, z)^T$  the pre-multiplication with the Givens rotation  $R_z(\theta)$  produces a new point  $\mathbf{x}' = (x', y', z')^T$  such that

$$R_z(\theta)\mathbf{x} = \begin{pmatrix} c_\theta & s_\theta & 0 \\ -s_\theta & c_\theta & 0 \\ 0 & 0 & 1 \end{pmatrix} \begin{pmatrix} x \\ y \\ z \end{pmatrix} = \begin{pmatrix} c_\theta x + s_\theta y \\ c_\theta y - s_\theta x \\ z \end{pmatrix} = \begin{pmatrix} x' \\ y' \\ z' \end{pmatrix} = \mathbf{x}' \quad (2.46)$$

The expressions for the  $x'$  and  $y'$  component of the new point correspond to a rotation of the  $(X, Y)$  coordinate system by  $\theta$  radians about the  $Z$  axis. These expressions are computed using simple trigonometrics where the point is decomposed into its  $x$  and  $y$  components which are then projected on the rotated  $(X', Y')$  axes as can be seen in figure 2.11.

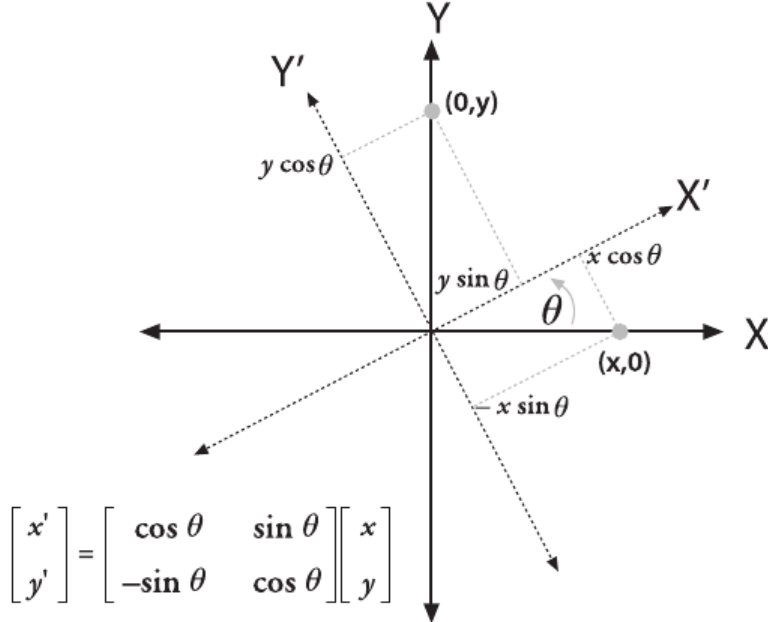


Figure 2.11: Transforming one point into another by rotating the coordinate system counterclockwise by  $\theta$  radians. The point  $[x, y]^T$  can be written as  $[x, 0]^T + [0, y]^T$ . These components are then individually transformed by projecting them onto the axes of the new coordinate system  $(X', Y')$  to obtain the new point  $[x', y']^T$ . The new point is the result of turning the original point clockwise by  $\theta$  radians. Take from [7].

After the transformation in equation 2.46 the  $z$  component of the original point is left unchanged. From similar calculations it can be seen that with matrix  $R_y$  the  $y$  component, with  $R_z$  the  $z$  component remain unchanged. It is therefore apparent that the matrix  $R_x(\phi)$  rotates by  $\phi$  about the  $X$  axis, matrix  $R_y(\psi)$  rotates by  $\psi$  about the  $Y$  axis and  $R_z(\theta)$  rotates by  $\theta$  about the  $Z$  axis. Any arbitrary rotation in 3D space can then be achieved using the total *rotation matrix*  $R = R_x(\phi)R_y(\psi)R_z(\theta)$  with the appropriate angles. Since all the total rotation matrix is a product of three orthogonal Givens rotations it likewise orthogonal with  $R^T R = R R^T = \mathbf{I}$ , with  $\mathbf{I}$  being the identity matrix. The three angles  $\theta$ ,  $\phi$  and  $\psi$  represent the three rotational degrees of freedom (DOF) of the object.

Any position in three dimensional space can be achieved through a linear combination of movements in any of the three unit directions given by the  $X$ ,  $Y$  and  $Z$  axes. The *translation vector* allows us to represent the shift from one coordinate system to another. In terms of the camera coordinate system and the object coordinate system, the translation vector is the offset between the origin of the camera system and the object system. Thus, to represent the position of the object we use the translation vector  $t = \text{origin}_{\text{object}} - \text{origin}_{\text{camera}}$ . The displacements in the the unit directions  $(1, 0, 0)^T$ ,  $(0, 1, 0)^T$ ,  $(0, 0, 1)^T$  are given by the components vector  $t = (t_x, t_y, t_z)^T$ .

Equation 2.47 shows how the rotation matrix and the translation vector allow us to transform a point  $P = (p_x, p_y, p_z)^T$  from the object coordinate system to the camera coordinate system.

$$\begin{pmatrix} x \\ y \\ z \end{pmatrix} = R \begin{pmatrix} p_x \\ p_y \\ p_z \end{pmatrix} + t \quad (2.47)$$

With homogeneous coordinates the 6 degrees of freedom (also known as the extrinsic parameters) can be used to construct a joint rotation-translation matrix which transforms the 3D point  $Q = (p_x, p_y, p_z, 1)^T$  in the object coordinate system to a point  $\mathbf{x} = (x, y, z, s)^T$  in the camera coordinate system as

$$\begin{pmatrix} x \\ y \\ z \\ s \end{pmatrix} = \begin{pmatrix} R & t \\ \mathbf{0} & 1 \end{pmatrix} \begin{pmatrix} p_x \\ p_y \\ p_z \\ 1 \end{pmatrix} \quad (2.48)$$

where  $\mathbf{0} = (0, 0, 0)$ .

### 2.2.3 Pose estimation with the POSIT algorithm

Davis and DeMenthon's POSIT algorithm [12], [7] is a simple and efficient method for solving the PnP problem. The POSIT algorithm estimates the rotation matrix  $R$  and the translation vector  $t$  of an object, given a perspective camera with known parameters, at least 4 non-coplanar feature points on the 3D object and the corresponding projections of these points in the 2D image. To compute an approximation of the true  $R$  and  $t$ , we first expresses the camera coordinate system in terms of the object coordinate system. Since the rotation matrix aligns the axes of the two coordinate systems we therefore know that the rows  $i$ ,  $j$  and  $k$  of the rotation matrix correspond to the unit vectors of the camera coordinate system expressed in the object coordinate system.

This is easy when on the example of the camera system unit vector  $u = (1, 0, 0)^T$ . The rotation matrix  $R$  transforms a vector  $x$  from the object coordinate system into  $u$ , therefore  $u = Rx$ . The rotation matrix is orthogonal so if we turn in the opposite direction we get  $x = R^T u$  as the object system equivalent of  $u$ . Since  $u = (1, 0, 0)^T$  we obtain the first row of the rotation matrix  $R$  as the object coordinate system vector which corresponds to  $u$ .

The rotation matrix can therefore be written as

$$R = \begin{pmatrix} i_1 & i_2 & i_3 \\ j_1 & j_2 & j_3 \\ k_1 & k_2 & k_3 \end{pmatrix} \quad (2.49)$$

Since the three vectors  $i$ ,  $j$  and  $k$  are all orthogonal we only need to find the first two and obtain the third as the cross product of the other two.

The translation vector is specified as the vector  $\overrightarrow{OM_0}$  between the origin of the camera system  $O$  and the origin of the object system  $M_0$ . The point  $M_0$  can be conveniently picked as one off the known feature points. Unfortunately, the camera coordinate system equivalent of this point is unknown since we do not know the rotation matrix. However, the translation vector can be expressed in terms of the 2D projection of this feature point as  $t = \frac{Z_0}{f} \overrightarrow{Om_0}$  where  $m_0$  is the known 2D projection of  $M_0$  and  $Z_0$  is the  $z$ -component of the translation vector. Therefore, to estimate the 3D pose we need to find the values of  $i$ ,  $j$  and  $Z_0$ .

The POSIT algorithm first makes a rough estimate these values using a *pose from orthography and scaling* (POS) step. In the POS step it is assumed that the points are far enough from the camera so that we can assume a weak-perspective camera model. Using this camera model the values  $i$ ,  $j$  and  $Z_0$  all have closed form solutions. After this first step, the 2D image are then projected back into the object coordinate space with using the true perspective camera and the pose (rotation, translation) estimated in the POS step. These new points are then used in further in POS steps until the algorithm converges, hence the name POS with iterations (POSIT). However, it is important to note that the convergence of the algorithm depends heavily on the weak-perspective assumption that the internal depth of the object is small compared to the distance from the pinhole camera.

The fundamental equations of the POSIT algorithm are

$$\overrightarrow{M_0 M_i} \cdot I = x_i(1 + \varepsilon_i) - x_0 \quad (2.50)$$

$$\overrightarrow{M_0 M_i} \cdot J = y_i(1 + \varepsilon_i) - y_0 \quad (2.51)$$

with

$$I = \frac{f}{Z_0} i, \quad J = \frac{f}{Z_0} j \quad \text{and} \quad \varepsilon_i = \frac{1}{Z_0} \overrightarrow{M_0 M_i} \cdot k$$

During the POSIT iterations, values are given to  $\varepsilon_i$  starting with 0 in the first iteration and then computed from  $\varepsilon_i = \frac{1}{Z_0} \overrightarrow{M_0 M_i} \cdot k$  with the  $k$  and  $Z_0$  being guesses from the previous iteration. Then the system of equations given by 2.50, 2.51 is solved to obtain the vectors  $I$  and  $J$ . These vectors are normalized to get the two rows of the rotation matrix  $i$  and  $j$ . The  $z$ -component of the translation vector  $Z_0$  is given by the norm of either  $I$  or  $J$ .

## 2.3 Feature Point Tracking

As we have seen, most model based recognition techniques rely on a number identified feature (landmark) points to estimate the model parameters. To be able to track a model between successive frames of a video recording, it is therefore necessary to either keep locating the points in every frame or to track the movement points themselves. This problem of tracking the movement points or objects between images has spurred the development of many algorithms. Most of these algorithms fall into the *optical flow* category since they determine the movement of points based on the intensity changes at pixels. One such algorithm is the Kanade-Lucas-Tomasi feature tracker.

### 2.3.1 Kanade-Lucas-Tomasi Feature Tracker

Kanade and Lucas first introduced an iterative feature point registration algorithm in [21]. Tomasi and Kanade developed a more generalized version of algorithm in [34], [2]. The derivation of the algorithm is given by Birchfield in [6].

The problem of registering a displaced image can between two images is formalized by assuming there are two images functions  $F(\mathbf{x})$  and  $G(\mathbf{x})$ . The image functions take a vector  $\mathbf{x} = (x, y)^T$  as input and output the pixel intensity at  $\mathbf{x}$ . The goal in image registration is to find a disparity vector  $\mathbf{h} = (h_x, h_y)^T$  which minimizes a measure of difference between  $F(\mathbf{x} + \mathbf{h})$  and  $G(\mathbf{x})$  for a given window of interest  $\mathcal{W}$ . The windows is required, since it is very difficult to track single pixels as they can be easily confused with other pixels unless they have very distinct brightness. The window of interest contains a number of pixels and should contain sufficient texture. The feature tracking is illustrated in figure 2.3.1 where the apple is the window of interest.



Figure 2.12: The image registration problem. The task is to find the disparity vector  $h$ .

The optimal displacement vector  $\mathbf{h}$  minimizes the error function  $E$  which is given by

$$E(\mathbf{h}) = \int_{\mathcal{W}} (F(x + h) - G(x))^2 dx \quad (2.52)$$

The naive way to locate this  $h$  would be to iterate through all the possible values of  $h$  and measure the  $E(\mathbf{h})$  norm. A better approach was proposed by Kanade and Lucas. The behavior of the function  $F(\mathbf{x})$  is approximated using a first order Taylor expansion as

$$F(\mathbf{x} + \mathbf{h}) \approx F(\mathbf{x}) + \mathbf{g}^T \mathbf{h} \quad (2.53)$$

where

$$\mathbf{g} = \left[ \frac{\partial}{\partial x} \left( \frac{F+G}{2} \right) \quad \frac{\partial}{\partial y} \left( \frac{F+G}{2} \right) \right]^T \quad (2.54)$$

This approximation is used instead of  $F(\mathbf{x} + \mathbf{h})$  in the error. Then the minimum of the error function is located by setting the derivative of the error function with respect to  $\mathbf{h}$  to zero. Therefore

$$\frac{\partial E}{\partial \mathbf{h}} = \frac{\partial}{\partial \mathbf{h}} \int_{\mathcal{W}} (F(x) + \mathbf{g}^T \mathbf{h} - G(x))^2 dx = 2 \int_{\mathcal{W}} g(F(x) + \mathbf{g}^T \mathbf{h} - G(x)) dx \quad (2.55)$$

Setting the above to zero and rearranging the terms we get the fundamental equation which relates the spatial intensity to the optimal displacement  $\mathbf{h}$  as

$$\left( \int_{\mathcal{W}} \mathbf{g} \mathbf{g}^T dx \right) \mathbf{h} = \int_{\mathcal{W}} g(F(x) - G(x)) dx \quad (2.56)$$

In matrix form the equation 2.56 can be expressed as

$$\mathbf{Z} \mathbf{h} = \mathbf{e} \quad (2.57)$$

The iterative Kanade-Lucas algorithm specifies the order in which possible values of  $\mathbf{h}$  will be explored. The procedure iteratively improves the guess for  $\mathbf{h}$  by solving the equation 2.56 with the spatial intensity gradients evaluated at each point  $\mathbf{x}$  in the image. Thus, the algorithm locally searches for the best disparity vector  $\mathbf{h}$  by using the information about the gradient at all points in the image. The estimation of the  $\mathbf{h}$  and the convergence of the algorithm is further improved by weighing contributions of the points  $\mathbf{x}$  inside the window. The weighing function can be a Gaussian or just set as  $w(\mathbf{x}) = 1$ .

The integrals simplify to sums when we are dealing with pixel values in real images. The iterative scheme for the Kanade-Lucas-Tomasi feature tracking algorithm is therefore:

$$\mathbf{h}_0 = 0 \quad (2.58)$$

$$\mathbf{h}_{k+1} = \mathbf{h}_k + \frac{\sum_{\mathbf{x} \in \mathcal{W}} w(\mathbf{x}) \mathbf{g} [G(x) - F(\mathbf{x} + \mathbf{h}_k)]}{\sum_{\mathbf{x} \in \mathcal{W}} w(\mathbf{x}) \mathbf{g} \mathbf{g}^T} \quad (2.59)$$

To further improve the technique it can be performed with several resolution levels, using the result from the coarser resolution as starting  $h_0$  of the algorithm with a finer resolution. An effective variation of the algorithm which utilizes this approach was developed by Bouguet [6]. Bouguet's implementation of the Kanade-Lucas-Tomasi algorithm uses several resolution levels from highest to lowest. These resolutions resemble a pyramid of images, which is why this implementation is called the pyramid Lucas-Kanade tracker. At every level of the pyramid the iterations are computed to and the guess is propagated to the lower of the pyramid.

The algorithm can also successfully compute the  $h$  even if the region of interest has been rotated or scaled. If the image has been rotated or scaled we express the matching problem as  $G(x) = F(xA + h)$  where  $A$  is a linear transformation matrix. This transformation allows us to apply the algorithm.

The Kanade-Lucas-Tomasi feature tracker has been successfully applied to tracking facial feature points [40]. Vlasic et al localized feature points in the initial frame manually and then used the Kanade-Lucas-Tomasi feature tracker to obtain the displacements between pairs of frames. From

these displacements they were able to derive parameters for their tensor-based multilinear model. This allowed them to transfer expressions to another video performance.

As a local iterative search method, the Kanade-Lucas-Tomasi feature tracker's performance depends heavily on the initial guess of the  $h$ . If the initial guess is too far from the region of interest then the algorithm does not perform well, since the scheme was derived using local approximations of functions. These local approximations will not hold for points far from the region of interest.

## 2.4 Optimization

The task of locating the correct model parameters which match the model to an object in the image is an optimization problem. It may not be possible to find an exact match which would explain the object in the image perfectly. Therefore, we are interested in finding an instance of the model which is most similar to the object in the image. One way to measure dissimilarity is through the use of an error function. If the value of the error function is large it means that the two entities are dissimilar. To find a model instance which is most similar we therefore need to minimize the error function. Optimization techniques make it possible to locate minima of functions.

### 2.4.1 Least Squares and Non Negative Least Squares

An important error function, which is often utilized in statistics and engineering, is the sum of squares error. This error function defines the dissimilarity between input values  $y_i$  and target values  $t_i$  using a numeric value given by

$$E(y) = \sum_i (y_i - t_i)^2 \quad (2.60)$$

Solving a problem in the least squares sense means minimizing this error function. Given is a linear system of equations defined in matrix notation by  $\mathbf{Ax} = \mathbf{b}$  with  $\mathbf{A} \in \mathbb{R}^{m \times n}$ ,  $\mathbf{x} \in \mathbb{R}^{n \times 1}$  and  $\mathbf{b} \in \mathbb{R}^{m \times 1}$ . This linear system may not have an exact solution if it is over determined  $m > n$ , underdetermined  $m < n$  or more generally when  $\mathbf{A}$  is not invertible. Solving this linear system in the least squares sense means finding a  $\hat{\mathbf{x}}$  for which the following error function is minimized

$$E(\hat{\mathbf{x}}) = \frac{1}{2} \|\mathbf{b} - \mathbf{A}\hat{\mathbf{x}}\|^2 \quad (2.61)$$

with  $\|\cdot\|$  being the vector norm (distance). To find this minimum we take the derivation of 2.62 with respect to  $\hat{\mathbf{x}}$  and set it to zero. The least squares solution is therefore

$$\hat{\mathbf{x}} = (\mathbf{A}^T \mathbf{A})^{-1} \mathbf{A}^T \mathbf{b} \quad (2.62)$$

where the expression  $(\mathbf{A}^T \mathbf{A})^{-1} \mathbf{A}^T$  is commonly known as the pseudo-inverse.

It is also possible to find the least squares solution of a linear system using singular value decomposition [27] if the matrix  $\mathbf{A}$  is square. Usually the linear system would be solved by inverting  $\mathbf{A}$  and pre-multiplying the equation with this inverse. Given the SVD  $\mathbf{A} = \mathbf{U}\Sigma\mathbf{V}^T$  we can easily invert  $\mathbf{A}$  by inverting the right hand side to get  $\mathbf{A}^{-1} = \mathbf{V}\Sigma^{-1}\mathbf{U}^T$ . If the square  $\mathbf{A}$  is not invertible it means that some of the diagonal elements in  $\Sigma$  are 0. However, We obtain a least squares solution by inverting the non-zero elements of  $\Sigma$  and pre-multiplying with  $\mathbf{V}\Sigma^{-1}\mathbf{U}^T$ .

In some case it may be necessary to enforce constraints on the function. This is particularly important when the variables represent real physical entities, which should not be negative. Such non negativity constraints are often introduced to a linear system. The goal of optimization is then to solve this non negativity linear system in the least squares sense. The problem is therefore to find the  $\mathbf{x}^*$  for which holds

$$\mathbf{x}^* = \underset{\mathbf{x} \geq 0}{\operatorname{argmin}} \frac{1}{2} \|\mathbf{b} - \mathbf{A}\mathbf{x}\|^2 \quad (2.63)$$

To optimize this constrained error function Franc et al reformulate the problem as an equivalent quadratic optimization problem [15], [9].

$$\mathbf{x}^* = \underset{\mathbf{x} \geq 0}{\operatorname{argmin}} \left( \frac{1}{2} \mathbf{x}^T \mathbf{H} \mathbf{x} + \mathbf{x}^T \mathbf{f} \right) \quad (2.64)$$

where  $\mathbf{H} = \mathbf{A}^T \mathbf{A}$  and  $\mathbf{f} = -\mathbf{A}^T \mathbf{b}$ . Franc et al solve this quadratic optimization problem by first formulating the Karush-Kuhn-Tucker (KKT) conditions and then applying a sequential coordinate descent algorithm. The KKT conditions for the non negative least squares solution are given by

$$\mathbf{H} \mathbf{x} + \mathbf{f} - \mu = \mathbf{0} \quad (2.65)$$

$$\mathbf{x} \geq \mathbf{0} \quad (2.66)$$

$$\mu \geq \mathbf{0} \quad (2.67)$$

$$\mathbf{x}^T \mu = 0 \quad (2.68)$$

The sequential coordinate-wise algorithm (SCA) then computes this solution so that the KKT conditions are satisfied. The SCA non-negativity least squares algorithm is given in 2.4.1. The input matrices are  $\mathbf{H} = \mathbf{A}^T \mathbf{A}$ ,  $\mathbf{f} = -\mathbf{A}^T \mathbf{b}$  and  $\mathbf{h}_k$  denotes a column of the matrix  $\mathbf{H}$ .

---

**Algorithm 1** Sequential Coordinate-wise Non-negativity Least Squares Algorithm

---

```

1: procedure SCANNLS( $\mathbf{H}, \mathbf{f}$ )
2:   Output  $\mathbf{x}^* \geq 0$  such that  $\mathbf{x}^* = \operatorname{argmin}_{\mathbf{x} \geq 0} \frac{1}{2} \|\mathbf{A}\mathbf{x} - \mathbf{b}\|^2$ 
3:   Initialization  $\mathbf{x}^0 = \mathbf{0}$  and  $\mu^0 = \mathbf{f}$ 
4:   repeat
5:     for  $k = 1 \dots n$  do
6:        $\mathbf{x}_k^{t+1} = \max\left(0, \mathbf{x}_k^t - \frac{\mu_k^t}{\mathbf{H}_{k,k}}\right)$ 
7:        $\mathbf{x}_i^{t+1} = \mathbf{x}_i^{t+1} \quad \forall i \neq k$ 
8:        $\mu^{t+1} = \mu^t + (\mathbf{x}_k^{t+1} - \mathbf{x}_k^t) \mathbf{h}_k$ 
9:     end for
10:    until stopping criteria (KKT conditions) are met.
11: end procedure
```

---

## 2.4.2 Nelder Mead Downhill Simplex

The downhill simplex is a local optimization method that does not require gradients to identify local extrema. With the downhill simplex method a local optimum is found by means of a sequence of fitness function evaluations.

The downhill simplex method was coined by Nelder and Mead in 1965 and has since proven itself to be comparable in efficiency to the more popular gradient based optimization methods. The method was designed for the optimization of multidimensional, unconstrained functions that have either no gradients or when the gradients exist only for portions of the search space such as in the case of discontinuous functions [30]. However, the drawback of the method is that many fitness function evaluations are required. Therefore, when the computational complexity of the fitness function is very high, other optimization methods need to be considered instead of the Nelder Mead downhill simplex [27].

The algorithm is based on the idea of isolating the minimum by geometrically transforming a *simplex*. The simplex is a convex hull of  $N + 1$  vertices, where  $N$  is the underlying problem's dimension. In a two dimensional space this simplex would therefore be a triangle, in three dimensions a tetrahedron. The algorithm is initialized so that the simplex encloses a portion of the search space and the goal is to move the simplex along the search space surface and deform so that all of its vertices converge on the local optimum. This is achieved with the help of geometric transformations of the simplex.

The process of transforming a multidimensional simplex, in order to isolate the minimum, is somewhat analogous to bracketing a minimum in a one dimensional search space. The one dimensional search space will have peaks and valleys in places of local optima. The simplex, which is a line in one dimensional space, makes it's way downhill through this search space, in search of a minimum by means of shrinking and stretching. When the simplex finds a local minimum, it shrinks itself to contain only the minimum and the algorithm terminates.

The behavior of the simplex during the algorithm parallels the expanding and collapsing movements of the amoeba organism. The Nelder Mead downhill simplex is in some publications referred to as the *amoeba* method due to this similarity but also to distinguish it from Dantzig's simplex method for linear programming [27].

#### 2.4.2.1 The Downhill Simplex Algorithm

To initialize the downhill simplex algorithm we need a nonlinear fitness function  $f : \mathbb{R}^N \rightarrow \mathbb{R}$  and an initial point  $P_0$ . The simplex will be a  $N + 1$  dimensional convex hull. The first vertex of the convex hull is the initial point. The remaining  $N$  vertices  $P_i$  are derived from the initial point. The shape of the simplex defines the way in which the points  $P_i$  are calculated[30].

The simplex shape can be one of the following:

- The simplex can have a regular shape where all sides are equally long. It is up to the user to pick this length.
- The simplex can be right angled in which case the vertices  $P_i$  are calculated according to formula 2.69.

$$P_i = P_0 + \lambda e_i \quad (2.69)$$

where  $e_i$  are unit vectors for the  $N$  dimensions and  $\lambda$  is a constant. This constant influences the size of the simplex and represents a guess of the problem's characteristic scale length [27].

After the initialization phase, three crucial steps are repeated until the simplex has encountered the local minimum. These steps are based around moving the vertex of the simplex with the largest fitness function value to a new point where the value will be smaller.

1. The first step is to sort the vertices  $x_i$  of the simplex from worst to best, where  $h$  is the index of the worst vertex,  $s$  the second worst index and  $l$  the best index.
2. Then the *centroid* of the best side is calculated according to formula 2.70.

$$c = \frac{1}{N} \sum_{j \neq h} x_j \quad (2.70)$$

3. In the final step, the centroid is used to geometrically transform the simplex in order to move the current worst vertex to a better position. To achieve this, the algorithm seeks a replacement point for  $x_h$  on the line that connects the worst index  $x_h$  and the centroid  $c$ . Three different points are then compared and the one with the best fitness value is chosen as the replacement point. These three candidates are obtained using reflection (formula 2.71), expansion (formula 2.72) and either inside or outside contraction (formula 2.73).

$$x_r = c + \alpha(c - x_h) \quad (2.71)$$

$$x_e = c + \gamma(x_r - c) \quad (2.72)$$

$$x_c = \begin{cases} c + \beta(x_r - c) & \text{if } x_h \leq x_r \\ c + \beta(x_h - c) & \text{otherwise} \end{cases} \quad (2.73)$$

In case neither of these three new replacement point candidates has a better fitness value than the worst vertex  $x_h$ , then the entire simplex is shrunk towards the best vertex  $x_l$ . In this case  $N$  new vertices will be computed as follows:

$$x_j = x_l + \delta(x_j - x_l) \quad j = 0, \dots, N \wedge j \neq l \quad (2.74)$$

The geometric implications of the transformations reflection, expansion, contraction and shrinking are depicted in figure 2.13.

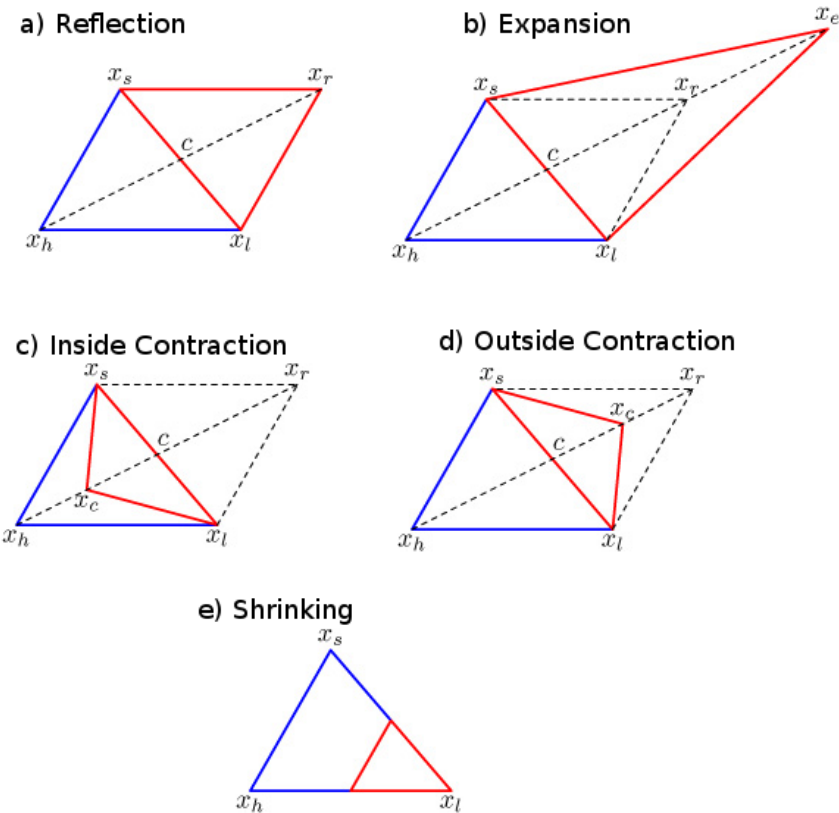


Figure 2.13: Geometric interpretations of the simplex transformations. Taken from [30].

The transformations are controlled by four parameters  $\alpha$  for reflection,  $\beta$  for contraction,  $\gamma$  for expansion and  $\delta$  for shrinking. Most implementations use the standard values  $\alpha = 1$ ,  $\beta = \frac{1}{2}$ ,  $\gamma = 2$  and a shrinking by a half with  $\delta = \frac{1}{2}$  [27, 30].

Finally, since the algorithm should terminate in finite time, it is necessary to establish a termination criterion. If the execution of the three aforementioned steps is considered one cycle of the algorithm, then possible termination criteria include terminating when the vector distance moved in the cycle was smaller than a constant tolerance  $tol$ , or when the difference between the fitness value of the newly obtained best and the old best is no larger than a tolerance  $ftol$ . Since either of these criteria could occur in a single anomalous step, restarts of the downhill algorithm are also sometimes utilized [27].

# Chapter 3

## Design

In this chapter we will design an application which understands the facial dynamics captured in a video recording of an individual. This understanding is accomplished by correctly modeling the shape of this individual's face.

The goal of the application is to transfer the expressions between two subjects. Given are video recordings of two persons and a database of faces. One recording is the source of the expressions, henceforth just source. The other recording is the target. The task is to alter the target recording so that the target person's face is animated to perform the expressions seen in the source.

We approach this problem by constructing a deformable shape model of a face from the face database. The model is constructed so that every expression corresponds to a specific instance of the model parameters. Since the goal is to transfer expressions, the model should be able to alter expression and identity of the subject separately. This suggests that the optimal model should have separate parameters for these two attributes, to allow the user to manipulate the identity independently of the expression or vice versa. As discussed in section 2.1.3.2, the tensor-based model possesses this very important quality of separability which makes it suitable to use as the deformable model of choice in the expression transfer application.

To find the values of the parameters, the model is fitted frame-by-frame to the source recording using an algorithm that estimates the 3D pose of the model, the expression parameters and the identity parameters. The model is also fitted to the target recording to obtain a model of the target face. The parameters from the source model are then used to animate the target model.

The application therefore needs to be designed to support the following functionality:

1. Pre-processing of the face database.
2. Learning a tensor-based model from the face scans in pre-processed database.
3. Implementation of an algorithm to find the expression, identity and pose parameters of the face in the source and target recording.
4. Animating the target face with the expression parameters estimated from the source face.

To make the application user-friendly, the implementation of this functionality should be encapsulated in graphical user interface (GUI). This GUI needs to be built with support for a 3D rendering framework since the application has to display the three-dimensional models and animate the target face. Additionally, most of the tasks that the application needs to solve either involve linear algebra computations or can be solved with standard computer vision algorithms. The implementations of these computations and algorithms need to be as efficient as possible to ensure that the application is highly responsive to the users actions and commands.

### 3.1 Design Challenges

While it may seem like a trivial problem to a human, the task of transferring expressions involves many challenges. The computer is attempting to understand a face using its model of what a face

should look like, as well as recognize the face in images and follow its movements through successive frames. All the while, the application has to correctly interpret all the observed deformations as corresponding expressions.

The first challenge lies in developing an algorithm that fits a model to a face in the image. Two expressions can differ in only very little detail and yet this small amount of detail can make a huge difference to how a human observer interprets the expression. A slight difference in the position of the corner of the mouth is all that separates a smirk from a genuine smile. However, model based recognition revolves around approximating an object in the image with an instance of the model. So if it is to correctly identify expression, the algorithm needs to operate on a large number of points to minimize the error between the approximation and the observed face as much as possible. This first of all causes the algorithm to take more time, but it also directly leads to the second problem of how these points are to be chosen.

The model fitting is performed with an error minimization algorithm. To perform this minimization, reference measurements are needed against which the minimization is performed. These measurements will be points in the frames which comprise the video sequences. These points should of course be points located on the face. So before the algorithm can begin fitting a model, it first needs some information about where the face is located in the image. However, it is not only necessary to identify the general position of the face – it is in fact imperative to know the position of points on the face which correspond to points in the model. Depending on how the face is located it may prove to be difficult to obtain more points to use in the fitting.

A convenient approach is to locate the face in only the first frame of the video sequence. Its position in the successive frames is then obtained by tracking the movement of the face from the first frame. Therefore, before applying the fitting algorithm the application needs to perform the following two steps:

1. Locating feature points in the first frame of both the source and target recording.
2. Tracking the movement of the feature points to obtain a guess for feature points in every frame.

Yet this tracking is again an approximation. It often also happens that certain points in the face are lost during the tracking procedure. So again it is impossible to guarantee that the fitting algorithm will be able to recover sufficient level of detail to correctly estimate the expression.

The final and most crucial problem lies in the fact that usually only very specific areas of the face contribute to expressions. The mouth or the brow are excellent areas for reference points for the fitting algorithm. However, should points in these areas be lost during tracking, or misidentified during face location then it is very likely that an incorrect expression will be estimated. Even if only a small number of points is lost, the algorithm can still fail badly if these were points from an important part of the face.

It is clear that error accumulates in every step of the model fitting. A robust application must therefore attempt to enforce constraints to limit this accumulation. The fitting algorithm and the model therefore need to be designed with these considerations in mind.

## 3.2 Frameworks and APIs

An important design and implementation question when constructing a large application, is deciding which software application programming interfaces (APIs) and software frameworks the application should employ. The great advantages of utilizing APIs and frameworks is that they provide efficient implementations of algorithms. The disadvantage is that some frameworks may require the user to install this framework on his machine to be able to use the application. Quite important is also the quality of cross-platform compatibility. To design a portable application only cross-platform frameworks and APIs should be chosen.

### 3.2.1 OpenCV

The expression transfer application processes images and utilizes many computer vision algorithms. An excellent library of computer vision algorithms and functions is the OpenCV library. The OpenCV is a multi-platform library written for C and C++ [7]. It was designed to provide a simple-to-use computer vision infrastructure for building vision applications. A large part of OpenCV was developed by Intel, specifically Intel's Russian branch. The expression application is build with OpenCV version 2.1.0.

Among the algorithms included in the OpenCV library are efficient implementations the Kanade-Lucas feature tracker and the POSIT algorithm for 3D pose estimation. The OpenCV library also provides an excellent matrix data structure.

### 3.2.2 OpenGL

Since the expression transfer application deals with a 3D model of the human face, it should be possible for this model to be presented graphically to the user. To this end we can use the popular graphics interface OpenGL. The Open Graphics Library (OpenGL) is a software interface to the graphics hardware [31]. It is currently being further developed and maintained by the Khronos Group. The OpenGL API provides a large number of commands to render 3D objects. These objects are constructed from graphics primitives like points, lines and polygons. The rendering of objects in OpenGL is implemented using a series of processing stages called the rendering pipeline. The pipeline also provides numerous useful graphics operations such transformations between camera and object coordinate systems, texture mapping and lighting.

### 3.2.3 Qt

The OpenGL graphical representation needs to be encapsulated in a user-friendly graphical user interface (GUI) to allow the user to load and process the video recordings. The GUI of choice for the expression transfer application is Trolltech's Qt, because it integrates well with the OpenGL framework. The Qt framework also includes a build system called qmake, which is likewise cross-platform. The Qt framework was developed by Trolltech in 1991. The software has since been acquired by Nokia.

## 3.3 Pre-processing

The primary drawback of the tensor-based model is that it requires the faces in the database to be in *correspondence*. To put faces in the database into correspondence so that a tensor model can be constructed, we must perform pre-processing of the database data.

### 3.3.1 Correspondence

For the purpose of this application we consider two polygon meshes to be in correspondence if for any point in one polygon mesh, the point in the other polygon mesh which corresponds to the same position on the object, has the same index value. So for example if the point corresponding to the tip of the nose has an index value of  $i$  in one face, then there will be a point in the other face with perhaps different  $x$ ,  $y$  and  $z$  but the same  $i$  index which also corresponds to the tip of the nose. So essentially, the order of the indices must be the same in both polygon meshes.

In the case when the two polygon meshes are not in correspondence, then a optimization algorithm must be applied to deform the mesh to correspond to a reference mesh. One mesh may have fewer vertices, or the vertices can be have a different ordering than in the reference mesh. To standardize the meshes the vertices in one mesh need to be aligned with vertices in the other mesh.

Correspondence may be computed in two ways. One approach is to use a registration algorithm which locates the rigid-transformations that transform a misaligned mesh into the reference mesh. A popular algorithm for 3D registration is the Iterated Closest Point (ICP) algorithm. Rusinkiewicz and Levoy give a comprehensive overview of efficient implementations of the ICP algorithm in [29].

The other approach involves finding the minimal deformation of the polygon mesh which transforms it into the reference mesh. An example of this type of algorithm was described by Sumner and Popovic in [33] who achieve this by transferring deformation between triangle meshes.

Other irregularities in the polygonal mesh can be present depending on how the 3D face scans in the database were obtained. For example there can be holes or spikes in the mesh, which need to be removed by interpolating new points to fill the holes or by Gaussian smoothing the spikes.

### 3.3.2 Database

The face database used in the application is the Binghamton expressions database [41]. This database of 3D face scans was developed at the Department of Computer Science of the State University of New York at Binghamton. The subjects in the face database perform seven expressions – neutral, angry, disgust, fear, happy, sad and surprise. Every subject carried out each of these expressions (except for neutral) in four levels of intensity. Examples of original face scans, along with the captured texture maps are shown in figure 3.1.

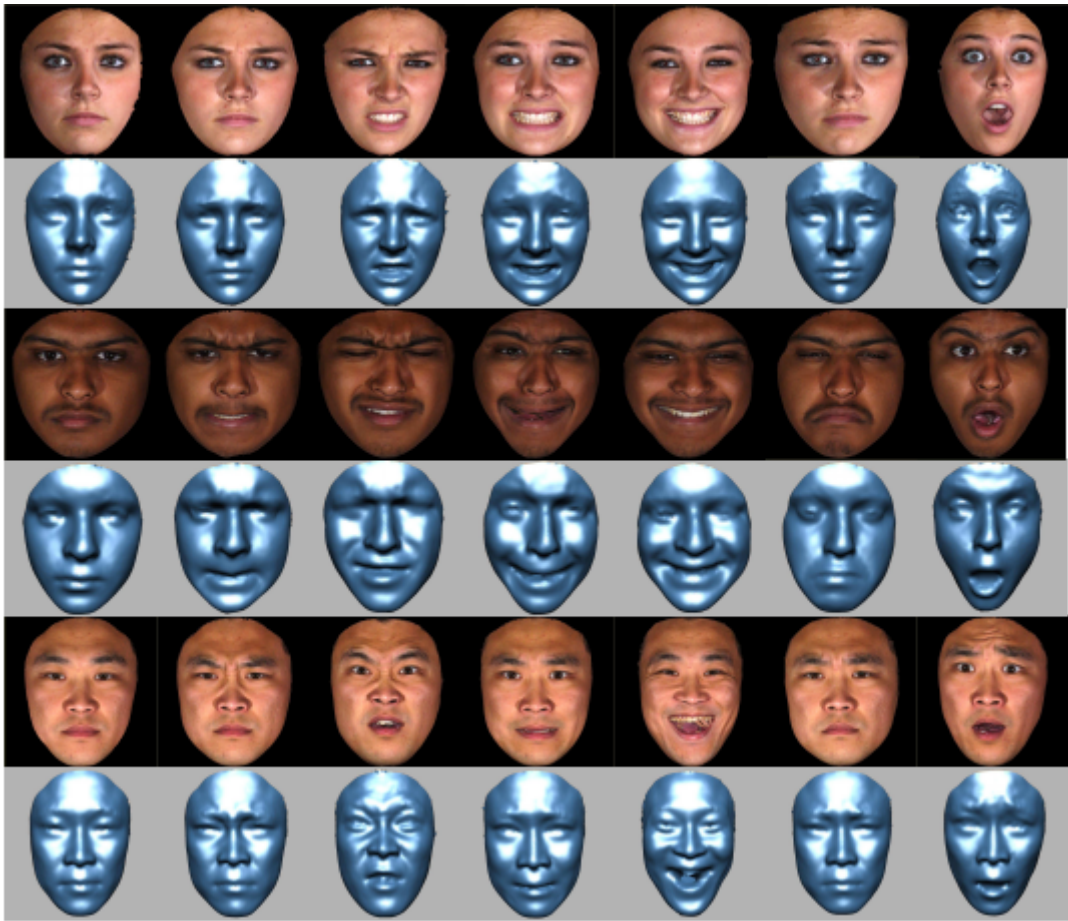


Figure 3.1: Sample 3D face scans from the Binghamton database along with the corresponding texture maps. Taken from [41].

The Binghamton database was constructed with the help of 100 students who participated in the face scans. Various ethnic groups are represented and the database consists of about 60% female and 40% male subjects. There is an unfortunate lack of middle aged to older subjects in the database, due to the fact that mostly students were involved in face scans. For purposes of the face transfer application this is a clear disadvantage since it makes the model we construct much less powerful.

The advantage of a 3D face database lies in the fact that it allows us to construct a 3D model. This 3D model will clearly be more powerful than a 2D model since it has more degrees of freedom. When the task is to transfer expressions between two recordings of 3D faces it is preferable to have

a 3D model which should in theory be able to duplicate the exact motions and rotations of the recorded objects. If the face database consisted of only 2D face images then the model would also have to be two-dimensional.

The face scans were captured using the 3DMD digitizer which utilizes structured light to calculate the depth. The captured surfaces contained between 20,000 and 35,000 polygons.

The Binghamton database consists of faces stored as polygon mesh data in VRML format and texture information in bitmap format. For the project the pre-processed Binghamton database was used. This pre-processed database was created by Dr. Lynn-Minoli [23] and consists of VTK files of the pre-processed polygon meshes. The VTK file lists the  $x$ ,  $y$  and  $z$  values of every vertex, the topology data of the face scan and the texture coordinates for every vertex. The face scans in pre-processed database are in correspondence, meaning that the order of the vertices in every face scan is the same. Conveniently, having the face scans in correspondence also means that the topology data stays constant.

The final pre-processing step before building a model is to move the center of the face scans to the origin of the object coordinate system. This step is not always required. However, the vertices in the pre-processed Binghamton database have a  $z$ -component with an average value of  $z_{avg} = -1500$ . It serves no purpose to have the face at such a distance. It can even cause problems to some algorithms like the POSIT algorithm discussed in 2.2.3. Moving the center of the face scans to the origin of the object coordinate system can be done by merely calculating the average  $x$ ,  $y$  and  $z$  of the entire dataset and then subtracting this average from every vertex.

## 3.4 Model Construction

Given a database of 3D face scans that are in correspondence, the tensor-based model can be constructed by first organizing this data into a tensor and then using multilinear algebra to find a decomposition of this tensor.

### 3.4.1 Data Tensor

The tensor model should be designed to address expression and identity as sources of variation in the data. We assume that the points are defined by a set of size  $I_{pts}$ , the expressions by a set of size  $I_{exp}$  and the identities with size  $I_{id}$ . Then we can construct a data tensor  $\mathcal{D} \in \mathbb{R}^{I_{pts} \times I_{id} \times I_{exp}}$ . Each face scan in the database is vector from  $R^{I_{pts}}$  and there are  $I_{id}I_{exp}$  such vectors in the database. To load data into the the tensor we need to read each vector representing a face into the tensor and index the elements of this vector appropriately. This is done as follows

---

#### Algorithm 2 Loading the Data Tensor

---

```

1: procedure LOAD(database, $\mathcal{D}$ )            $\triangleright$  Input the database and the empty data tensor
2:   for  $i = 1 \dots I_{id}$  do
3:     for  $j = 1 \dots I_{exp}$  do
4:        $v \leftarrow \text{database}(i, j)$ 
5:       for  $k = 1 \dots I_{pts}$  do
6:          $\mathcal{D}(i, j, k) \leftarrow v_k$ 
7:       end for
8:     end for
9:   end for
10:  return  $\mathcal{D}$                                  $\triangleright$  return the initialized data tensor
11: end procedure
```

---

Due to the fact that most algorithms operate on matrices instead of tensors, it may be preferable to flatten the data tensor right after loading it. Flattening the tensor along a mode is done by successively fixing the values of the index of the corresponding mode and iterating through the values of the other indices to obtain the data. The procedure for flattening a tensor along the identity mode space is given in Algorithm 3.

**Algorithm 3** Flattening a Tensor along the identity mode space

---

```

1: procedure FLATTEN( $\mathcal{D}$ ,  $\mathbf{D}_{(2)}$ )                                 $\triangleright$  The input tensor, the output matrix
2:   for  $i = 1 \dots I_{id}$  do
3:     for  $j = 1 \dots I_{exp}$  do
4:       for  $k = 1 \dots I_{pts}$  do
5:         index  $\leftarrow j * I_{pts} + k$ 
6:          $\mathbf{D}_{(2)}(i, \text{index}) \leftarrow \mathcal{D}(i, j, k)$ 
7:       end for
8:     end for
9:   end for
10:  return  $\mathbf{D}_{(2)}$                                           $\triangleright$  return the flattened tensor
11: end procedure

```

---

The data tensor itself will need to be loaded once and flattened three times for the computation of the HOSVD decomposition.

### 3.4.2 Computing the HOSVD

The generative tensor model for the face transfer application is given by the formula

$$\mathbf{f} = \mathcal{M} \times_2 \mathbf{w}_i^T \times_3 \mathbf{w}_e^T \quad (3.1)$$

where  $\mathbf{f}$  is the generated 3D face scan in form of a vector and  $\mathbf{w}_i$  with  $\mathbf{w}_e$  are column vectors of identity and expression parameters respectively. Ideally, we should be able to generate new faces using equation 3.1 by choosing values for the identity and expression parameters and obtaining a 3D face scan in form of the  $\mathbf{f}$  vector. To implement this generative function it is necessary to compute the multilinear model  $\mathcal{M}$  tensor which governs this mapping between the vector spaces.

As seen in equation 2.36, the core tensor is obtained by reversing the HOSVD decomposition. The multilinear model tensor  $\mathcal{M}$  is obtained by the mode product of the core tensor and the mode matrix of the points. This is equivalent to not factoring along the point mode space during the HOSVD. To construct the model we therefore have to implement the following formula

$$\mathcal{M} = \mathcal{C} \times_1 \mathbf{U}_{pts}^T = \mathcal{D} \times_2 \mathbf{U}_{id}^T \times_3 \mathbf{U}_{exp}^T \quad (3.2)$$

which relates the data tensor  $\mathcal{D}$  with the mode matrices  $\mathbf{U}_{id}$  and  $\mathbf{U}_{exp}$ . The column vectors of  $\mathbf{U}_{id}$  span the space of identities and its row vectors are point invariant encodings of each identity seen in the database. Similarly, the column vectors of  $\mathbf{U}_{exp}$  form the basis of the space of expressions and the rows are invariant representations of the various expressions. These matrices are obtained through singular value decomposition of the flattened matrices as

$$\mathbf{D}_{(2)} = \mathbf{U}_{id} \boldsymbol{\Sigma}_{id} \mathbf{V}_{id}^T \quad (3.3)$$

$$\mathbf{D}_{(3)} = \mathbf{U}_{exp} \boldsymbol{\Sigma}_{exp} \mathbf{V}_{exp}^T \quad (3.4)$$

However, computing the mode matrices using the above equations is often not feasible due to computer memory constraints. This can be easily seen from the magnitude of the matrices involved in the computation. Consider the dimensions of the flattened matrices seen in 3.3 and 3.4. The data tensor we described in section 3.4.1 has dimensions  $I_{pts} \times I_{id} \times I_{exp}$ . The flattened matrix  $\mathbf{D}_{(2)}$  is flattened along the identity mode and has dimensions  $I_{id} \times I_{exp}I_{pts}$ . For the SVD of this matrix we therefore need three matrices  $\mathbf{U}_{id}$ ,  $\boldsymbol{\Sigma}_{id}$  and  $\mathbf{V}_{id}$  of dimensions  $I_{id} \times I_{id}$ ,  $I_{id} \times I_{exp}I_{pts}$  and  $I_{exp}I_{pts} \times I_{exp}I_{pts}$  respectively. Flattening along the expression mode produces the  $\mathbf{D}_{(3)}$  matrix with dimensions  $I_{exp} \times I_{pts}I_{id}$ . The matrices obtained from the decomposition of this matrix are  $\mathbf{U}_{exp}$ ,  $\boldsymbol{\Sigma}_{exp}$  and  $\mathbf{V}_{exp}$  with dimensions  $I_{exp} \times I_{exp}$ ,  $I_{exp} \times I_{pts}I_{id}$  and  $I_{pts}I_{id} \times I_{pts}I_{id}$ .

The memory requirements are best illustrated on an actual application. For instance, consider an application with 56 identities, 7 expressions and 5090 vertices, where the data tensor has three

dimensions and a size  $56 \times 7 \times (5090 * 3)$ . A matrix flattened along the expression mode space then has two dimensions and a size  $7 \times (56 * 5090 * 3)$ . Decomposing this flattened matrix into  $\mathbf{U}_{exp} \Sigma_{exp} \mathbf{V}_{exp}^T$  requires the allocation of memory for matrices of sizes  $7 \times 7$  for  $\mathbf{U}_{exp}$ , 7 non-zero singular values in  $\Sigma_{exp}$  and a matrix of size  $(56 * 5090 * 3) \times (56 * 5090 * 3)$  for  $\mathbf{V}_{exp}$ . This means that the  $\mathbf{V}_{exp}$  matrix needs to be represented using  $855120 * 855120$  float values. The memory requirement of this is approximately  $4 * 700 * 10^9$  bytes. Clearly the  $\mathbf{V}_{exp}$  matrix is too large and exceeds the memory capacity of most personal computers.

We are not interested in the matrix  $\mathbf{V}$  so ideally we should try to avoid computing it and thereby avoid needing to allocate memory for it. To compute a simplified and less memory demanding version of the SVD we can post-multiply the matrix with its transpose. To illustrate this approach lets take a matrix  $\mathbf{A}$  with dimensions  $m \times n$ . The SVD of this matrix is  $\mathbf{A} = \mathbf{U}\Sigma\mathbf{V}^T$ , where  $\mathbf{U}$  is a  $m \times m$  orthonormal matrix,  $\Sigma$  a  $m \times n$  diagonal matrix and  $\mathbf{V}$  is a  $n \times n$  orthonormal matrix. If the goal is to obtain the left singular matrix  $U$  then finding this matrix by means of SVD of  $\mathbf{A}$  will be memory inefficient if  $m \ll n$ . However, note that

$$\mathbf{A}^T = (\mathbf{U}\Sigma\mathbf{V}^T)^T = (\mathbf{V}^T)^T(\mathbf{U}\Sigma)^T = \mathbf{V}\Sigma^T\mathbf{U}^T = \mathbf{V}\Sigma\mathbf{U}^T \quad (3.5)$$

Therefore if we post-multiply  $\mathbf{A}$  with  $\mathbf{A}^T$  we obtain

$$\mathbf{A}\mathbf{A}^T = \mathbf{U}\Sigma\mathbf{V}^T\mathbf{V}\Sigma\mathbf{U}^T \quad (3.6)$$

Because  $\mathbf{V}$  is orthonormal this means that  $\mathbf{V}^T\mathbf{V} = \mathbf{I}$ , where  $\mathbf{I}$  is the identity matrix. Using this relationship equation 3.6 simplifies to

$$\mathbf{A}\mathbf{A}^T = \mathbf{U}\Sigma^2\mathbf{U}^T \quad (3.7)$$

The square of a diagonal matrix is trivially again a diagonal matrix. Since  $\Sigma^2$  is diagonal, this means that we can calculate the left singular matrix  $\mathbf{U}$  in a memory efficient way by computing the SVD of  $\mathbf{A}\mathbf{A}^T$ . The approach defined by equation 3.7 is crucial for the first step of the HOSVD algorithm in the expression transfer application.

Once the mode matrices  $\mathbf{U}_{id}$  and  $\mathbf{U}_{exp}$  have been computed, the next step of the HOSVD algorithm is to calculate the multilinear model using equation 3.2. This can be done by utilizing the relationship between the Kronecker product and mode- $n$  multiplication. The HOSVD decomposition of the data tensor which is given by

$$\mathcal{D} = \underbrace{\mathcal{S} \times_1 \mathbf{U}_{pts}}_{\mathcal{M}} \times_2 \mathbf{U}_{id} \times_3 \mathbf{U}_{exp} \quad (3.8)$$

where  $\mathcal{S}$  is the core tensor and  $\mathcal{M}$  is the multilinear model which is to be computed. The HOSVD decomposition can then be rewritten using Kronecker products by flattening the core tensor and the data tensor along the first mode. Thus

$$\mathbf{D}_{(1)} = \underbrace{\mathbf{U}_{pts}\mathbf{S}_{(1)}}_{\mathbf{M}_{(1)}}(\mathbf{U}_{id} \otimes \mathbf{U}_{exp})^T \quad (3.9)$$

As seen in 2.30, the Kronecker product of orthogonal matrices is again orthogonal. Therefore equation 3.9 can be post-multiplied with  $\mathbf{U}_{id} \otimes \mathbf{U}_{exp}$  to give

$$\begin{aligned} \mathbf{D}_{(1)}(\mathbf{U}_{id} \otimes \mathbf{U}_{exp}) &= \mathbf{M}_{(1)}(\mathbf{U}_{id} \otimes \mathbf{U}_{exp})^T(\mathbf{U}_{id} \otimes \mathbf{U}_{exp}) \\ \mathbf{D}_{(1)}(\mathbf{U}_{id} \otimes \mathbf{U}_{exp}) &= \mathbf{M}_{(1)} \\ \mathbf{M}_{(1)} &= \mathbf{D}_{(1)}(\mathbf{U}_{id} \otimes \mathbf{U}_{exp}) \end{aligned} \quad (3.10)$$

Equation 3.10 is essentially equation 3.2 rewritten using Kronecker products. It is not necessary to compute the multilinear model tensor  $\mathcal{M}$  from the flattened multilinear model matrix  $\mathbf{M}_{(1)}$ . This is due to the fact that the flattened multilinear model is obtained from the decomposition of the flattened data tensor  $\mathbf{D}_{(1)}$  as seen in equation 3.9. This flattened data tensor is composed

of the 3D face scans arranged as the columns of the matrix. The goal of the model is to be able to synthesize faces. These new faces should be generated as linear combinations of the original faces. This implies that generating new faces can be done by linear combination of columns of the flattened matrix  $\mathbf{D}_{(1)}$ . Since the flattened multilinear model  $\mathbf{M}_{(1)}$  is part of the decomposition of  $\mathbf{D}_{(1)}$ , it can therefore be used to perform this linear combination.

**HOSVD algorithm** The expression transfer HOSVD algorithm calculates the flattened multilinear model  $\mathbf{M}_{(1)}$  in four steps as follows:

- **Step 1.** Flatten the data tensor along all modes to obtain the matrices  $\mathbf{D}_{(1)}$ ,  $\mathbf{D}_{(2)}$  and  $\mathbf{D}_{(3)}$ .
- **Step 2.** Compute the identity mode matrix  $\mathbf{U}_{id}$  using SVD as

$$\mathbf{D}_{(2)}\mathbf{D}_{(2)}^T = \mathbf{U}_{id}\Sigma_{id}^2\mathbf{U}_{id}^T \quad (3.11)$$

- **Step 3.** Compute the expression mode matrix  $\mathbf{U}_{exp}$  using SVD as

$$\mathbf{D}_{(3)}\mathbf{D}_{(3)}^T = \mathbf{U}_{exp}\Sigma_{exp}^2\mathbf{U}_{exp}^T \quad (3.12)$$

- **Step 4.** Finally, calculate the multilinear model flattened along the first mode using the Kronecker product as

$$\mathbf{M}_{(1)} = \mathbf{D}_{(1)}(\mathbf{U}_{id} \otimes \mathbf{U}_{exp}) \quad (3.13)$$

### 3.4.3 Generating new faces

As previously mentioned, the general idea that motivates the use of statistical analysis techniques when building models, is that novel faces can be obtained from linear combinations of the faces in the 3D face scan database. This linear combination can be understood as moving one face in a direction given by another face. The resulting new face will look realistic provided that the new face is close in terms of standard deviation to the mean. Therefore, one approach to generating new faces from the data tensor is to flatten the tensor along the points mode to obtain  $\mathbf{D}_{(1)}$  and synthesize new faces using a linear combination of the columns of this matrix. A face model would therefore be by choosing a set of parameters  $\mathbf{w}$  and generating a new face  $\mathbf{f}$  as

$$\mathbf{f} = \mathbf{D}_{(1)}\mathbf{w} \quad (3.14)$$

The HOSVD algorithm calculates the multilinear model  $\mathbf{M}_{(1)}$  along with the mode matrices  $\mathbf{U}_{id}$  and  $\mathbf{U}_{exp}$ . These matrices form the decomposition of the data matrix  $\mathbf{D}_{(1)}$  as per equation 3.9. Thus, the generative model becomes

$$\mathbf{f} = \mathbf{M}_{(1)}(\mathbf{U}_{id} \otimes \mathbf{U}_{exp})^T\mathbf{w} \quad (3.15)$$

Since we are free to choose the coefficients  $\mathbf{w}$ , they can be thought of as composed through a Kronecker product as  $\mathbf{w} = \mathbf{w}_{id} \otimes \mathbf{w}_{exp}$ . The transpose of a Kronecker product is equal to transposing the operands of the product. Therefore

$$\mathbf{f} = \mathbf{M}_{(1)}(\mathbf{U}_{id} \otimes \mathbf{U}_{exp})^T(\mathbf{w}_{id} \otimes \mathbf{w}_{exp}) \quad (3.16)$$

$$= \mathbf{M}_{(1)}(\mathbf{U}_{id}^T \otimes \mathbf{U}_{exp}^T)(\mathbf{w}_{id} \otimes \mathbf{w}_{exp}) \quad (3.17)$$

$$= \mathbf{M}_{(1)}(\mathbf{U}_{id}^T\mathbf{w}_{id} \otimes \mathbf{U}_{exp}^T\mathbf{w}_{exp}) \quad (3.18)$$

where we have used the relationship between multiplication and the Kronecker product shown in 2.27. So to recover the  $i$ -th of the original faces from the multilinear model, the parameter vector  $\mathbf{w}$  will have a 1 at the  $i$ -th position. When this parameter vector is multiplied with the flattened data tensor, the  $i$ -th column will be recovered. This  $i$ -th column is the  $i$ -th face scan in the database.

With the multilinear model even more powerful recovery is possible. For example, to obtain the face which corresponds to the  $j$ -th identity and  $k$ -th expression, the parameter vector will be

composed from the identity and expression vectors. This identity parameter vector will have a 1 at the  $j$ -th position and the expression parameter vector will have a 1 at the  $k$ -position. Taking the Kronecker product of these two will produce the parameter vector  $\mathbf{w}$  with a 1 at the  $(j * I_{exp} + k)$ -th position which reconstructs the face with the  $j$ -th identity and the  $k$ -th expression when the parameter vector is multiplied with the flattened data tensor as per equation 3.14.

Furthermore, any arbitrary interpolation, or indeed extrapolation of the faces in the database can be obtained from the multilinear model based on the choice of the attribute parameters. This is because any vector  $\mathbf{w}$  can be written as a sum of vectors which have zeros at all positions except one. If we define  $\mathbf{e}_i$  to be a vector which has a 1 at the  $i$ -th position and a zero everywhere else then  $\mathbf{w} = a_1\mathbf{e}_1 + a_2\mathbf{e}_2 + \dots + a_n\mathbf{e}_n$  where the  $a_i$  are arbitrary coefficients. Therefore to show that the model produces any arbitrary linear combination of the original faces we proceed as

$$\mathbf{M}_{(1)}(\mathbf{U}_{id} \otimes \mathbf{U}_{exp})^T \mathbf{w} = \mathbf{M}_{(1)}(\mathbf{U}_{id} \otimes \mathbf{U}_{exp})^T(a_1\mathbf{e}_1 + a_2\mathbf{e}_2 + \dots + a_n\mathbf{e}_n) \quad (3.19)$$

$$= a_1\mathbf{D}_{(1)}\mathbf{e}_1 + a_2\mathbf{D}_{(1)}\mathbf{e}_2 + \dots + a_n\mathbf{D}_{(1)}\mathbf{e}_n \quad (3.20)$$

This is due to the fact that the multiplication of  $\mathbf{D}_{(1)}\mathbf{e}_i$  recovers the  $i$ -th face. Therefore any linear combination can be generated using the multilinear model.

If the goal is to linearly interpolate a face from the original faces, then the coefficients  $a_i$  must all be greater or equal to 0 and they must all sum to 1. This interpolation can equivalently be done by choosing the  $\mathbf{w}_{id}$  and  $\mathbf{w}_{exp}$  to have all components greater or equal to 0 and both weight vectors summing to 1. The Kronecker product of two such vectors has components all greater or equal to 0 and summing to one and it therefore satisfies the interpolation condition. If the Kronecker product is the vector  $\mathbf{w} = \mathbf{w}_{id} \otimes \mathbf{w}_{exp}$ , then the elements of this vector are all possible combinations of  $\mathbf{w}_{id_i}\mathbf{w}_{exp_j}$  which are the  $i$ -th and  $j$ -th components of the identity and expression vectors. The sum of the elements of  $\mathbf{w}$  is therefore

$$\sum_i \left( \mathbf{w}_{id_i} \sum_j \mathbf{w}_{exp_j} \right) = \sum_i \mathbf{w}_{id_i} = 1$$

All the elements of the vector  $\mathbf{w}$  are also trivially greater or equal to 0 as well.

If we are not interested in interpolating between the original faces, then it is not necessary to store the mode matrices  $\mathbf{U}_{id}$  and  $\mathbf{U}_{exp}$ . These mode matrices are invertible and thus form a basis for the subspaces  $\mathbb{R}^{I_{id}}$  and  $\mathbb{R}^{I_{exp}}$  respectively. The operands  $\mathbf{U}_{id}^T \mathbf{w}_{id}$  and  $\mathbf{U}_{exp}^T \mathbf{w}_{exp}$  of the Kronecker product in equation 3.18 can therefore generate any vector from these subspaces. Since any vector from these subspaces can be obtained inside the Kronecker product, we can safely drop the mode matrices to obtain the generative model:

$$\mathbf{f} = \mathbf{M}_{(1)}(\mathbf{w}_{id} \otimes \mathbf{w}_{exp}) \quad (3.21)$$

**Summary.** The matrices computed through HOSVD make it possible to synthesize a novel face by choosing values for the identity and expression model parameters  $\mathbf{w}_{id}$  and  $\mathbf{w}_{exp}$ . Due to the separability of the multilinear model, these parameters can be given values independently of each other, allowing the user to alter the corresponding attribute on its own. It is therefore possible to enforce linear interpolation constraints on one attribute but not the other. The expressive power of the multilinear model depends solely on the variance of the faces in the database, since new face are generated as linear combinations of original faces.

## 3.5 Model Parameter Estimation

Once the face model is constructed, the objective becomes to correctly adjust the parameters that control this model in order to match a face in an image. This fitting algorithm must also allow the face in the image to be scaled, rotated or moved. So in addition to estimating the model parameters the algorithm also needs to approximate the 3D pose of the object. As discussed in section 2.2, the 3D pose is defined by a rotation matrix  $\mathbf{R}$  and a translation vector  $\mathbf{t}$ . There are 3 parameters which

uniquely describe a rotation matrix and 3 components in a translation vector. The total number of model parameters depends on the amount of persons in the database and on how many expressions these individuals perform. In the model construction section we defined these numbers to be  $I_{id}$  and  $I_{exp}$  respectively. Thus, to fit the model to an image there are  $6 + I_{id} + I_{exp}$  parameters which need to be estimated. To determine these parameters the fitting algorithm will need to minimize the difference between the face in the image and the model with the changed pose.

However, the model is three dimensional and the images are just two dimensional. Therefore, to compare the two in an optimization algorithm, the 3D points of the model must be projected to a 2D space using a camera model.

After the model has been projected, an error between the projection and the face in the image is calculated. To be able to calculate this error, it is necessary to know a set of 2D reference points in the image. These reference points, or feature points, correspond to known points on the model. The idea behind the fitting algorithm is to find how the model needs to be deformed and what 3D pose it needs to have so that these corresponding points on the 3D model are projected onto the feature points. How these feature points are selected is therefore crucial to determining the difference between the model and the face in the image. Minimizing this difference is the purpose of the fitting algorithm. Moreover, finding feature points is not a trivial task since they need to correspond to points on the model.

The goal of the expression transfer application is to understand the facial dynamics of an individual from a video recording – so therefore a sequence of images. Since we are dealing with a video it means that the fitting algorithm will need to be performed for each frame of the video recording and for that it will need reference points in each and every frame. The application therefore needs to track the movement of the feature points so that there are feature points available for the fitting algorithm in every frame.

### 3.5.1 Locating Feature Points

The first problem that needs to be addressed before the fitting algorithm is designed, is how the application locates feature points. These feature points need to correspond to points in the 3D model so that they can be used as reference points in the parameter optimization step. The feature points therefore cannot be picked randomly or even independently of the model.

One approach is to designate which points on the model will be used as correspondences to the feature points during the model construction step. In the case of the expression transfer application these points should be chosen so that their positions can be used to determine expressions. Good feature points may be the corners of the mouth, the tip of the nose and other easily distinguishable features on the face model. Given this predefined set of points on the model, the feature points which correspond to them are located in the image. This may for example be done manually by a user who selects the locations of these feature points one by one. Reference points selection in the image could likewise be performed with an automatic feature detector such as the Viola-Jones object detection framework [39].

The manual approach is more flexible, simple and less error prone. The flexibility comes from the fact that adding a new feature point to the model does not necessitate the writing of a new feature detector. However, it can be tedious for the user to have to select a large number of points in the image and it is certainly not as impressive as when these points are located automatically.

The drawback of using automatic feature detectors is the fact that they introduce error. The feature locations they detect are guesses. One of the challenges that the expression transfer application faces is that estimating the correct expression requires a considerable amount of detailed information. Any amount of error is significantly counterproductive since it will inevitably increase during the latter stages of the fitting algorithm.

For the sake of flexibility and simplicity the expression transfer application is designed with a fixed set of feature points on the model. The user is then asked to provide the corresponding image feature points on the first frame of the video. The default feature points on the model are shown in figure 3.2.

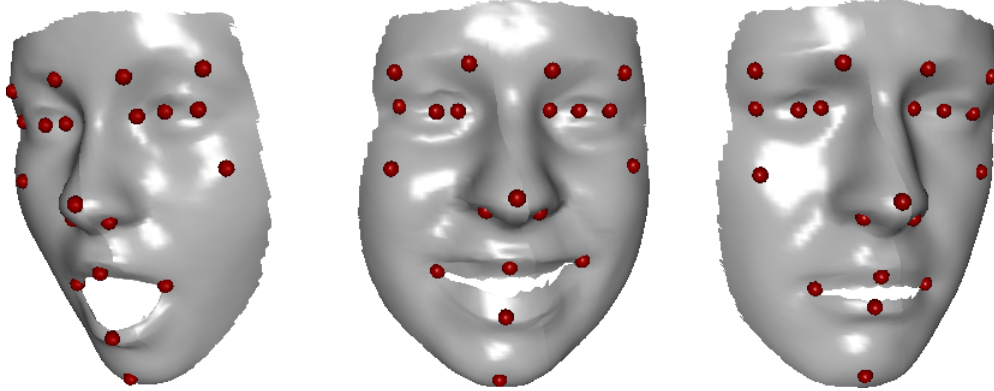


Figure 3.2: Three newly generated faces with twenty feature points (denoted by the red spheres). These feature points define the correspondence between the model and the image.

The user selects the feature points simply by clicking on the correct pixel in the image. During the selection process, a label guides the user and informs him which feature point he should select next. This design is shown in figure 3.3.



Figure 3.3: The user selects points in the image which correspond to the feature points on the model (see figure 3.2 ).

How well the corresponding image feature points are selected plays a very important role during the optimization process of the fitting algorithm. This again is due to the sensitivity of expression estimation to detail.

### 3.5.2 Tracking Feature Points

After the user (or an automatic algorithm) has identified the position of the projections of model feature points in the first frame of the recording, it is necessary to find the positions of these points in all the successive frames. This is done automatically using an optical flow algorithm. This algorithm attempts to estimate the movement of the points.

The movement of points is what allows the fitting algorithm to recognize an expression. Clearly, there are always feature points which provide more information about an expression than other.

Points around the mouth for example are especially important for the algorithm since most expressions are characterized by unique mouth movements. Points on the eyebrows are also a good source of information about the expression. Conveniently, these points are also very good for tracking since the mouth and the eyebrows are easily distinguishable in terms of texture from other points on the face.

On the other hand, the features which are imperative to the recognition of a person's identity are mostly static. These features include the distance between the corners of the mouth, the location of the chin, the displacements between the mouth and the nose and even the size of the eyes. The problem with feature points which are good for estimating identity is they are often located in areas where texture is largely constant and they are thus difficult to track. For example, selecting feature points on the forehead or the cheeks may be crucial to determine the measurements of the face. However, the movement of these points will be very difficult to predict due to the lack of unique texture in their surroundings.

The Kanade-Lucas feature tracker, which was discussed in 2.3.1, is an optical flow algorithm well suited for tracking a small number of points. A pyramidal implementation of the Kanade-Lucas feature tracker is available in the OpenCV library as the function `calcOpticalFlowPyrLK()`. The OpenCV implementation is described in detail by Bouguet in [6].

Feature points may sometimes get lost during tracking process with the Kanade-Lucas feature tracker. This can happen if the texture around the point changes so drastically that it is impossible for the algorithm to predict the point's movement. This may for instance happen to feature points on the eye when a person blinks. There are two possible approaches to dealing with lost points. The algorithm may for example assume that the point did not move at all, which is a reasonable assumption for feature points on the eye. The other possibility is to discard such points altogether. The second approach works better with more general disturbances. Consider a situation when a hand is moving in front of the face. It should usually take several frames for the hand to pass. As the hand appears some points will get lost. If the algorithm assumed their position did not change they would begin moving with the hand in the following frames.

### 3.5.3 Camera Parameters

The feature points on the 3D model need to be projected into 2D so that their difference from user selected points may be calculated. These points are projected using a camera model. The parameters of this camera model must be obtained by calibrating the camera which was used to capture the image. There are three main camera (intrinsic) parameters. As seen in section 2.2.1, often it is preferable to use four parameters. These are the two components of the principal point  $c_x$ ,  $c_y$  and two parameters  $f_x$  and  $f_y$  which are computed from the focal length  $f$  and pixel to real world conversion values. The camera model used in the expression transfer application is

$$\gamma \begin{pmatrix} x \\ y \\ 1 \end{pmatrix} = \begin{pmatrix} f_x & 0 & c_x & 0 \\ 0 & f_y & c_y & 0 \\ 0 & 0 & 1 & 0 \end{pmatrix} \begin{pmatrix} X \\ Y \\ Z \\ 1 \end{pmatrix} \quad (3.22)$$

The process of computing camera parameters is called camera calibration. There are numerous algorithms for camera calibration. Most of them are based on first using the camera to produce images of a pattern with a known 3D geometry. The calibration algorithm is then provided with a set of marked points on the images which correspond to points in the 3D geometry. A commonly used planar pattern for camera calibration is the chessboard pattern. The feature points in the chessboard pattern image are often chosen to be the inside corners of the chessboard squares. These can be located automatically since they are easily distinguishable using edge and corner detection filters. OpenCV provides the `cvFindChessboardCorners(.)` function for this purpose.

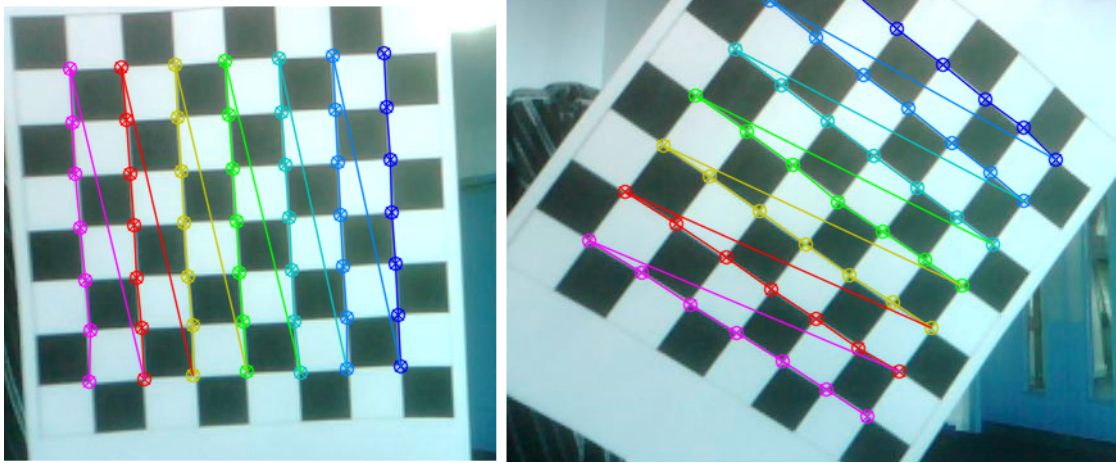


Figure 3.4: Locating feature points in a chessboard pattern.

The expression transfer application uses Zhang's camera calibration algorithm [42]. Computing the camera parameters with Zhang's algorithm requires only a few images of a planer pattern (such as the chessboard) at different orientations. An implementation of this algorithm is provided in OpenCV under the function `cvCalibrateCamera()`.

Utilizing OpenCV, we can thus implement camera calibration in a few steps as

- **Step 1.** The user inputs two or more images of a chessboard pattern.
- **Step 2.** The images are processed with `cvFindChessboardCorners()` to find all the inner corners inside the chessboard.
- **Step 3.** The function `cvCalibrateCamera()` is called with the found corners and with the 3D geometry of the board. This geometry need only be defined once when writing the algorithm.

Camera calibration can only be performed if the user has access to the camera and can take images of a chessboard pattern. To allow for more flexibility, it must also be possible for the user to input camera parameters into the application manually. The GUI of the expression transfer application therefore includes the possibility of either specifying the parameters manually or calling the automatic calibration process. The GUI of application provides a dialog for camera calibration.

### 3.5.4 Minimizing the Error Function

The goal of the fitting algorithm is to estimate the model and 3D pose parameters given a set of  $N$  feature points  $f_1, \dots, f_N$  in every frame of the recording. In order to find the parameters that are closest to the true parameters we need an error function to measure the dissimilarity between the projected 3D model and the image. A convenient error function is the sum of squares error function which measures this dissimilarity as the sum of the distances between the feature points and the projection of their corresponding 3D model points. The sum of squares function that we need to minimize with respect to the parameters is therefore

$$E(\text{parameters}) = \sum_{i=1}^N \left\| \mathbf{f}_i - \text{proj}(\text{model point}) \right\|^2 \quad (3.23)$$

The point on the model which corresponds to the feature point  $\mathbf{f}_i = (u_i, v_i)^T$  is defined as  $\mathbf{p}_i = (x_i, y_i, z_i)^T$ . The 3D model points are a function of the model parameters. For the expression transfer model this function is given by 3.18. This function generates a vector  $\mathbf{X}$  which is obtained as a linear combination of the 3D face scans, therefore

$$\mathbf{X} = g(\mathbf{w}_{id}, \mathbf{w}_{exp}) = \mathbf{M}_{(1)}(\mathbf{U}_{id}^T \mathbf{w}_{id} \otimes \mathbf{U}_{exp}^T \mathbf{w}_{exp}) \quad (3.24)$$

If we were only interested in generating 3D points as linear combinations of the 3D face scans then the generative function could also be specified in a more concise form by formula 3.21. However, by avoiding this simplification the weights maintain their meaning. This meaning stems from the direct relation of the expression and identity weights to the weight vector  $\mathbf{w}$  which was used to generate a linear combination of the columns of the flattened data tensor as seen in equation 3.14. The model parameters  $\mathbf{w}_{id}$  and  $\mathbf{w}_{exp}$  are therefore the decomposition of the coefficients which produced this linear combination of the data tensor columns. As such, we can impose meaningful constraints to enforce realistic results as will be seen later.

The components of the model point  $\mathbf{p}_i$  form three successive components of the vector  $\mathbf{X}$ . The point is therefore generated by the corresponding rows from the flattened multilinear model. We specify these row as  $(\mathbf{M}_{(1)})_{i,*}$ ,  $(\mathbf{M}_{(1)})_{i+1,*}$  and  $(\mathbf{M}_{(1)})_{i+2,*}$  respectively. To simplify the notation these three rows collectively stacked on top of each other will be denoted as  $[\mathbf{M}_{(1)}]_i$ . The points  $\mathbf{p}_i$  can be thus generated by the function

$$\mathbf{p}_i = g_i(\mathbf{w}_{id}, \mathbf{w}_{exp}) = [\mathbf{M}_{(1)}]_i (\mathbf{U}_{id}^T \mathbf{w}_{id} \otimes \mathbf{U}_{exp}^T \mathbf{w}_{exp}) \quad (3.25)$$

In addition to the model parameters, we need to estimate the 3D pose parameters of the 3D model so that the optimization can account for all the degrees of freedom which are available to the subject in the recording. The 3D pose is defined by the rotation of the object and its translation. These are specified using the rotation matrix  $\mathbf{R}$  and the translation vector  $\mathbf{t}$ . This rotation and translation is applied to all model points allowing us to generate a 3D representation of any arbitrarily rotated or moved face. The augmented generative function is thus

$$\mathbf{p}_i = g_i(\mathbf{w}_{id}, \mathbf{w}_{exp}, \mathbf{R}, \mathbf{t}) = \mathbf{R}[\mathbf{M}_{(1)}]_i (\mathbf{U}_{id}^T \mathbf{w}_{id} \otimes \mathbf{U}_{exp}^T \mathbf{w}_{exp}) + \mathbf{t} \quad (3.26)$$

Lastly, to measure the dissimilarity between the feature points  $\mathbf{f}_i$  and the corresponding 3D model points  $\mathbf{p}_i$  it is necessary to project the model points into 2D. This projection is done using the perspective camera model with a camera matrix  $\mathbf{P}$  which consists of the calibrated (or user provided) intrinsic parameters  $f_x$ ,  $f_y$ ,  $c_x$  and  $c_y$ . The result of projecting the model point  $\mathbf{p}_i$  is

$$\gamma \begin{pmatrix} \mathbf{f}_i \\ 1 \end{pmatrix} = \begin{pmatrix} f_x & 0 & c_x \\ 0 & f_y & c_y \\ 0 & 0 & 1 \end{pmatrix} \mathbf{p}_i = \mathbf{P} \mathbf{p}_i \quad (3.27)$$

Given the augmented generative function  $g_i$  and the projection matrix we can now expand the sum of square error function 3.23 to obtain

$$E(\mathbf{w}_{id}, \mathbf{w}_{exp}, \mathbf{R}, \mathbf{t}) = \sum_{i=1}^N \left\| \begin{pmatrix} \mathbf{f}_i \\ 1 \end{pmatrix} - \frac{1}{\gamma} \mathbf{P} g_i(\mathbf{w}_{id}, \mathbf{w}_{exp}, \mathbf{R}, \mathbf{t}) \right\|^2 \quad (3.28)$$

The generative function can be further expanded to give

$$E(\mathbf{w}_{id}, \mathbf{w}_{exp}, \mathbf{R}, \mathbf{t}) = \sum_{i=1}^N \left\| \begin{pmatrix} \mathbf{f}_i \\ 1 \end{pmatrix} - \frac{1}{\gamma} \mathbf{P} [\mathbf{R}[\mathbf{M}_{(1)}]_i (\mathbf{U}_{id}^T \mathbf{w}_{id} \otimes \mathbf{U}_{exp}^T \mathbf{w}_{exp}) + \mathbf{t}] \right\|^2 \quad (3.29)$$

$$= \sum_{i=1}^N \left\| \begin{pmatrix} \mathbf{f}_i \\ 1 \end{pmatrix} - \frac{1}{\gamma} \mathbf{P} \mathbf{R}[\mathbf{M}_{(1)}]_i (\mathbf{U}_{id}^T \mathbf{w}_{id} \otimes \mathbf{U}_{exp}^T \mathbf{w}_{exp}) - \frac{1}{\gamma} \mathbf{P} \mathbf{t} \right\|^2 \quad (3.30)$$

The optimal values of the error function parameters  $\mathbf{w}_{id}$ ,  $\mathbf{w}_{exp}$ ,  $\mathbf{R}$  and  $\mathbf{t}$  can be obtained by setting the derivative of the error function with respect to the parameter in question to zero and then solving the resulting equation. These optimal parameters describe a model that gives the smallest possible error between its projection and the image feature points.

However, the problem with the perspective projection is that to obtain the feature point we need to dehomogenize the result of the projection by dividing with  $\gamma$ . This  $\gamma$  will be equal to the unknown value of the  $z$ -component of the point which is being projected using the camera matrix, making the scaling factor  $\gamma$  a function of the model parameters and the rotation matrix given by

$\gamma(\mathbf{w}_{id}, \mathbf{w}_{exp}, \mathbf{R}, \mathbf{t})$ . The perspective projection is therefore ill-suited for optimization, because the derivative of the error function will be a nonlinear function depending on the partial derivatives of the function  $\gamma(\mathbf{w}_{id}, \mathbf{w}_{exp}, \mathbf{R}, \mathbf{t})$ . Setting the derivative to zero would then result in a nonlinear equation which is difficult to solve.

The presence of the scaling factor means that the perspective projection is not a linear transformation since  $\gamma$  is a function of the point  $p_i$ . The weak-perspective projection, however, is a linear transformation and it may be used to approximate the perspective projection. The idea behind the weak-perspective projection is that when the distance of the object from the camera is large enough then the points on the object can be thought to have effectively same  $z$ -component. Fortunately, the points on a face are very close to each other in depth, which justifies using the weak-perspective camera model as an approximation of the perspective camera model in the fitting algorithm.

The weak-perspective projection uses the same parameters  $f_x$ ,  $f_y$ ,  $c_x$  and  $c_y$  as the perspective camera model. Unlike the perspective model however, the result is divided by the average depth  $z_{avg}$  of the model instead of  $\gamma$ . The average depth is essentially the average  $\gamma$  value of all points in the object. The weak-perspective camera model is defined by the camera matrix  $\mathbf{P}_w$  as

$$\mathbf{f}_i = \frac{1}{z_{avg}} \begin{pmatrix} f_x & 0 & c_x \\ 0 & f_y & c_y \end{pmatrix} \mathbf{p}_i = \frac{1}{z_{avg}} \mathbf{P}_w \mathbf{p}_i \quad (3.31)$$

For the weak-perspective projection to provide a reasonable approximation of the perspective projection, the points must be far enough from the origin so that the differences in their depth are small in comparison to this distance. If this condition is not fulfilled, it is possible to still make the weak-perspective approximation acceptable by increasing the distance from the origin to the image plane (defined by the focal length  $f$ ). Increasing the focal length is essentially equivalent to moving the object in the  $z$  direction.

**Error function.** With the weak-perspective camera model we can now define the error function for the tensor-based model fitting algorithm as

$$E(\mathbf{w}_{id}, \mathbf{w}_{exp}, \mathbf{R}, \mathbf{t}) = \sum_{i=1}^N \left\| \mathbf{f}_i - \frac{1}{z_{avg}} \mathbf{P}_w \left( \mathbf{R}[\mathbf{M}_{(1)}]_i (\mathbf{U}_{id}^T \mathbf{w}_{id} \otimes \mathbf{U}_{exp}^T \mathbf{w}_{exp}) + \mathbf{t} \right) \right\|^2 \quad (3.32)$$

which uses the weak-perspective camera matrix  $\mathbf{P}_w$  to project the rotated model point and the translation vector  $t$ .

Given the error defining function  $E(\mathbf{w}_{id}, \mathbf{w}_{exp}, \mathbf{R}, \mathbf{t})$ , the goal is to find the optimal parameters  $\mathbf{w}_{id}^*$ ,  $\mathbf{w}_{exp}^*$ ,  $\mathbf{R}^*$  and  $\mathbf{t}^*$  which minimize this error. The minimum can be found by setting the partial derivatives to zero as

$$\frac{\partial E}{\partial \mathbf{w}_{id}} = \mathbf{0}, \quad \frac{\partial E}{\partial \mathbf{w}_{exp}} = \mathbf{0}, \quad \frac{\partial E}{\partial \mathbf{R}} = \mathbf{0}, \quad \frac{\partial E}{\partial \mathbf{t}} = \mathbf{0} \quad (3.33)$$

The resulting equations are unfortunately nonlinear due to the square in the error function. Consider the derivative with respect to the identity parameters given by

$$\begin{aligned} \frac{\partial E}{\partial \mathbf{w}_{id}} &= \frac{\partial}{\partial \mathbf{w}_{id}} \sum_{i=1}^N \left\| \mathbf{f}_i - \frac{1}{z_{avg}} \mathbf{P}_w \mathbf{R}[\mathbf{M}_{(1)}]_i \underbrace{(\mathbf{U}_{id}^T \mathbf{w}_{id} \otimes \mathbf{U}_{exp}^T \mathbf{w}_{exp})}_{\mathbf{Z}} - \frac{1}{z_{avg}} \mathbf{P}_w \mathbf{t} \right\|^2 \\ &= \sum_{i=1}^N \frac{\partial}{\partial \mathbf{w}_{id}} \left\| \mathbf{f}_i - \frac{1}{z_{avg}} \mathbf{P}_w \mathbf{R}[\mathbf{M}_{(1)}]_i \mathbf{Z} - \frac{1}{z_{avg}} \mathbf{P}_w \mathbf{t} \right\|^2 \\ &= \sum_{i=1}^N -\frac{2}{z_{avg}} \left( \frac{\partial \mathbf{P}_w \mathbf{R}[\mathbf{M}_{(1)}]_i \mathbf{Z}}{\partial \mathbf{w}_{id}} \right) \left( \mathbf{f}_i - \frac{1}{z_{avg}} \mathbf{P}_w \mathbf{R}[\mathbf{M}_{(1)}]_i \mathbf{Z} - \frac{1}{z_{avg}} \mathbf{P}_w \mathbf{t} \right) \end{aligned}$$

where the chain rule of matrix calculus was used.

The order of the derivations in the chain rule for vectors depends on whether the gradient is a row or column vector. Here we will adopt the notation that the gradient is a row vector. The chain rule is therefore “build toward the left” [14]. For example, if  $\mathbf{w}$  is a function of  $\mathbf{z}$ , which is a function of  $\mathbf{y}$ , which is a function of  $\mathbf{x}$  then the derivative of  $\mathbf{w}$  with respect to  $\mathbf{x}$  is computed using the chain rule as

$$\frac{\partial \mathbf{w}}{\partial \mathbf{x}} = \frac{\partial \mathbf{y}}{\partial \mathbf{x}} \frac{\partial \mathbf{z}}{\partial \mathbf{y}} \frac{\partial \mathbf{w}}{\partial \mathbf{z}}$$

which is reverse order of the scalar chain rule where multiplication is commutative.

The derivative of a vector function  $\mathbf{Ax}$  with respect to a vector  $\mathbf{x}$  is defined as

$$\frac{\partial \mathbf{Ax}}{\partial \mathbf{x}} = \mathbf{A}^T$$

Using the chain rule and then expanding  $\mathbf{Z}$  we obtain

$$\begin{aligned} \frac{\partial \mathbf{P}_w \mathbf{R}[\mathbf{M}_{(1)}]_i \mathbf{Z}}{\partial \mathbf{w}_{id}} &= \frac{\partial \mathbf{P}_w \mathbf{R}[\mathbf{M}_{(1)}]_i (\mathbf{U}_{id}^T \mathbf{w}_{id} \otimes \mathbf{U}_{exp}^T \mathbf{w}_{exp})}{\partial \mathbf{w}_{id}} \\ &= \frac{\partial \mathbf{U}_{id}^T \mathbf{w}_{id}}{\partial \mathbf{w}_{id}} \frac{\partial (\mathbf{U}_{id}^T \mathbf{w}_{id} \otimes \mathbf{U}_{exp}^T \mathbf{w}_{exp})}{\partial \mathbf{U}_{id}^T \mathbf{w}_{id}} \frac{\partial \mathbf{P}_w \mathbf{R}[\mathbf{M}_{(1)}]_i (\mathbf{U}_{id}^T \mathbf{w}_{id} \otimes \mathbf{U}_{exp}^T \mathbf{w}_{exp})}{\partial (\mathbf{U}_{id}^T \mathbf{w}_{id} \otimes \mathbf{U}_{exp}^T \mathbf{w}_{exp})} \\ &= \mathbf{U}_{id} \underbrace{\frac{\partial (\mathbf{U}_{id}^T \mathbf{w}_{id} \otimes \mathbf{U}_{exp}^T \mathbf{w}_{exp})}{\partial \mathbf{U}_{id}^T \mathbf{w}_{id}}}_{\mathbf{W}} (\mathbf{P}_w \mathbf{R}[\mathbf{M}_{(1)}]_i)^T \end{aligned} \quad (3.34)$$

Computing the  $\mathbf{W}$  requires us to take the derivative of a Kronecker product. In [13] the derivative of the Kronecker of a  $m \times n$  matrix  $\mathbf{A}$  and a  $p \times q$  matrix  $\mathbf{B}$  with respect to the matrix  $\mathbf{A}$  is defined as

$$\frac{\partial \mathbf{A} \otimes \mathbf{B}}{\partial \mathbf{A}} = (\mathbf{I}_n \otimes \text{vec}(\mathbf{B}) \otimes \mathbf{I}_m) (\mathbf{I}_{nq} \otimes \mathbf{T}_{pm}) \quad (3.35)$$

where  $\mathbf{I}_n$  is the  $n \times n$  identity matrix,  $\text{vec}$  a vectorization operator which stacks the columns of the operand into a vector and  $\mathbf{T}_{pm}$  a  $p \times m$  permutation matrix called the transpose matrix. This permutation matrix  $\mathbf{T}_{pm}$  has the special property that it reverses the Kronecker product.

$$\mathbf{B} \otimes \mathbf{A} = \mathbf{T}_{pm}(\mathbf{A} \otimes \mathbf{B})\mathbf{T}_{nq} \quad (3.36)$$

However, since we are taking the derivation of the Kronecker product with respect to a vector, we can utilize the fact that the operands are vectors to simplify the equation  $\mathbf{Z} = \mathbf{U}_{id}^T \mathbf{w}_{id} \otimes \mathbf{U}_{exp}^T \mathbf{w}_{exp}$  using the relationship between multiplication and the Kronecker product given by

$$(A \otimes B)(C \otimes D) = (AC \otimes BD)$$

The expression  $\mathbf{U}_{exp}^T \mathbf{w}_{exp}$  is a  $I_{exp} \times 1$  matrix (or in other words a vector) which is a constant when taking the derivation with respect to  $\mathbf{w}_{id}$ . We can therefore substitute the vector  $\mathbf{a} = \mathbf{U}_{exp}^T \mathbf{w}_{exp}$  into  $\mathbf{Z}$  to get

$$\begin{aligned} \mathbf{Z} &= \mathbf{U}_{id}^T \mathbf{w}_{id} \otimes \mathbf{U}_{exp}^T \mathbf{w}_{exp} \\ &= \mathbf{U}_{id}^T \mathbf{w}_{id} \otimes \mathbf{a} \\ &= \mathbf{I}_{I_{id}} \mathbf{U}_{id}^T \mathbf{w}_{id} \otimes \mathbf{a} \mathbf{I}_1 \\ &= (\mathbf{I}_{I_{id}} \otimes \mathbf{a})(\mathbf{U}_{id}^T \mathbf{w}_{id} \otimes \mathbf{I}_1) \\ &= (\mathbf{I}_{I_{id}} \otimes \mathbf{U}_{exp}^T \mathbf{w}_{exp}) \mathbf{U}_{id}^T \mathbf{w}_{id} \end{aligned} \quad (3.37)$$

since  $\mathbf{I}_1 = 1$ . Using a similar approach it is also possible to extract  $\mathbf{w}_{exp}$  out of  $\mathbf{Z}$  to obtain

$$\mathbf{U}_{id}^T \mathbf{w}_{id} \otimes \mathbf{U}_{exp}^T \mathbf{w}_{exp} = (\mathbf{U}_{id}^T \mathbf{w}_{id} \otimes \mathbf{I}_{I_{exp}}) \mathbf{U}_{exp}^T \mathbf{w}_{exp} \quad (3.38)$$

With this result we can now evaluate  $\mathbf{W}$  to obtain

$$\begin{aligned}\mathbf{W} &= \frac{\partial(\mathbf{U}_{id}^T \mathbf{w}_{id} \otimes \mathbf{U}_{exp}^T \mathbf{w}_{exp})}{\partial \mathbf{U}_{id}^T \mathbf{w}_{id}} = \frac{\partial(\mathbf{I}_{I_{id}} \otimes \mathbf{U}_{exp}^T \mathbf{w}_{exp}) \mathbf{U}_{id}^T \mathbf{w}_{id}}{\partial \mathbf{U}_{id}^T \mathbf{w}_{id}} \\ &= (\mathbf{I}_{I_{id}} \otimes \mathbf{U}_{exp}^T \mathbf{w}_{exp})^T = (\mathbf{I}_{I_{id}} \otimes \mathbf{w}_{exp}^T \mathbf{U}_{exp})\end{aligned}$$

This result, obtained using 3.37, adheres with the derivation of the Kronecker product, since for transpose matrices it holds that  $\mathbf{T}_{n1} = \mathbf{T}_{1n} = \mathbf{I}_n$  for any  $n$ .

With the known  $\mathbf{W}$  we can complete the derivation we began in 3.34 to get

$$\begin{aligned}\frac{\partial \mathbf{P}_w \mathbf{R}[\mathbf{M}_{(1)}]_i \mathbf{Z}}{\partial \mathbf{w}_{id}} &= \mathbf{U}_{id} \frac{\partial(\mathbf{U}_{id}^T \mathbf{w}_{id} \otimes \mathbf{U}_{exp}^T \mathbf{w}_{exp})}{\partial \mathbf{U}_{id}^T \mathbf{w}_{id}} (\mathbf{P}_w \mathbf{R}[\mathbf{M}_{(1)}]_i)^T \\ &= \mathbf{U}_{id} (\mathbf{I}_{I_{id}} \otimes \mathbf{w}_{exp}^T \mathbf{U}_{exp}) [\mathbf{M}_{(1)}]_i^T \mathbf{R}^T \mathbf{P}_w^T\end{aligned}\quad (3.39)$$

The results from equations 3.37 and 3.38 also allow us to decompose the Kronecker product in the error function as well. Thus we obtain the derivation of the error function with respect to  $\mathbf{w}_{id}$  to be

$$\begin{aligned}\frac{\partial E}{\partial \mathbf{w}_{id}} &= \sum_{i=1}^N -\frac{2}{z_{avg}} \left( \frac{\partial \mathbf{P}_w \mathbf{R}[\mathbf{M}_{(1)}]_i \mathbf{Z}}{\partial \mathbf{w}_{id}} \right) \left( \mathbf{f}_i - \frac{1}{z_{avg}} \mathbf{P}_w \mathbf{R}[\mathbf{M}_{(1)}]_i \mathbf{Z} - \frac{1}{z_{avg}} \mathbf{P}_w \mathbf{t} \right) \\ &= \sum_{i=1}^N -\frac{2}{z_{avg}} \underbrace{\left( \mathbf{U}_{id} (\mathbf{I}_{I_{id}} \otimes \mathbf{w}_{exp}^T \mathbf{U}_{exp}) [\mathbf{M}_{(1)}]_i^T \mathbf{R}^T \mathbf{P}_w^T \right)}_{\mathbf{H}_i^T} \left( \mathbf{f}_i - \frac{1}{z_{avg}} \mathbf{P}_w \mathbf{R}[\mathbf{M}_{(1)}]_i \mathbf{Z} - \frac{1}{z_{avg}} \mathbf{P}_w \mathbf{t} \right) \\ &= \frac{2}{z_{avg}} \sum_{i=1}^N \left( \mathbf{H}_i^T \frac{1}{z_{avg}} \mathbf{P}_w \mathbf{R}[\mathbf{M}_{(1)}]_i \mathbf{Z} \right) - \frac{2}{z_{avg}} \sum_{i=1}^N \mathbf{H}_i^T \left( \mathbf{f}_i - \frac{1}{z_{avg}} \mathbf{P}_w \mathbf{t} \right) \\ &= \frac{2}{z_{avg}^2} \sum_{i=1}^N \left( \mathbf{H}_i^T \underbrace{\mathbf{P}_w \mathbf{R}[\mathbf{M}_{(1)}]_i (\mathbf{I}_{I_{id}} \otimes \mathbf{U}_{exp}^T \mathbf{w}_{exp}) \mathbf{U}_{id}^T}_{\mathbf{H}_i} \mathbf{w}_{id} \right) - \frac{2}{z_{avg}} \sum_{i=1}^N \mathbf{H}_i^T \left( \mathbf{f}_i - \frac{1}{z_{avg}} \mathbf{P}_w \mathbf{t} \right) \\ &= \frac{2}{z_{avg}^2} \sum_{i=1}^N (\mathbf{H}_i^T \mathbf{H}_i \mathbf{w}_{id}) - \frac{2}{z_{avg}} \sum_{i=1}^N \mathbf{H}_i^T \left( \mathbf{f}_i - \frac{1}{z_{avg}} \mathbf{P}_w \mathbf{t} \right)\end{aligned}$$

To find the optimal identity parameters  $\mathbf{w}_{id}^*$  which minimize the error function we set this derivative to zero to obtain the system of equations

$$\begin{aligned}\frac{2}{z_{avg}^2} \sum_{i=1}^N (\mathbf{H}_i^T \mathbf{H}_i \mathbf{w}_{id}^*) - \frac{2}{z_{avg}} \sum_{i=1}^N \mathbf{H}_i^T \left( \mathbf{f}_i - \frac{1}{z_{avg}} \mathbf{P}_w \mathbf{t}^* \right) &= 0 \\ \frac{2}{z_{avg}^2} \sum_{i=1}^N (\mathbf{H}_i^T \mathbf{H}_i \mathbf{w}_{id}^*) &= \frac{2}{z_{avg}} \sum_{i=1}^N \mathbf{H}_i^T \left( \mathbf{f}_i - \frac{1}{z_{avg}} \mathbf{P}_w \mathbf{t}^* \right) \\ \frac{1}{z_{avg}} \sum_{i=1}^N (\mathbf{H}_i^T \mathbf{H}_i \mathbf{w}_{id}^*) &= \sum_{i=1}^N \mathbf{H}_i^T \left( \mathbf{f}_i - \frac{1}{z_{avg}} \mathbf{P}_w \mathbf{t}^* \right)\end{aligned}$$

This system of equations can be written in matrix form as

$$\frac{1}{z_{avg}} \mathbf{H}^T \mathbf{H} \mathbf{w}_{id}^* = \mathbf{H}^T \left( \mathbf{f} - \frac{1}{z_{avg}} \mathbf{P}_w \mathbf{t}^* \right) \quad (3.40)$$

with

$$\mathbf{H} = \begin{pmatrix} \mathbf{H}_1 \\ \mathbf{H}_2 \\ \vdots \\ \mathbf{H}_N \end{pmatrix} \quad \text{and} \quad \mathbf{f} = \begin{pmatrix} \mathbf{f}_1 \\ \mathbf{f}_2 \\ \vdots \\ \mathbf{f}_N \end{pmatrix} \quad (3.41)$$

The solution of this system of equations in matrix form is the optimal identity parameter vector  $\mathbf{w}_{id}^*$  which is given by

$$\mathbf{w}_{id}^* = z_{avg}(\mathbf{H}^T \mathbf{H})^{-1} \mathbf{H}^T (\mathbf{f} - \frac{1}{z_{avg}} \mathbf{P}_w \mathbf{t}^*) \quad (3.42)$$

with

$$\mathbf{H}_i = \mathbf{P}_w \mathbf{R}^* [\mathbf{M}_{(1)}]_i (\mathbf{I}_{I_{id}} \otimes \mathbf{U}_{exp}^T \mathbf{w}_{exp}^*) \mathbf{U}_{id} \quad (3.43)$$

The optimal expression parameter vector  $\mathbf{w}_{exp}^*$  is obtained in the same manner by setting the derivative of the error function with respect to  $\mathbf{w}_{exp}^*$  to zero. The result is

$$\mathbf{w}_{exp}^* = z_{avg}(\mathbf{G}^T \mathbf{G})^{-1} \mathbf{G}^T (\mathbf{f} - \frac{1}{z_{avg}} \mathbf{P}_w \mathbf{t}^*) \quad (3.44)$$

with

$$\mathbf{G}_i = \mathbf{P}_w \mathbf{R}^* [\mathbf{M}_{(1)}]_i (\mathbf{U}_{id}^T \mathbf{w}_{id}^* \otimes \mathbf{I}_{I_{exp}}) \mathbf{U}_{exp} \quad (3.45)$$

From equations 3.42 and 3.44 we see that solving for the optimal parameters reduces to a system of nonlinear equations. Both the  $\mathbf{w}_{exp}^*$  and  $\mathbf{w}_{id}^*$  depend on the other optimal parameter vector as well as on the optimal rotation matrix  $\mathbf{R}^*$  and the optimal translation vector  $\mathbf{t}^*$ , which are likewise obtained by setting the respective derivative to zero. The resulting nonlinear system may be solved using a Newton or quasi-Newton optimization method to obtain approximations to these optimal solutions.

**Coordinate-Descent Method** Instead of approximating the solution using a Newton optimization method, it is possible to linearize the nonlinear system by fixing each of the parameters except for one to their current guesses. Only the one free parameter is thereby allowed to vary. The resulting linear system is then solved to give a new guess for the free parameter. In the next iteration, this free parameter is then fixed to this new guess and the process is restarted on one of the other parameters. The cycle is repeated until convergence. This approach is known as minimization by coordinate descent [27]. Coordinate-descent was also used by Vlasic et al in [40] to approximate the optimal parameters of a tensor model during each iteration of the Kanade-Lucas feature tracker.

Newton's method may not converge if the starting point is far from the optimum. Therefore to avoid using the Newton's method on a nonlinear system, we minimize the expression transfer error function (3.32) using a coordinate-descent method which combines the equations 3.42, 3.44 with the POSIT algorithm discussed in section 2.2.3. An implementation of the POSIT algorithm is available in OpenCV as the function `solvePnP()`. As arguments, the function requires a camera matrix, a set of image feature points and the corresponding model points which can be generated from the model identity and expression parameters using equation 3.21.

The optimization algorithm is initialized with a guess for the model parameters  $\mathbf{w}_{exp}$  and  $\mathbf{w}_{id}$  which correspond to a realistic face. Using this guess, the POSIT algorithm estimates a rotation matrix and a translation vector. Given the estimated 3D pose, first the expression is updated using equation 3.44. Then the updated guess for  $\mathbf{w}_{exp}$  is used to solve equation 3.42 to give a new guess for the identity parameters  $\mathbf{w}_{id}$ . The updated model parameters are used to generate a new face using equation 3.21. The updated face is then used to update the 3D pose using the POSIT algorithm, completing one iteration of the algorithm. The iterations are repeated until convergence. The values  $\hat{\mathbf{w}}_{exp}$ ,  $\hat{\mathbf{w}}_{exp}$ ,  $\hat{\mathbf{R}}$  and  $\hat{\mathbf{t}}$  of the parameters at convergence approximate the values of the optimal parameters.

One issue with this approach lies in the average depth  $z_{avg}$ . The value of  $z_{avg}$  must be an average of the rotated and translated object's depth. This value is therefore only available once both the 3D pose and the model parameters have been computed.

There are two ways to deal with the  $z_{avg}$  problem. One way is to assume that  $z_{avg}$  is just another parameter of the model and then update it during the coordinate descent minimization until at termination the sequence of  $z_{avg}$  guesses converges to the true average depth. The  $z_{avg}$  guess is easily obtained after performing the POSIT update by averaging the rotated and translated generated points.

The second approach is to move the  $z_{avg}$  into the model parameters. Since the average depth is a constant we can simply scale the model parameters with this constant to obtain the scaled parameters  $\tilde{\mathbf{w}}_{exp}^*$ ,  $\tilde{\mathbf{w}}_{id}^*$  as

$$\tilde{\mathbf{w}}_{exp}^* = \frac{1}{z_{avg}} \mathbf{w}_{exp}^* \quad \text{and} \quad \tilde{\mathbf{w}}_{id}^* = \frac{1}{z_{avg}} \mathbf{w}_{id}^*$$

We then attempt to approximate these scaled model parameters during the coordinate-descent without needing to worry about average depth.

The advantage of the second approach is that it decreases the number of steps in the algorithm. However, the disadvantage is that the scaled parameter vector may be scaled with perhaps a negative value which may cause difficulties during constrained optimization when constraints are enforced on the parameter vectors. To keep the optimization as general as possible the expression transfer application therefore utilizes the first approach.

The expression transfer coordinate-descent method for one frame is thus

---

**Algorithm 4** Coordinate-descent for one frame

---

```

1: procedure COORDDESC( $f_1, \dots, f_N, [\mathbf{M}_{(1)}]_1 \dots, [\mathbf{M}_{(1)}]_N, \mathbf{P}_w$ )
2:   Output  $\hat{\mathbf{w}}_{id}$ ,  $\hat{\mathbf{w}}_{exp}$ ,  $\hat{\mathbf{R}}$  and  $\hat{\mathbf{t}}$ 
3:   Initialization  $\hat{\mathbf{w}}_{id} = [0, 0, \dots, 1, \dots, 0]^T$ ,  $\hat{\mathbf{w}}_{exp} = [0, 0, \dots, 1, \dots, 0]^T$ 
4:   repeat
5:      $\mathbf{X} = \mathbf{M}_{(1)}(\mathbf{w}_{id} \otimes \mathbf{w}_{exp})$ 
6:      $\hat{\mathbf{R}}, \hat{\mathbf{t}} \leftarrow \text{opencv.solvePnP}(f_1, \dots, f_N, \mathbf{X}, \mathbf{P}_w)$ 
7:
8:      $z_{avg} \leftarrow \text{z-mean}(\hat{\mathbf{R}}\mathbf{X} + \hat{\mathbf{t}})$ 
9:
10:     $\mathbf{G}_i = \mathbf{P}_w \hat{\mathbf{R}} [\mathbf{M}_{(1)}]_i (\mathbf{U}_{id}^T \hat{\mathbf{w}}_{id} \otimes \mathbf{I}_{I_{exp}}) \mathbf{U}_{exp}$ 
11:     $\mathbf{G} \leftarrow \text{stack-horizontally}(\mathbf{G}_i)$ 
12:
13:     $\hat{\mathbf{w}}_{exp} = z_{avg} (\mathbf{G}^T \mathbf{G})^{-1} \mathbf{G}^T (\mathbf{f} - \frac{1}{z_{avg}} \mathbf{P}_w \hat{\mathbf{t}})$ 
14:
15:     $\mathbf{H}_i = \mathbf{P}_w \hat{\mathbf{R}} [\mathbf{M}_{(1)}]_i (\mathbf{I}_{I_{id}} \otimes \mathbf{U}_{exp}^T \hat{\mathbf{w}}_{exp}) \mathbf{U}_{id}$ 
16:     $\mathbf{H} \leftarrow \text{stack-horizontally}(\mathbf{H}_i)$ 
17:
18:     $\hat{\mathbf{w}}_{id} = z_{avg} (\mathbf{H}^T \mathbf{H})^{-1} \mathbf{H}^T (\mathbf{f} - \frac{1}{z_{avg}} \mathbf{P}_w \hat{\mathbf{t}})$ 
19:   until stopping criteria fulfilled
20: end procedure

```

---

### 3.5.5 Overfitting

As pointed out earlier the generative model only generates realistic representations of a face when the model parameters are within several standard deviations of the mean. In [4], [23] the model parameters are constrained to be in the range of  $\pm 3$  standard deviations for the PCA based model. However, the upper and lower bound are not known in the tensor-based shape model utilized by the expression transfer application.

So that the application generates believable results, the optimization through coordinate-descent should find only model parameters that represent a realistic face. The optimal parameters  $\mathbf{w}_{exp}^*$ ,  $\mathbf{w}_{id}^*$ ,  $\mathbf{R}^*$  and  $\mathbf{t}^*$  obtained through minimization of the error function may not be realistic. This is due to the fact that the model may not be able to generate any arbitrary face if it is not present in the database. The model can only build linear combinations of the faces in the database. A face present in the image may not be obtainable as this linear combination. In such a case the optimal model parameters which minimize the error will therefore not be the parameters of the optimal face. Instead they will be the parameters of the one shape which minimizes the error for

the feature points  $f_1, \dots, f_N$ . If this shape is more than a few standard deviations from the mean it not resemble a face.

This problem is well known to machine learning where it is known as *overfitting*. The minimization finds the parameters of a shape which is too specific, because it minimizes the error for a specific set of feature points. However, since the model parameters are too specific they cause a large error for other points on the image which were not used to fit the model.

The model fitting algorithm should therefore be *general* enough so that the obtained model parameters minimize the error function not only for the feature points used during the fitting stage, but also for any arbitrary point on the face. This can be achieved trivially by increasing the number of feature points. Such an approach is, however, error prone since it is not always clear how many points is enough to make the fitting general.

The expression transfer application supports two techniques which ensure that the fitting algorithm generates realistic faces. They are *regularization* and *constrained minimization*.

**Regularization.** As discussed, unrealistic faces are produced when the model parameters are far from the mean. To manipulate the minimization to prefer parameters which are close to the mean we can add a regularization term to the error function. A reasonable choice for this term is one which penalizes the distance of the parameters from their respective mean. The augmented error function is then given by

$$E = \sum_{i=1}^N \left\| \mathbf{f}_i - \frac{1}{z_{avg}} \mathbf{P}_w \mathbf{R} [\mathbf{M}_{(1)}]_i (\mathbf{U}_{id}^T \mathbf{w}_{id} \otimes \mathbf{U}_{exp}^T \mathbf{w}_{exp}) + \mathbf{t} \right\|^2 + \frac{\lambda}{2} \left\| \begin{array}{l} \mathbf{w}_{id} - \bar{\mathbf{w}}_{id} \\ \mathbf{w}_{exp} - \bar{\mathbf{w}}_{exp} \end{array} \right\|^2 \quad (3.46)$$

where  $\bar{\mathbf{w}}_{exp}$  is the mean expression parameter vector and  $\bar{\mathbf{w}}_{id}$  the mean identity parameter vector. The parameter  $\lambda$  is the regularization parameter. By increasing  $\lambda$  the fitting algorithm is made more general, by decreasing  $\lambda$  it is made more specific.

Setting the partial derivatives with respect to identity and expression of 3.46 to zero and solving gives us the following update equations for the model parameters

$$\mathbf{w}_{id}^* = z_{avg} (\mathbf{H}^T \mathbf{H} + \lambda \mathbf{I}_{id})^{-1} \mathbf{H}^T (\mathbf{f} - \frac{1}{z_{avg}} \mathbf{P}_w \mathbf{t}^*) + \lambda z_{avg} \bar{\mathbf{w}}_{id} \quad (3.47)$$

$$\mathbf{w}_{exp}^* = z_{avg} (\mathbf{G}^T \mathbf{G} + \lambda \mathbf{I}_{exp})^{-1} \mathbf{G}^T (\mathbf{f} - \frac{1}{z_{avg}} \mathbf{P}_w \mathbf{t}^*) + \lambda z_{avg} \bar{\mathbf{w}}_{exp} \quad (3.48)$$

with the matrices  $\mathbf{H}$  and  $\mathbf{G}$  unchanged.

**Constrained Optimization.** Regularization suffers from the fact that the optimal value of regularization parameter  $\lambda$  must be found either manually by the user or using prior knowledge about the distribution of the parameters. Ideally, we would like to obtain a technique that does not depend on the value of  $\lambda$ .

The fundamental problem is that the linear combination of the original face scans may generate non-realistic faces. However, with a linear interpolation of the original faces it is always the case that a realistic face is generated. This is because linear interpolation produces faces from the convex hull spanned by faces in the database. At the center of this convex hull is the mean. On the sides, the hull is bounded by the original faces. Therefore any face inside this hull consists of points which are interpolations of the points on the original faces. With linear interpolation the fitting algorithm is able to generate realistic faces without needing to resort to regularization.

To ensure that we obtain a linear interpolation we must enforce constraints on the model parameters. For both the identity and the expression parameter vector it must hold that all the components are greater or equal to zero and that they sum to one. The constrained minimization

problem that the fitting algorithm must solve is therefore given by

$$\text{minimize}_{\mathbf{w}} \quad \sum_{i=1}^N \left\| \mathbf{f}_i - \frac{1}{z_{avg}} \mathbf{P}_w \mathbf{R}[\mathbf{M}_{(1)}]_i (\mathbf{U}_{id}^T \mathbf{w}_{id} \otimes \mathbf{U}_{exp}^T \mathbf{w}_{exp}) + \mathbf{t} \right\|^2 \quad (3.49)$$

$$\text{subject to} \quad \sum_{i=1}^{I_{id}} w_{id_i} = 1 \quad (3.50)$$

$$\sum_{i=1}^{I_{exp}} w_{exp_i} = 1 \quad (3.51)$$

$$w_{id_i} \geq 0 \quad i = 1, \dots, I_{id} \quad (3.52)$$

$$w_{exp_i} \geq 0 \quad i = 1, \dots, I_{exp} \quad (3.53)$$

Constrained minimization of a nonlinear function is a difficult task. It involves setting up the Karush-Kuhn-Tucker conditions or the Lagrangian function and taking the derivatives. We can, however, solve the problem using the Nelder Mead downhill simplex discussed in section 2.4.2. The downhill simplex method does not require the derivatives. It finds the minimum by evaluating the function at specific points in order to move towards the minimum.

To solve a constrained optimization problem the downhill simplex method needs to be augmented. The simplest way to do this is to make the function evaluation return infinity when the constraints are not satisfied.

The drawback of the downhill simplex method is that it usually performs a large number of function evaluations. However, every evaluation amounts to computing the error function for all feature points. The downhill simplex method is thus not very efficient.

Experimentation showed that unrealistic faces are generated only when the non-negativity constraints 3.52 and 3.53 are violated. When the constraints which ensure the sum are violated then the resulting face is merely larger but still a realistic representation. We can therefore ensure that the fitting algorithm produces only realistic faces by solving the minimization problem 3.49 given only the non-negativity conditions. The simplified constrained optimization problem is therefore

$$\text{minimize}_{\mathbf{w}} \quad \sum_{i=1}^N \left\| \mathbf{f}_i - \frac{1}{z_{avg}} \mathbf{P}_w \mathbf{R}[\mathbf{M}_{(1)}]_i (\mathbf{U}_{id}^T \mathbf{w}_{id} \otimes \mathbf{U}_{exp}^T \mathbf{w}_{exp}) + \mathbf{t} \right\|^2 \quad (3.54)$$

$$\text{subject to} \quad w_{id_i} \geq 0 \quad i = 1, \dots, I_{id} \quad (3.55)$$

$$w_{exp_i} \geq 0 \quad i = 1, \dots, I_{exp} \quad (3.56)$$

This makes it possible to update the identity and expression model parameters at every iteration of the coordinate descent algorithm using the Sequential Coordinate-wise Non-negativity Least Squares Algorithm introduced in 2.4.1.

The reason why only non-negative parameters produce unrealistic faces is most likely due to the fact that during the linear combination only a subtraction of faces can produce the zero vector. The null space of the data tensor thus spans only the negative parameter space.

It is entirely possible to generate some realistic faces even when the non-negativity conditions are violated, so by enforcing these constraints the model loses expressive power. However, it is impossible to generate an unrealistic face when they are satisfied, which warrants enforcing the non-negativity constraints.

### 3.5.6 Fitting Algorithm

Before the complete fitting algorithm can be established two problems need to be addressed.

**Multi-Frame Coordinate Descent.** First of all the coordinate descent algorithm discussed so far was designed to optimize the parameters for just one frame. The fitting algorithm should, however, find the identity and the expressions of a person by examining a sequence of frames.

As an additional constraint, the identity parameters should stay the same in all frames since the identity of the person in the video sequence should not change. In the multi-frame coordinate descent algorithm we therefore first find the expression parameters for every frame using a guess for the identity parameters. Then we use the feature points and the estimated expression parameter vectors collected from all frames to solve for the identity parameters. This process can then be iteratively repeated until convergence.

**Feature point generation.** The second problem concerns the feature points. To find a reasonable approximation of the expression in the video sequence, it is necessary to use a large number of feature points. The user cannot be expected to enter that many points. The algorithm must therefore be able to generate a number of new points to use in addition to the feature points specified by the user. These points cannot be picked just randomly, they must correspond to known points on the model so that they can be used in the error function.

The task is thus to generate feature points which correspond to known points on the model. This can be done by either selecting new 3D points on the model and projecting them to generate the new feature points in the image, or inversely by selecting points in the 2D image and reprojecting them into 3D. When points are projected from the model the correspondence is already given. When they are reprojected from the image into 3D then the corresponding 3D point to the 2D image is chosen to be the 3D point on the model which is closest in terms of Euclidean distance to the reprojected point.

To establish the correspondence in this manner the camera matrix and the 3D pose need to be known. These define the projection from object coordinate space into image space. When using a weak-perspective camera model, this projection can be inverted to give the reprojection from image space into object coordinate space. Likewise, it is necessary to know the shape of the face in 3D space. This shape is generated using the expression and identity parameters. So to be able to generate new points with known correspondences we require all the unknown parameters we are attempting to find. This is clearly a problem. The best approach is to find the 3D pose and model parameters of the first frame by means of optimization using only the small number of user provided feature points. These rough estimations of the parameters can then be used to generate more points with known correspondences which are then tracked using optical flow and used in the error function of the following frames. Finding these parameter estimates for the first frame is known as *first frame alignment*.

The first frame alignment approach to generating new feature points raises an important issue. The problem lies in the fact that an estimate of the model parameters and 3D pose is used to generate most of the feature points. These are later utilized to minimize the error. Thus, it is clear that with each and every newly generated point we are influencing our result. The error for every point that was generated using the estimates is of course minimized exactly when the parameters assume the values of the model and 3D pose parameter estimates. Fortunately, the fitting algorithm utilizes information obtained from the movement of these tracked points not from their static position. Therefore, as long as the reprojected point is not static and at least close enough to the true model point, then this reprojected point still supports the correct model parameters even though it does not correspond to the true 3D model point. For the reprojection to be close enough it is necessary to have a good estimate of the rotation matrix and the translation vector. This is because the rotation and translation account for most of the movement of points in 3D. The variation due to the model parameters is small in comparison.

**Expression Transfer Fitting Algorithm.** Given are  $N$  image feature points  $f_1, \dots, f_N$ , the calibrated weak perspective camera matrix  $\mathbf{P}_w$  and the regularization parameter  $\lambda$ . To fit the tensor-based shape model to these point the parameters  $\mathbf{w}_{id}$ ,  $\mathbf{w}_{exp}$ ,  $\mathbf{R}$  and  $\mathbf{t}$  are located as follows

- **Step 1.** Calculate the first frame alignment using the single frame coordinate descent algorithm 3.5.4 optimizing with regularization for the  $N$  feature points  $f_1, \dots, f_N$  to obtain initial estimates of  $\mathbf{w}_{id}$ ,  $\mathbf{w}_{exp}$ ,  $\mathbf{R}$  and  $\mathbf{t}$ .

- **Step 2.** Generate new  $M$  points using the 3D pose and model parameters. Do this by uniformly sampling points in the 2D image around important feature like the mouth and the eyebrows to obtain new feature points  $f_{N+1}, \dots, f_{N+M}$ . Then reproject these points into 3D to obtain 3D points  $p_{N+1}, \dots, p_{N+M}$  using

$$p_i = \mathbf{R}^T(\mathbf{P}_w^{-1}f_i - \mathbf{t})$$

utilizing the parameters obtained through first frame alignment. Finally establish correspondences to model points by finding the closest 3D model point  $m_i$  to the point  $p_i$  using Euclidean distance.

- **Step 3.** Track the  $N + M$  point using the Kanade-Lucas feature tracker (OpenCV function `calcOpticalFlowPyrLK()`), dropping lost points, to obtain  $R_i \leq N + M$  image feature points in every  $i$ -th frame.
- **Step 4.** Perform the multi-frame coordinate descent algorithm by repeating
  - **Step 5.** Update the 3D pose estimates for every frame using the POSIT algorithm (OpenCV function `solvePnP()`).
  - **Step 6.** Update the expression parameter vector estimate for every frame using

$$\mathbf{w}_{exp} = z_{avg}(\mathbf{G}^T\mathbf{G} + \lambda\mathbf{I}_{exp})^{-1}\mathbf{G}^T(\mathbf{f} - \frac{1}{z_{avg}}\mathbf{P}_w\mathbf{t}) + \lambda z_{avg}\bar{\mathbf{w}}_{exp}$$

with

$$\mathbf{G}_i = \mathbf{P}_w\mathbf{R}[\mathbf{M}_{(1)}]_i(\mathbf{U}_{id}^T\mathbf{w}_{id} \otimes \mathbf{I}_{I_{exp}})\mathbf{U}_{exp}$$

- **Step 7.** Collect the feature points from all frame and update the identity parameter vector using

$$\mathbf{w}_{id} = z_{avg}(\mathbf{H}^T\mathbf{H} + \lambda\mathbf{I}_{id})^{-1}\mathbf{H}^T(\mathbf{f} - \frac{1}{z_{avg}}\mathbf{P}_w\mathbf{t}) + \lambda z_{avg}\bar{\mathbf{w}}_{id}$$

with

$$\mathbf{H}_i = \mathbf{P}_w\mathbf{R}[\mathbf{M}_{(1)}]_i(\mathbf{I}_{I_{id}} \otimes \mathbf{U}_{exp}^T\mathbf{w}_{exp})\mathbf{U}_{id}$$

- **Step 8.** Until convergence

The above algorithm enforces realistic faces using regularization. To use constrained optimization instead, it is only necessary to change the update steps 6. and 7. so that the parameter vectors are updated using the Sequential Coordinate-wise Non-negativity Least Squares Algorithm given in 2.4.1.

## 3.6 Expression Transfer

Ideally, the expression transfer application should be able to seamlessly change the expressions of the individual in the target video with the expressions from the source video. This of course involves correctly generating the texture for the respective expressions. Since the tensor model we have constructed is a shape model and not an appearance model, it cannot be used to directly generate the correct texture. The shape model does, however, provide the application with an understanding of the source and target face. This understanding can be utilized to transfer the texture between the target subject in the 2D frames of the video.

The simplest way of transferring the texture between the two video sequences is to create a texture map of the target face and then map the texture onto the estimated 3D model of this face. The application can construct the texture map after all the model and pose parameters have been estimated by projecting all the model points into the image to obtain their image coordinates. The RGB values at these image coordinates make up the texture map's contents and

the image coordinates themselves can be used as the texture coordinates. Usually, this texture itself is captured from the first frame of the target video sequence. If the subject has a neutral expression in the first frame and a smiling expression is transferred onto him, then this will cause the original texture to contract and stretch to fit the new configuration of model points. It is clear that this approach alone cannot produce very realistic results.

However, we may utilize the information available about the target and source face shape to generate more realistic results. If the exact measurements of the source subject's smile and the size of the target's mouth are known then the texture of the source smile can be transferred into the target frame and blended with its surroundings. This blending has to be seamless so that the result appears believable.

**Poisson Cloning.** Realistic blending of images can be achieved using Poisson image editing techniques. The Poisson cloning method, described by Perez et al in [26], and Leyvand [20] allows for seamless cloning of regions between images. The method is based on the two observations. Firstly, it is known to psychologists [26] that second-order variations, rather than slow gradients of intensity, are most important perceptually. Secondly, a scalar function is uniquely defined by its Laplacian and the values at its boundary. Since the Laplacian of an image filters everything but the second order variations in intensity, we blend a region  $\Omega$  of a source image  $g$  into a target image  $f^*$  seamlessly by finding the Laplacian  $\Delta g$  over this region and solving an optimization problem to obtain the seamlessly cloned interior  $f$ . The minimization is performed over the region  $\Omega$ , constrained so that values at the region boundary ( $\partial\Omega$ ) match. The optimization problem is therefore

$$\min_f \iint_{\Omega} |\nabla f - \nabla g|^2 \quad \text{with} \quad f|_{\partial\Omega} = f^*|_{\partial\Omega} \quad (3.57)$$

The solution of this problem is given by the equation

$$\Delta f = \Delta g \text{ over } \Omega \quad \text{with} \quad f|_{\partial\Omega} = f^*|_{\partial\Omega} \quad (3.58)$$

This equation reduces to a sparse linear system of equations where the unknowns are the pixels values inside the region. It can be solved using a sparse linear equation solver.

The result of cloning two regions using Poisson image editing is shown in figure 3.5

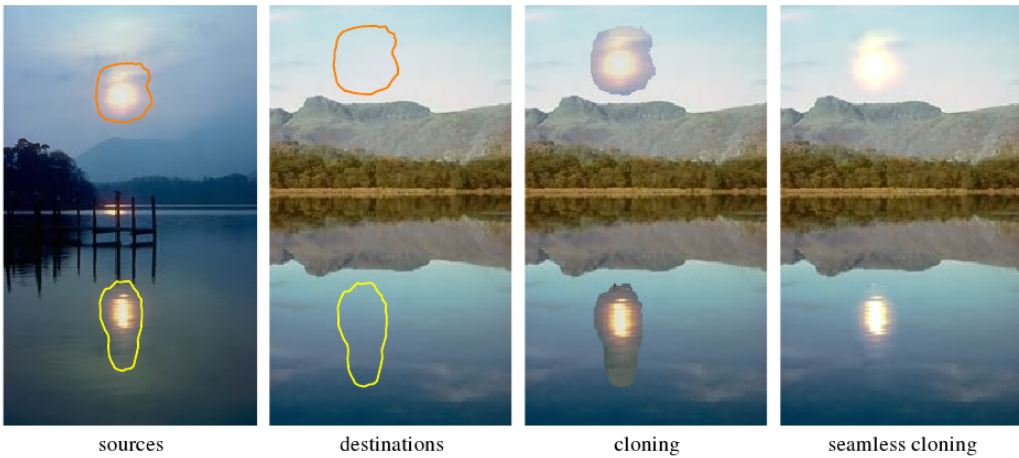


Figure 3.5: The seamless blending of regions into a target image using Poisson image editing.

**Expression transfer algorithm.** Having established how faces will be reanimated using textures, we can now summarize the expression transfer algorithm:

- **Step 1.** Apply the fitting algorithm to the **source** video sequence to obtain the identity, expression model parameters and the 3D pose parameters for every frame.

- **Step 2.** Apply the fitting algorithm to the **target** video sequence to obtain the identity, expression model parameters and the 3D pose parameters for every frame.
- **Step 3.** Compute a sequence of 3D faces using the identity parameters along with the 3D pose from the target and the expression parameter from the source. Each face in the sequence will share the identity parameter but will have different values for the expression and 3D pose parameters. These are the faces with transferred expressions.
- **Step 4.** For each frame.
  - Use the geometry and topology of the **source face** obtained in step 1 to find the mouth.
  - Use the geometry and topology of the **target face** obtained in step 2 to find the mouth.
  - Poisson clone the mouth from the source texture into the target texture using the size of the target face with the transferred expression as the region size.

## 3.7 System Architecture

The system architecture of the expression transfer application follows a model-view-controller (MVC) design. There are three conceptual layers – the view layer which is responsible for interacting with the user, the controller layer which processes the commands coming from the view and the model or data layer. The MVC architecture is depicted in figure 3.6

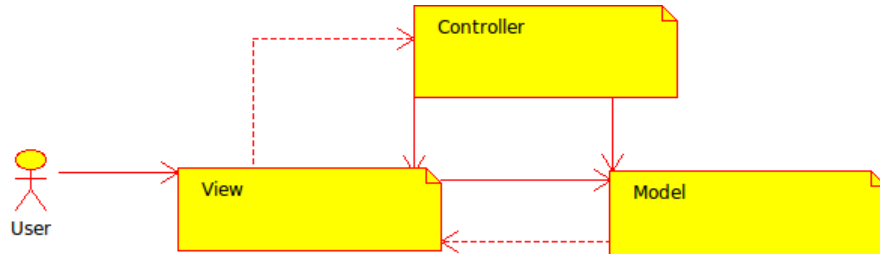


Figure 3.6: System architecture of the expression transfer application.

Each layer contains a number of classes and interfaces, chosen so that the coupling between layers is decreased and the cohesion inside the layer is increased.

### 3.7.1 View Layer

The view layer of the expression transfer application contains the classes which are responsible for user interface related tasks such as displaying the 3D model and providing interactive images for feature point selection. There are four crucial components in the expression transfer view layer. The OpenGL widget class, a class hierarchy of interactive images, the main window and the GUI.

**OpenGL widget** The expression transfer application needs to allow the user to view the estimated 3D model or to view the 3D face scans from the database. The GUI is build with Qt which supports OpenGL and provides the widget class `QGLWidget`. This widget class integrates with the OpenGL graphics interface and includes a canvas onto which objects can be rendered. The class implements three functions with protected visibility which can be overwritten in any class inheriting from `QGLWidget`. These functions are `initializeGL()`, `resizeGL()` and `paintGL()`. The first of these functions, `initializeGL()`, is called when the widget class is constructed to set up the rendering context. The function `resizeGL()` is called when the window which holds the widget is resized and should be overwritten so that it correctly sets the viewport and the projection parameters. The most important of the three function is `paintGL()` which controls the drawing of the scene.

In addition to the rendering functions, there are also useful public functions such as `bindTexture(.)` and `grabFrameBuffer(.)` to support adding texture or grabbing the frame buffer and returning it in form of an image.

The expression transfer application's view layer includes the class `FaceWidget` which extends the `QGLWidget`. The `FaceWidget` class overwrites the rendering functions of `QGLWidget` to allow for a 3D face scan to be displayed. The class also intercepts mouse events so that the object on the canvas can be rotated or enlarged.

Inheriting from `FaceWidget`, the class `CustomizableFaceWidget` makes it possible to load a custom projection matrix into OpenGL.

**Interactive Image Hierarchy** In a Qt based user interface, images are displayed using the `QLabel` class. Since the face transfer application needs to allow the user to select points on the image it is necessary to extend this base class. The main subclass which stores and displays clicked points is `ClickableQLabel`. This class is extended by `FeaturePointQLabel` which maps clicked points to corresponding 3D feature points and `VectorFieldQLabel` which is used to display an optical flow vector field.

**Main Window** The GUI is itself is encapsulated in a main window. In the expression transfer application the main window's functionality is implemented in the class `ExpTranWindow`. This class is responsible for all the GUI objects such as labels, OpenGL widgets and buttons. It also holds references to the controller layer and connects the signals emitted by the GUI objects to the appropriate controller objects.

**GUI** The graphical user interface is separated into three tabs. The face tab allows the user to view a 3D face model and change its expression and identity using sliders. The design for this tab is shown in figure 3.7

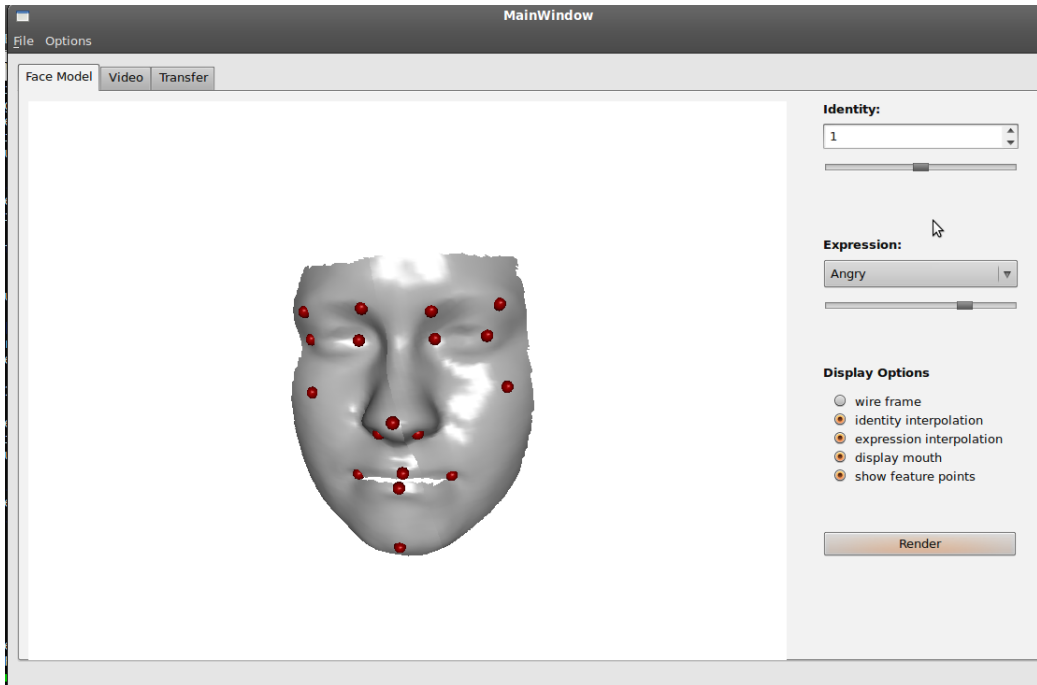


Figure 3.7: The face tab part of the GUI which allows the user to view and move the 3D face.

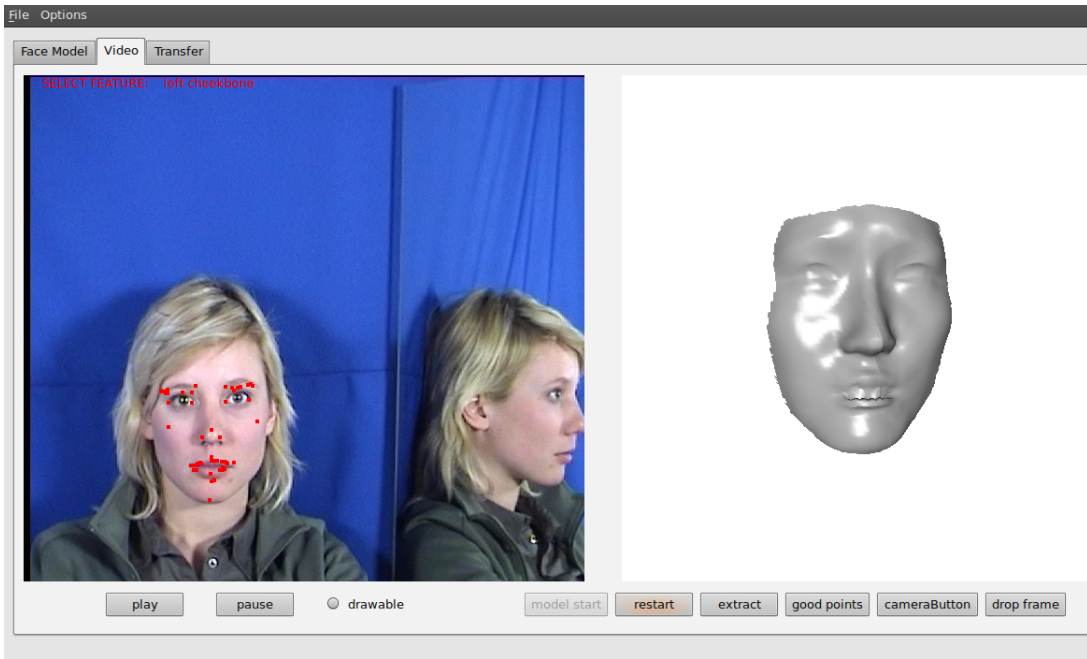


Figure 3.8: The video tab which provides model fitting and feature point tracking functionality.

The face tab also includes an options group which allows the user to customize how the face is displayed. The menu bar of the window contains a File and an Options drop down menu. Using the file menu the user can load a .VTK file containing a face object or a video file to use in the video tab.

The video tab processes the loaded video, providing functionality related to tracking points, extracting 3D pose and fitting the model to the video. The design of this tab is shown in figure 3.8

This tab contains a `ClickableQLabel` which represents the current frame of the video. Feature points can be selected on this frame. The OpenGL widget is then used to display the model which is extracted from the image.

The expression transfer functionality is provided in the transfer tab. This tab allows the user to load a source and a target video files needed for the expression transfer.

### 3.7.2 Model Layer

The model layer contains classes that participate in constructing and fitting the tensor based model. A diagram of the class hierarchy in this layer is depicted in figure 3.9

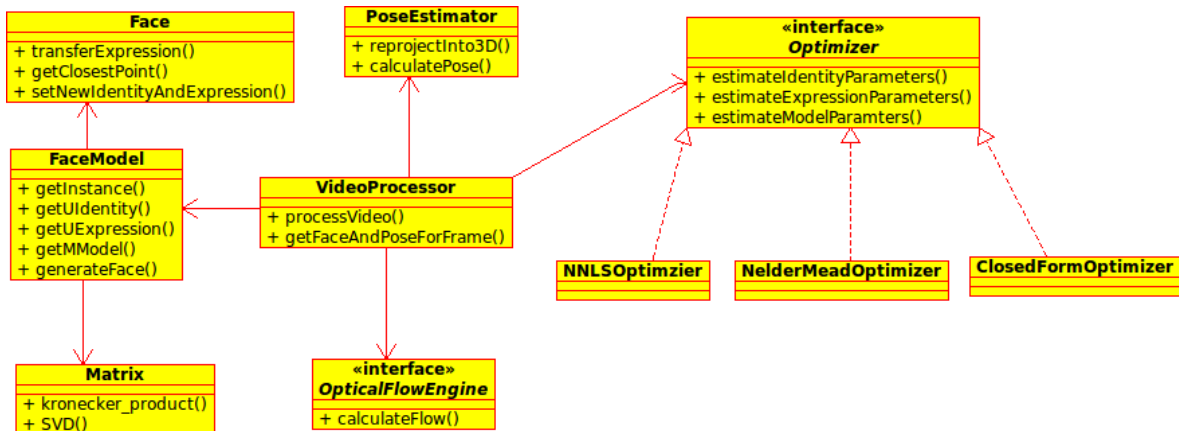


Figure 3.9: UML class diagram of the model layer.

The model layer can be divided based on responsibility into two parts. The first part is composed

of the classes which are used to construct the tensor model and generate new faces. The second part of the model layer is responsible for fitting the model to an image.

**Model Construction** The model construction algorithm is encapsulated in the persistable `FaceModel` class. Persistence means that the tensor model needs to be computed only once. After the initial computation the class persists the identity mode matrix, the expression mode matrix and the flattened multilinear model matrix in a file. When the application is started it will look for this file and if found it will load these matrices without having to recompute them.

The `FaceModel` class follows the singleton design pattern and stores a static instance of a `FaceModel` object. It also provides a function to obtain a reference to this static instance. By hiding its constructor, the class ensures that the only instance of the class at runtime will be the one static instance. The use of the singleton pattern makes the code more effective since the mode and model matrices are quite large and it would require a considerable amount of memory to have more than just one instance of the `FaceModel` class at any time.

The tensor model also provides a function to generate new faces given an identity and expression parameter vector.

The faces themselves are made up of a number of vertices and the identity and expression parameters. The application represents a face object using the `Face` class.

**Model Fitting** The model fitting algorithm discussed in paragraph 3.5.6 is implemented in the class `VideoProcessor`. To prevent blocking of the application during the computation of the fitting algorithm, the class extends `QThread` so that each processing of a video can be started in a separate thread.

A `VideoProcessor` object communicates with an `Optimizer` object, a `PoseEstimator` object and a `OpticalFlowEngine` object. The `Optimizer` provides an interface for model parameter estimation. This interface is implemented in a number of subclasses each of which applies a different optimization method to find the parameters. The `PoseEstimator` class reprojects points into 3D and calculates the 3D pose using the OpenCV implementation of the POSIT algorithm. The `OpticalFlowEngine` is an interface to a feature tracker algorithm. By default, the engine uses the OpenCV Kanade-Lucas feature tracker.

The communication between the classes during an invocation of the `VideoProcessor` thread is shown in figure 3.10

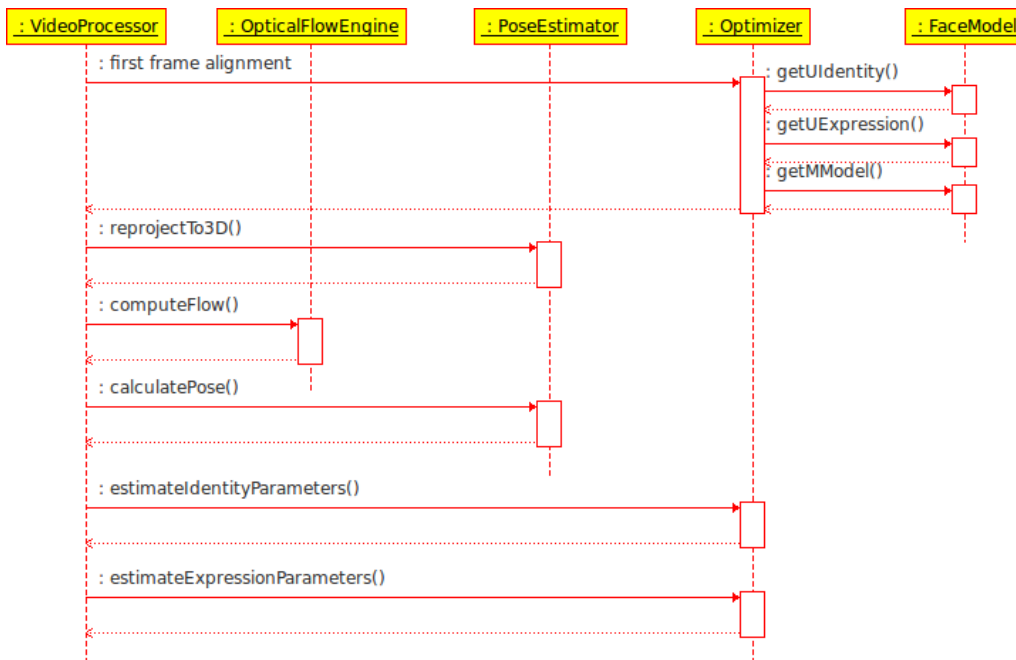


Figure 3.10: The sequence diagram showing an invocation of the `VideoProcessor` thread.

### 3.7.3 Controller Layer

The classes in the controller layer intercept signals and events from the GUI, process these requests and return the result to the view layer. There are three controller classes – one for each tab in the user interface. The `FaceTabController` reacts to movements of the sliders by calling the face generation functions from `FaceModel` and then updating the OpenGL widget. The `VideoTabController` starts `VideoProcessor` threads or computes the optical flow using the appropriate classes from the model layer. Finally, the `TransferTabController` provides functionality to transfer expression between two video files. It allows the user to load a source and a target video file and to start the expression transfer process which estimates the face model parameters, exchanges the expression and transfers texture.

# Chapter 4

## Results and Evaluation

The expression transfer application's performance depends heavily on the speed and accuracy of the fitting algorithm and the expressive power of the tensor model. This chapter presents results obtained from the application which can be analyzed to evaluate the performance of the tensor model and the fitting algorithm designed in chapter 4.

### 4.1 Face Generation

The model's power depends on its ability to generate a large variety of different faces. Since the tensor model generates novel faces from linear combinations of faces from the database its expressive power is limited by the shape variance inherent in the database. In the face tab of the GUI the user is allowed to explore this generative power of the model by altering the model parameters using GUI sliders. The original faces from the database can be recovered from the model by setting exactly one identity and one expression slider to one and the rest to zero.

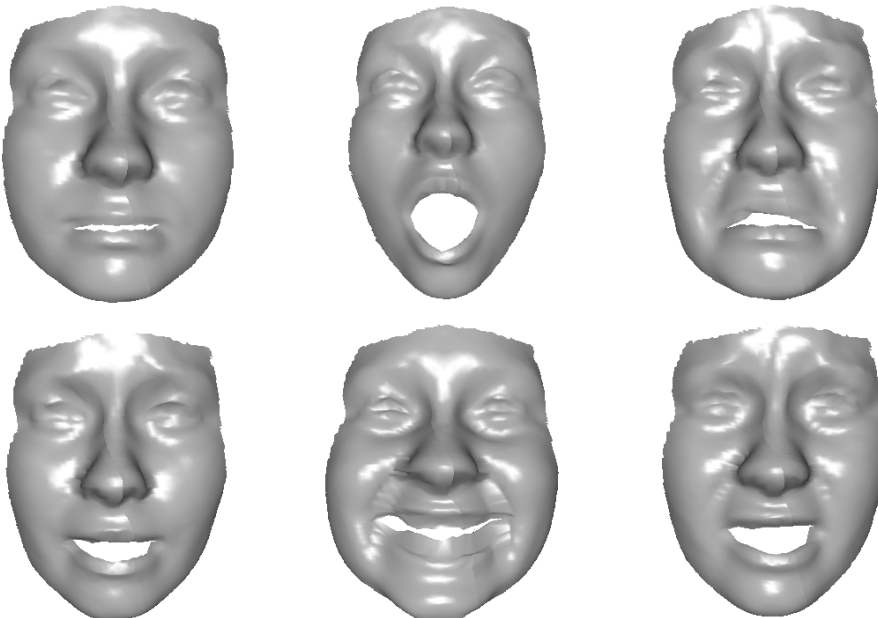
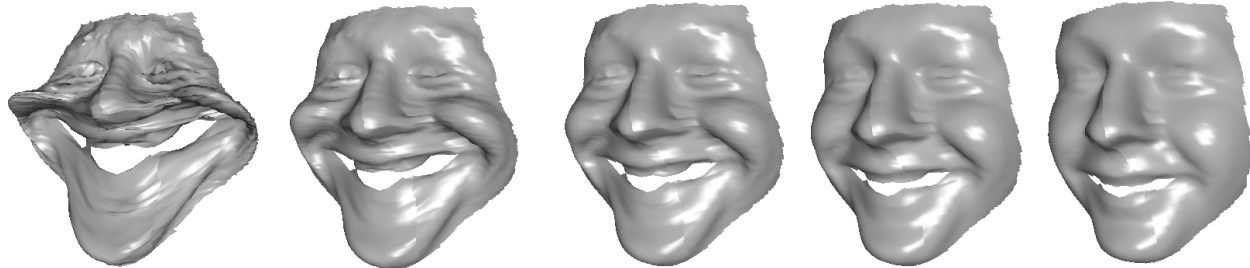


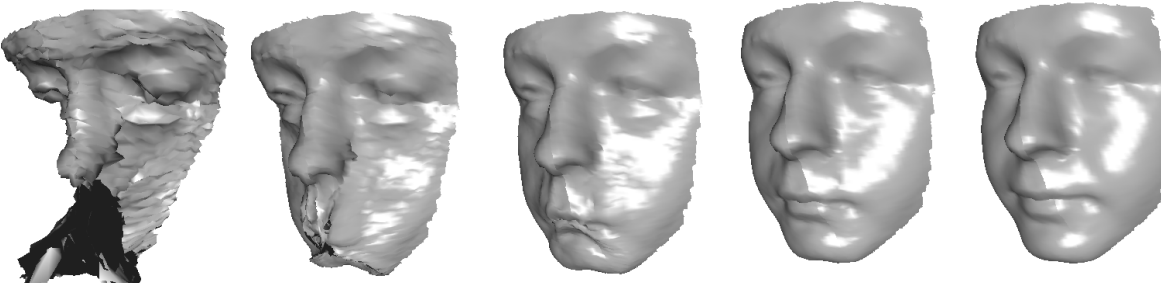
Figure 4.1: The graphic shows six expressions of the seven expressions present in the database. From left to right, top to bottom: neutral, surprise, sadness, fear, happiness and disgust.

The expression transfer can use the multilinear model to generate novel faces as linear combinations of original faces. The variance of the model is thus equivalent to the variance of the vertices

of which the original faces consist. The extent of the variance of a tensor model constructed from the Binghamton database is depicted in figure 4.2.



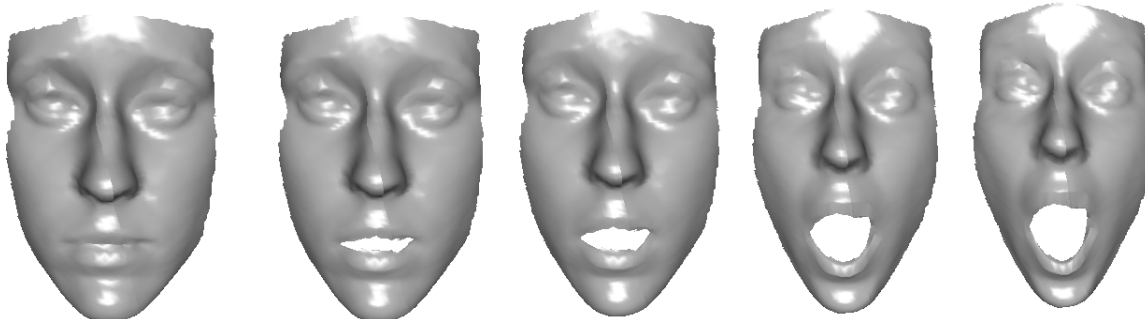
(a) Moving a happy face in the negative neutral direction from right to left.



(b) Moving a neutral face in the negative happy direction from right to left.

Figure 4.2: New expressions are generated by moving the points in the direction of one of the vectors of the expression mode matrices. This movement is mathematically equivalent to taking a linear combination.

From the results shown in figure 4.2 we can see that by subtracting too much of one expression from another it is possible to generate shapes which do not resemble faces. On the other hand, interpolating between faces always generates realistic faces since no coefficient in the linear combination can be negative. This means that faces are only added together and not subtracted from each other. Figure 4.3 shows experimental results for interpolating between the base 7 expressions (happy, neutral, angry, fear, sad, surprise, disgust).



(a) Interpolating between a neutral and surprised expression.

Figure 4.3: Generating new face through linear interpolation of the original faces.

The tensor model is well-suited for expression transfer applications since it to manipulates the identity and the expression of the subject separately. This is shown in figure 4.4, where we interpolate the identity between two subjects from the database first with a neutral expression and then with a happy expression.

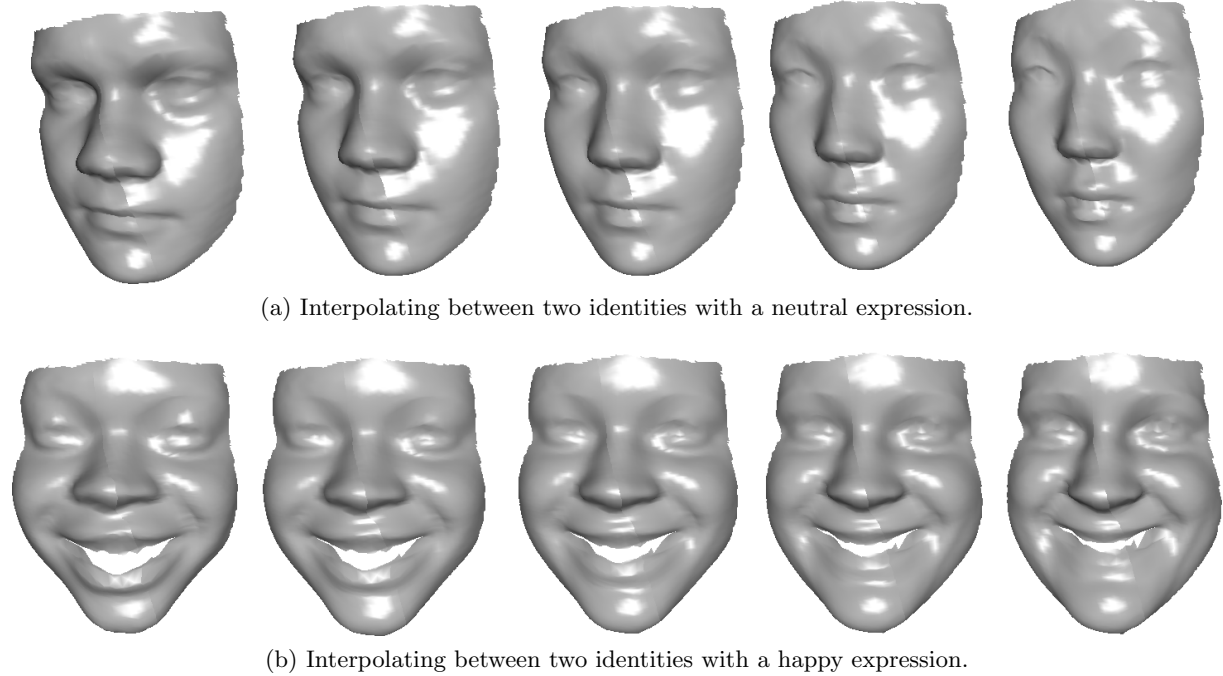


Figure 4.4: Linear interpolation between subjects from the Binghamton database.

The fitting algorithm finds the model parameters by minimizing the difference between projected model feature points and corresponding feature points in the image. For this approach to work the feature points on the model must move as they would on a real face. For the pre-processed Binghamton database this holds as can be seen in figure 4.5.

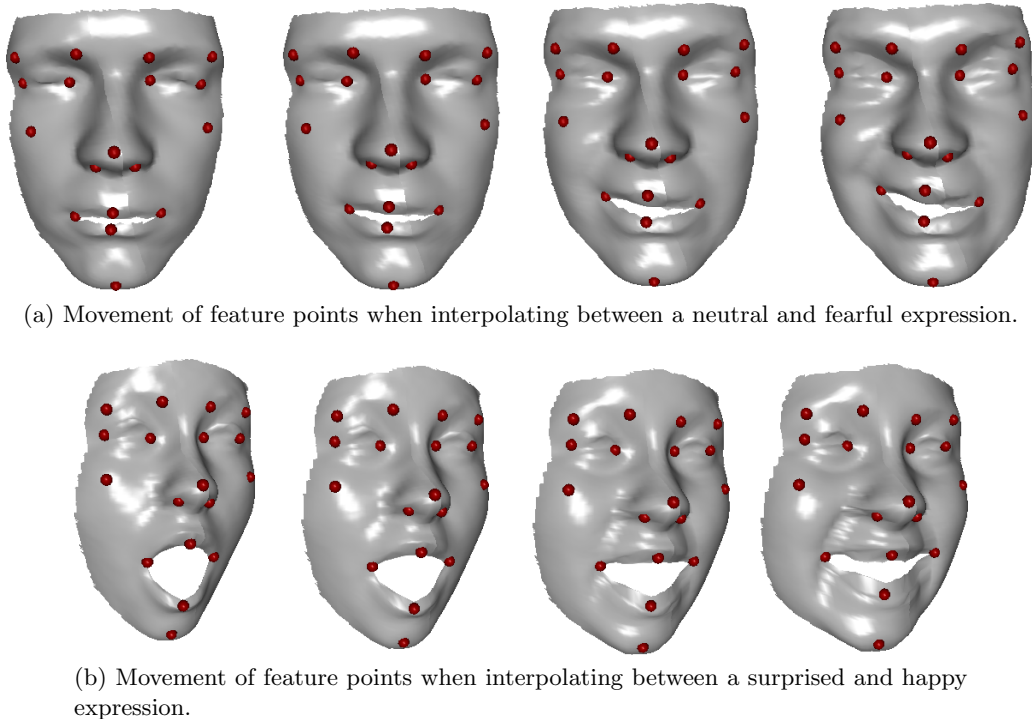


Figure 4.5: The movement of feature points (designated by red spheres).

In summary, the tensor based shape model allows the user to easily synthesise realistic expressions. Thereby, it is made possible for casual users and beginning animators to generate believable 3D models of faces. These models then allow the user to manipulate identity and expression sepa-

rately. The only requirement is that a database of face scans is necessary to construct the model. The generative power of the model depends only on the variance of the faces used to build to model.

## 4.2 Tracking Results

The most important part of the fitting algorithm is feature point tracking. Without identifying how the feature points are moving in the image, it is impossible to determine the correct expression and 3D pose during using the fitting algorithm. The task of tracking points becomes more difficult if there are changes in lighting in the image or if the object is moving very quickly. Likewise, points located in large areas of constant texture often drift away from their true positions.

The main parameter which affects the performance of the Kanade-Lucas feature point tracker is the window size. As discussed in section 2.3.1, the window size is the area around the point, the texture of which the tracker uses to determine the movement of the point. If the window size is chosen too small then points may jump around since the texture in the window is too small to be unique enough. Figure 4.6 shows the tracking of a moving face with a  $3 \times 3$  window size around every feature point.

If, on the other hand, the window size is chosen too large then small movements of points will be subdued. This happens because even though textures close to the point change, the ones far from the point may not and the evidence from the far off textures will outweigh the small contribution from the nearby textures. Figure 4.7 shows tracking with a  $50 \times 50$  window size. It can be seen that although points are not jumping anymore, the smile and the eyebrows do not move as much as the actual pixels of the image.

The fitting algorithm of the expression transfer application uses a  $15 \times 15$  window size. This window size provided the best results with our test videos. An example is shown in figure 4.8.

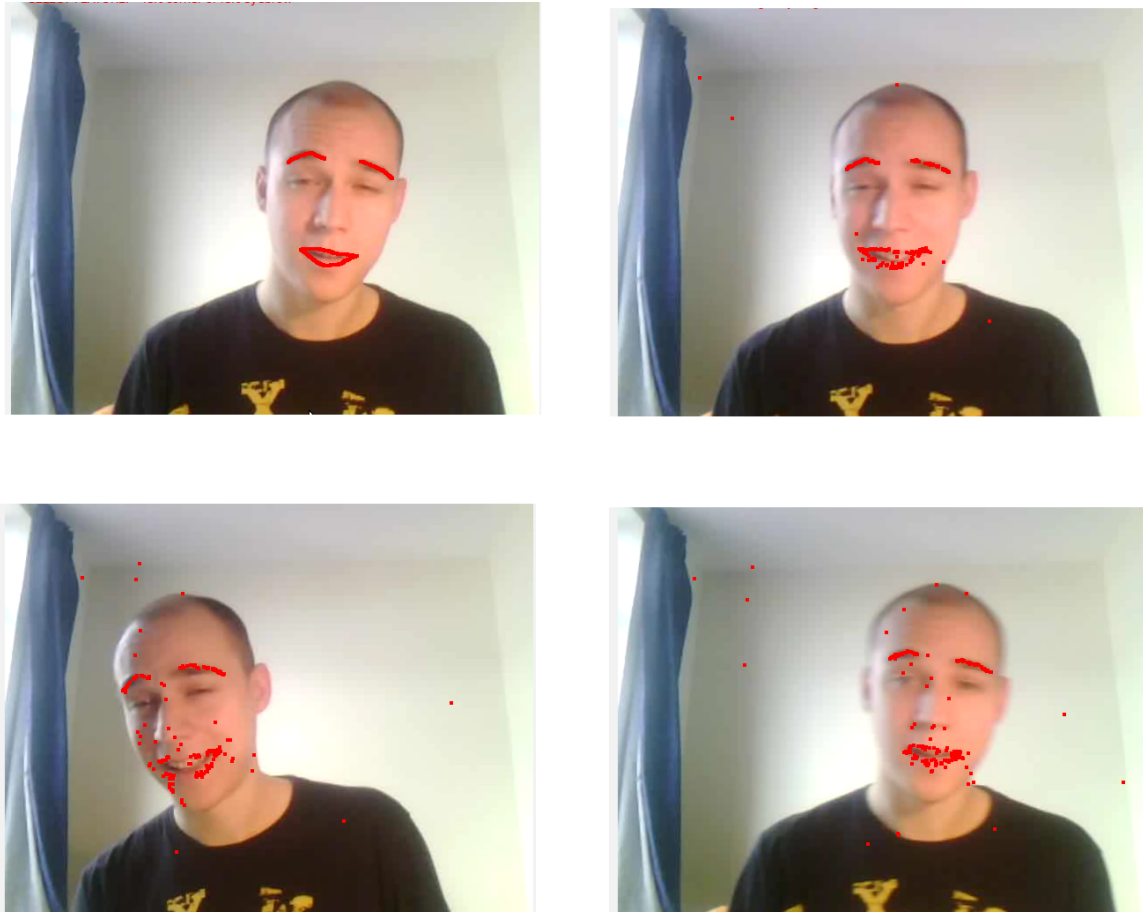


Figure 4.6: Tracking of feature point using a  $3 \times 3$  window size. A large number of feature points jump into incorrect positions, since the window size is too small.

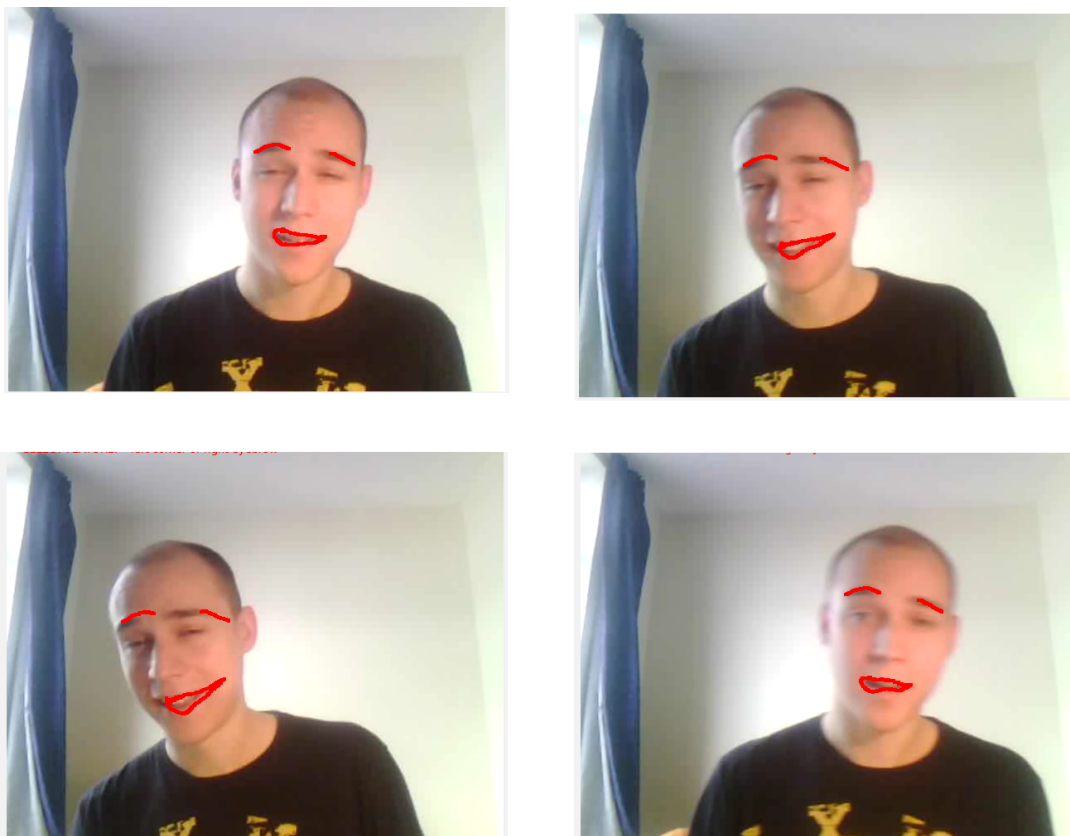


Figure 4.7: Tracking of feature point using a  $50 \times 50$  window size. The features do not follow their true counterparts because the window size is too large.

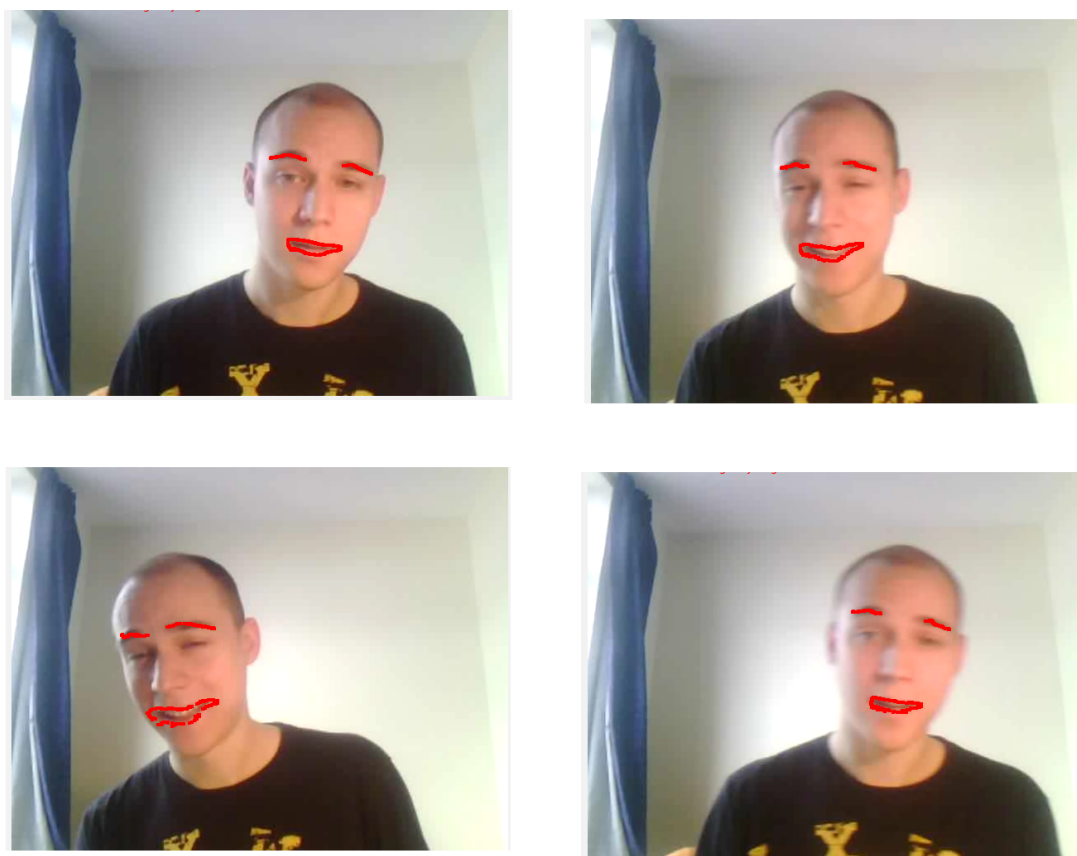


Figure 4.8: Best tracking results obtained using a  $15 \times 15$  window size.

## 4.3 Fitting Algorithm Results

The performance of the fitting algorithm is determined primarily by the four following factors

- The quality of the user provided feature points.
- The number of newly generated points and the correctness of their established 3D correspondence.
- The optimization algorithm, which can be based on regularization or constrained optimization.
- The number of frames in the video recording.

In this section we will provide fitting algorithm results and evaluate them based on these factors.

**Feature point selection.** The quality of the model and 3D pose parameter estimation depends on the input set of feature points. This is due to the fact that the first frame alignment is calculated purely using these user provided (or automatically located) feature points. The first frame alignment is then used to determine the 3D model correspondences of a large number of newly generated feature points. These correspondences bias the fitting process toward the identity, expression and 3D pose of the first alignment. This is especially the case when the individual does not perform dynamic expressions in the recording. On the other hand, the user cannot be expected to input a large number of feature points and an automatic algorithm is likewise only effective for a small number of unique features such as the mouth corners, eye corners etc.

The more points the fitting algorithm utilizes the more information it will have about the movement of the facial features. Using more points also helps avoid overfitting. However, the more points are generated the more biased the result is toward the first frame alignment parameters. Figures 4.9a and 4.9b illustrate this trade-off between bias and improved optimization result on an interesting frames of a 100 frame video sequence optimized using a coonstrained non-negativity minimization scheme.

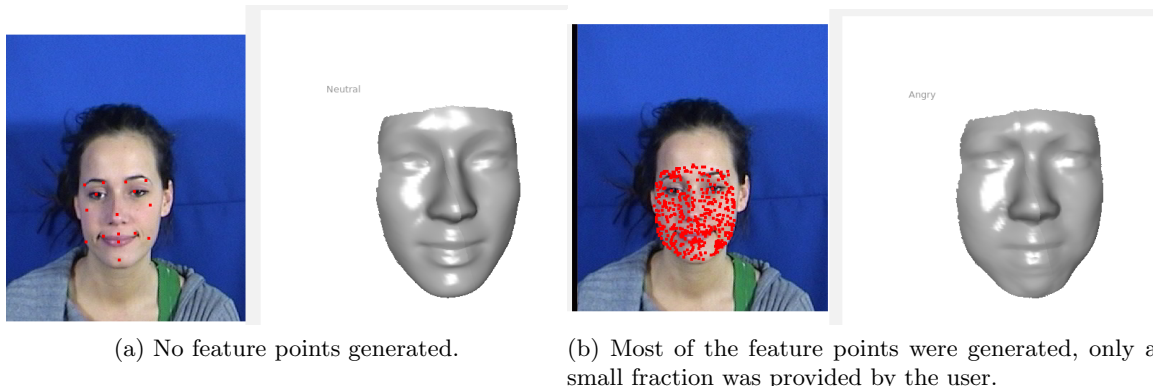


Figure 4.9: The above images illustrate the trade-off between quality of optimization and the introduced bias. With too few points the identity estimate can never be very accurate. With too many points, the result becomes biased for the first frame alignment face which is different from the one in the image.

From figure 4.9 we see that when the first frame alignment is very different from the true identity, expression and 3D pose of the subject, the fitting algorithm also returns an incorrect estimate of the face. However, to obtain a good estimate of a person's identity a large number of points is necessary. The identity depends small details such as the width of the nose, the fullness of lips and others. A user cannot manually select all these these features.

**Optimization scheme.** The two optimization approaches to finding model parameters which generate realistic face are regularization and constrained optimization. Of the two, regularization is more difficult to use since it requires a regularization parameter  $\lambda$  to control the distance from the mean. Reasonable values of this parameter can be obtained through trial and error. The regularization parameter also needs to be increased when more frames or more points are utilized. This is due to the fact that the error function generally increases when more frames or points are used, making the penalty value of the regularization parameter smaller by comparison. Constrained optimization is easier to use, however, a fitting algorithm using constrained optimization has a weaker expressive power since it prohibits parameter vectors with negative components.

The convergence of both fitting approaches is shown in figure 4.10. Regularization-based fitting algorithms are faster, but they are also more likely to overfit if the regularization parameter is poorly chosen.

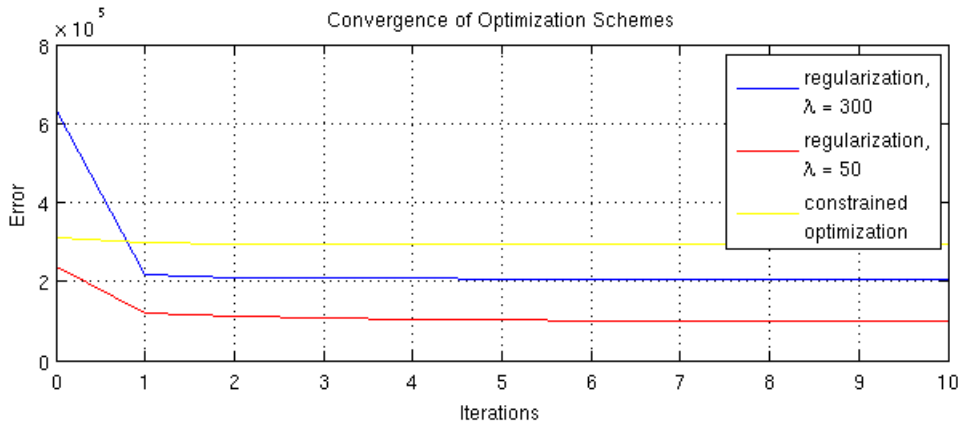


Figure 4.10: The convergence behaviour of the two fitting algorithm variations. Regularization converges to a lower error value faster but often produces unrealistic face scans for low values of the regularization parameter  $\lambda$ .

The results of applying the various optimization schemes to a fitting problem is shown in figure 4.11. An almost inhuman face is generated with  $\lambda = 100$ . On the other hand, the best result was obtained with constrained optimization.

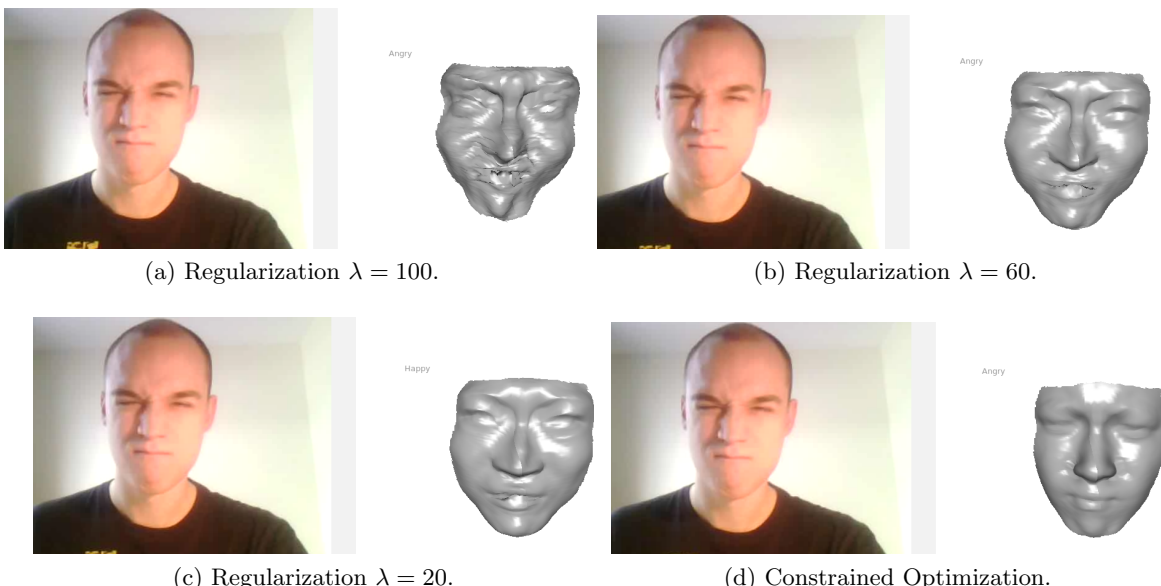


Figure 4.11: The result of fitting the model to an image using the various fitting algorithms.

Experiments with regularization have shown that this approach tends to keep the mouth

on the model open when fitting the model to image. This is due to the fact that the mean face from the Binghamton database has an open mouth. Since the regularization algorithm penalizes any large discrepancy from the mean face, it therefore often falsely approximates the face in the image with an open mouthed model instance, as can be seen in figure 4.12b. The results for fitting faces with the regularized fitting algorithm are shown in figures 4.12 and 4.13.



Figure 4.12: Results obtained from applying the regularized fitting algorithm.

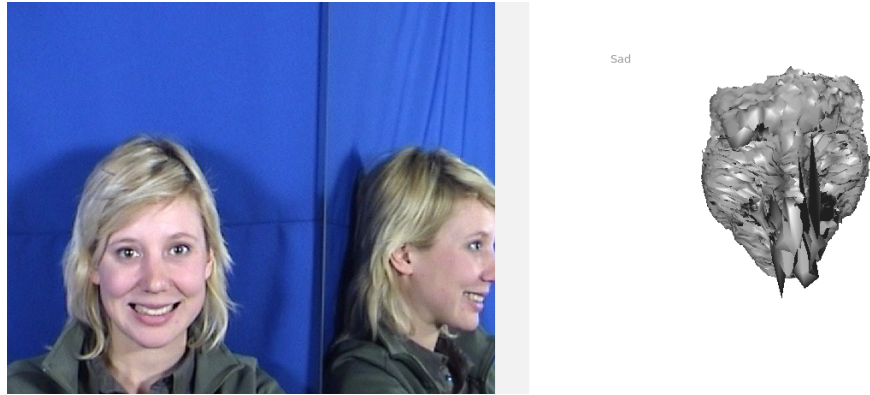
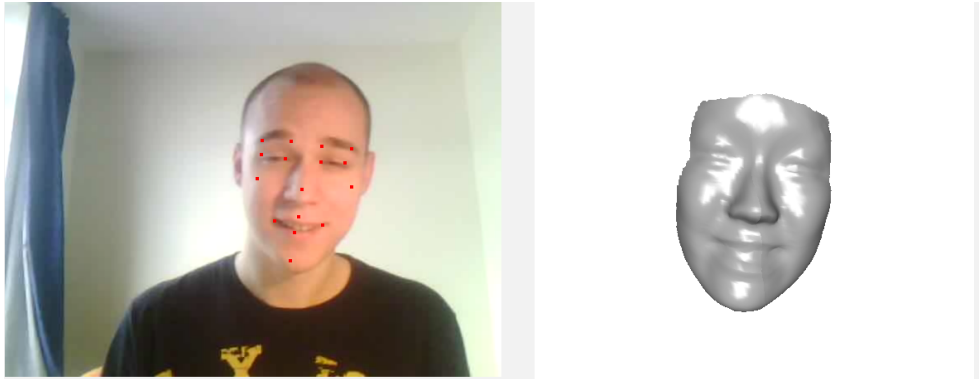


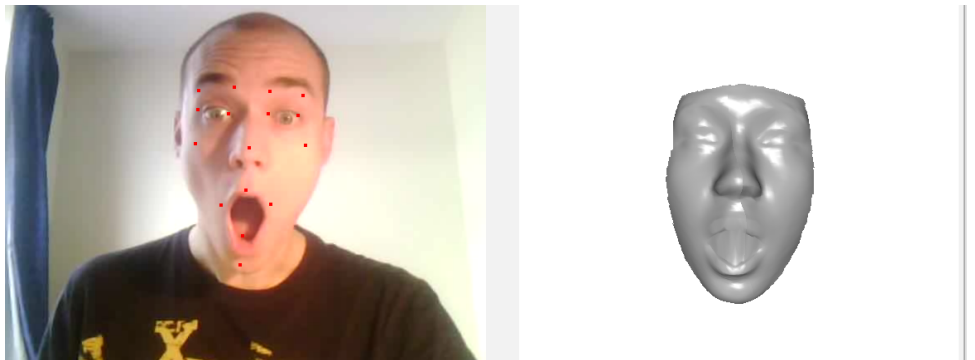
Figure 4.13: The fitting algorithm is prone to overfitting when no regularization is performed ( $\lambda = 0$ ) and there is only a small number of feature points available.

From 4.12c, we can see that the regularized algorithm even matches face shapes which are very different from the shapes in the database. However, there are two significant disadvantages. Firstly, the choice of the regularization parameter  $\lambda$  has to be done by trial and error. Secondly, the fitting algorithm often falsely identifies subjects as having their mouth open, since this enables the algorithm to achieve a better error function minimum.

On the other hand, the constrained optimization algorithm only fits realistic models to faces in images, without requiring the user to provide a value for a regularization parameter. However, unlike the regularized fitting algorithm, it limits the variance available in the database by allowing only positive coefficients in the linear combination. The face scans from the data tensor are therefore only added together and never subtracted from each other. This means that effectively only a small portion of the space spanned by the columns of the data tensor is available to us. Results for constrained fitting are shown in figures 4.14 and 4.15.



(a) Using only 16 feature points, the constrained algorithm finds a good match.



(b) The constrained algorithm correctly identifies a surprised expression.

Figure 4.14: Result obtained using the constrained fitting algorithm

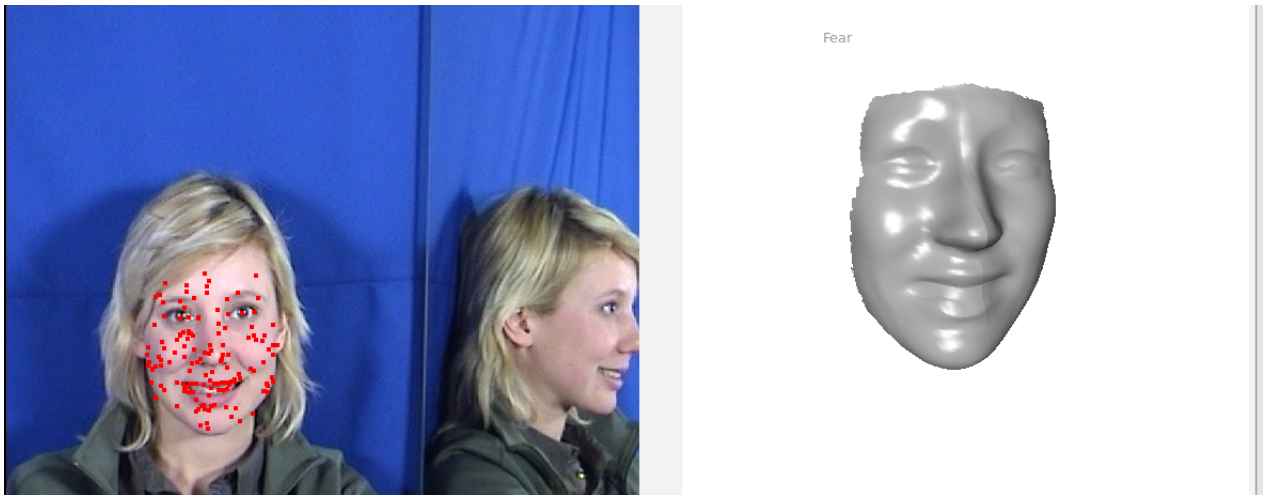


Figure 4.15: Using a larger number of automatically generated feature points, the constrained algorithm correctly perceives the facial dynamics, but misidentifies the expression as fear.

In summary, we have discussed and explored two approaches to avoiding overfitting in the fitting algorithm. This overfitting is exemplified by unrealistic face shapes.

The regularization approach yields realistic face shapes for certain values of a regularization parameter  $\lambda$ . However, this parameter must often be found by trial and error. The parameter's magnitude controls the attraction to the mean and can cause the algorithm to recover incorrect shapes, such as ones with an open mouth even when the mouth in the image is closed.

With the constrained optimization approach we exchange a significant portion of the expressive power of the model for being able to only recover realistic faces. The constrained fitting algorithm does not require any input parameters which makes the application more accessible to the casual user.

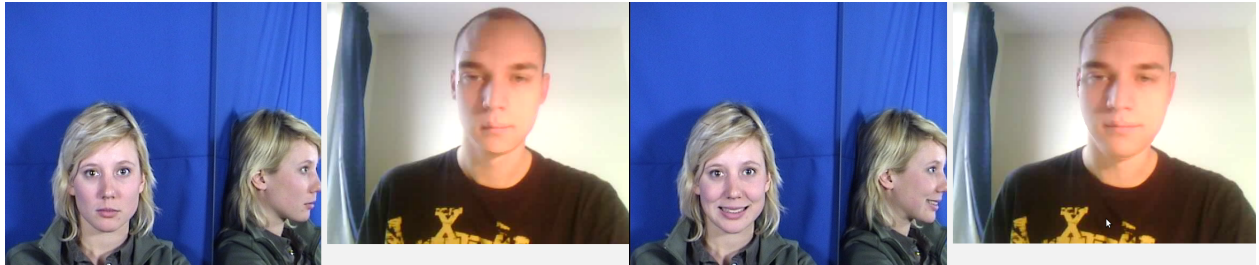
**Video Length.** In the expression transfer algorithm (section 3.6), we require that the identity of the person will not change during the video recording. This means that the multi-frame coordinate descent algorithm has to find an expression parameter vector for each frame but just one identity parameter vector for the entire video sequence. This is essentially a constraint on the fitting algorithm. This constraint also limits the algorithm's performance. It first of all it necessitates that the solution of a large linear system, obtained by collecting the feature points from all frames. Secondly, some identities in the database did produce certain expressions.

## 4.4 Expression Transfer Results

Given a 3D model of the source subject and a 3D model of the target subject, the final task is transfer the source expression to the target and then reanimate the target in the target video recording. Transferring the expression between the two models is trivial since we only need to input the source expression parameters along with the target identity parameters into the generative function. This may not provide us with exactly the same facial movements as displayed by the source. The target subject may have a different type of smile than the source individual for example.

On the other hand, the second step is a very challenging one. As discussed in section 3.6, since we only have a model of a face shape and not a model of the texture, we cannot directly use the tensor model to synthesize the correct appearance. We therefore must utilize shape information to transfer texture.

This can be done by finding the texture coordinates by projecting the newly generated face into target the image and using the image as a texture. This leads to decent results as seen in figure 4.16. However, certain expressions such as a strong smile may stretch the texture in an unrealistic way.



(a) Step 1: Transfer of a neutral expression.

(b) Step 2: Transfer of a weak smile.



(c) Step 3. The stronger smile stretches the texture.

(d) The 3D model with the transferred expression.

Figure 4.16: Expression transfer by reanimating the augmented target subject with texture data obtained from the first target recording frame.

In figure 4.17 a smiling expression is transferred causing a noticeably skewed texture in the target image.



Figure 4.17: Transfer of a smile using the first frame of the target recording as texture.

The other approach to reanimating faces is to exploit the knowledge of the shape of both faces to clone the features from the source texture into the target texture. So that the result seems realistic this is done with seamless blending to produce results depicted in figures 4.18 and 4.19

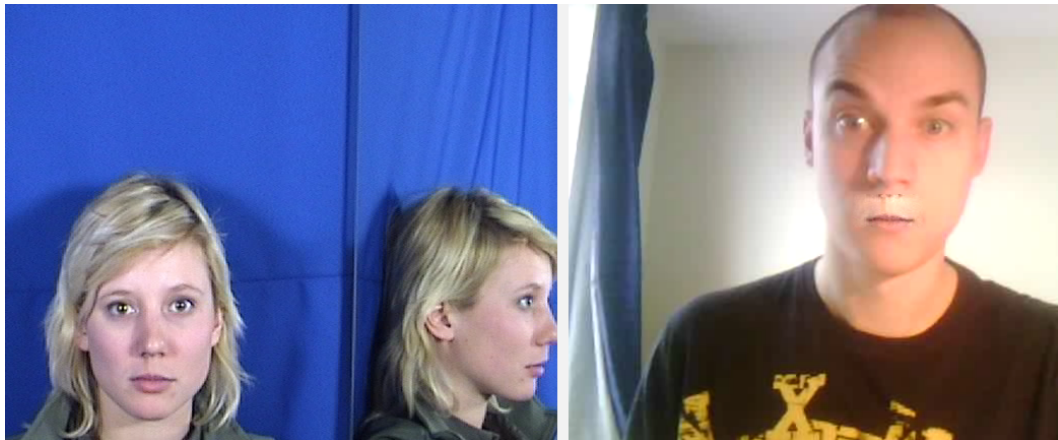


Figure 4.18: The cloning of the smile from the source (left) image into the target (right) image.

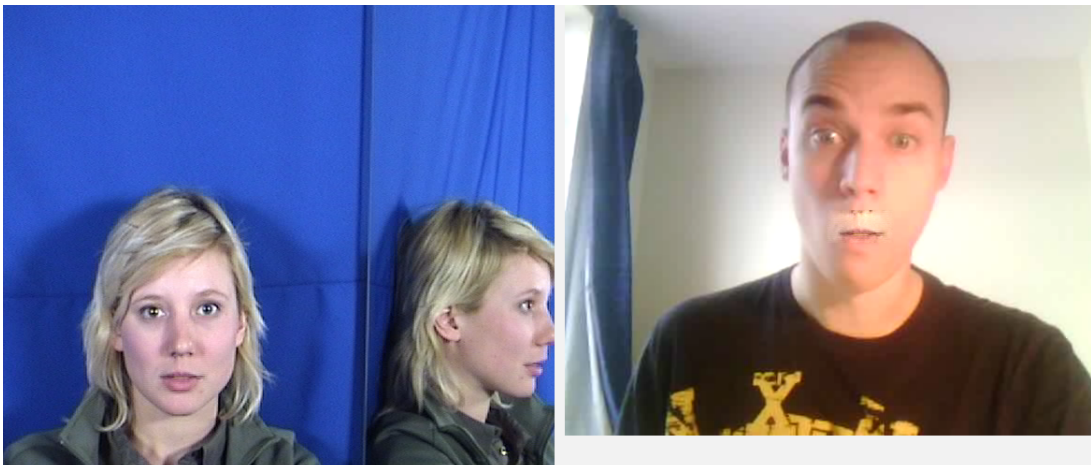


Figure 4.19: Another example of using poisson cloning to achieve a somewhat realistic expression transfer result.

Since the geometry of both 3D models is known from fitting algorithm, the transfer is done by simply taking smile texture from the source image and cloning it over the mouth on the target image. This approach was also utilized by Vlasic et al [40] in their expression transfer application. It produces good results when both faces are the same size. Figure 4.20 illustrates the case when one face is considerably larger than the other. Note that a small fragment of the source nose is transferred as well. This occurred because the mouth of the target image was larger than mouth of the source.



(a) Step 1: Transfer of a neutral expression.



(b) Step 2: Transfer of the beginnings of a smile.

Figure 4.20: Texture transfer using poisson cloning. Depicted is a case where the technique does not work well due to the discrepancy in size.

## 4.5 Performance

The expression transfer application was tested on the following system

- **System Type:** Thinkpad Laptop
- **Operating System:** Ubuntu 9.10 (kernel 2.6.31-22)
- **Processor:** Intel(R) Core(TM)2 Duo CPU P8400 @ 2.26GHz
- **RAM:** 2GB DDR2
- **Graphics Card:** Intel GMA 4500MHD

On this system, constructing a tensor model from the Binghamton databases with 5090 vertices, 7 expressions and 56 identities averages at around 2 minutes. This includes loading the data from the database and computing the HOSVD.

Fitting the tensor model using a linear combination algorithm with regularization takes on average about a third of a second per frame. For a 100 feature points the runtime averages at around 13 seconds for 40 frames and 18 seconds for 50 frames.

The runtime of fitting the model parameters by enforcing linear interpolation through non-negativity constraints and solving using the sequential coordinate-wise non-negativity least squares algorithm is around 25 seconds for 40 frames and around 28 seconds for 50 frames for 100 feature points, thus averaging a little over 0.6 seconds per frame.

The slower runtime of the non-negativity least squares algorithm is due to the fact that it performs a sequence of iterations until convergence during every parameter update step in the coordinate descent expression transfer fitting algorithm. The linear combination fitting algorithm, on the other hand, updates parameters using a closed form solution, which is computationally much more effective.

# Chapter 5

## Conclusion

To summarize, we developed the expression transfer application for

### 5.1 Future Work

As part of the expression transfer application, we constructed a deformable model from a simple database of 3D face scans displaying expressions. An intriguing prospect for future work would be to perform data gathering and construct larger, more powerful 3D databases, with more attributes than identity and expression. For example it would be interesting to build an appearance tensor model with attributes for expressions, identities, lighting and texture of the faces as well. Tensor based shape models of other objects such as hands and entire bodies are an area which has not been researched as thoroughly as face models by the computer vision community. It would therefore be possible to contribute to the deformable modelling field by exploring tensor models of such objects. Constructing and fitting the model using a new database would not necessitate the reworking of the algorithms derived in the paper. The HOSVD and the fitting algorithm could be easily adapted to work with databases not consisting of face scans by simply adapting the number of parameters and mode matrices.

Of course, to build a new database it would be necessary to perform 3D data gathering. It should, however, be possible to perform this gathering without the need for expensive equipment. Structured light based scanning equipment and other 3D shape recovery approaches such as computational or photometric stereo are increasingly becoming more readily available to casual users and they would lend themselves well for data gathering purposes. The application could for instance be extended to allow the user to perform their own data gathering on an object of their choosing and then to construct a tensor model from it. If it were not possible to gather 3D despite the availability of data gathering techniques, more variability could be introduced to existing databases by utilizing a FEM based model to generate new faces and using these to expand the database.

To improve the usability of the application it would also be intriguing to link a feature point detection algorithm into the expression transfer algorithm. An automatic feature detection framework such as the Viola-Jones feature tracker [39] would make the application more accessible to casual users. The automatic detector could be trained to locate corners of the mouth, eyebrows or the tip of the nose. These points are easily distinguishable and are conveniently already utilized as feature points in the application. Even an external feature point tracker could therefore be seamlessly linked with the application if it produced a set of 2D feature point coordinates which would then be used by the expression transfer fitting algorithm.

The main limitation we encountered with the shape tensor-based model is the need for correspondences between feature and model points. Correspondences are not elegant and weaken the power of the model fitting approaches. This limitation could be overcome by utilizing an appearance based tensor model. Since this model generates a textured representation of the face its projection into 2D is a textured image of the face. It therefore is less constrained in how the error is computed meaning that more elegant and flexible fitting algorithms could be developed. To construct such a model it would be necessary to know the RGB values at every vertex so a database with texture

maps and texture coordinates would be required. A tensor-based model of appearance would also be able to reanimate faces without having to resort to Poisson image editing techniques.

Lastly, a future project could explore the performance of Newton and quasi-Newton fitting algorithms for the tensor model of shape. Section 3.5.4 provides the starting point of such approaches and derives two of the four optimal parameters non-linear equations.

# Bibliography

- [1] Klaus-Juergen Bathe. *Finite Element Procedures*. Prentice Hall, 1996.
- [2] Stan Birchfield. Derivation of kanade-lucas-tomas tracking equation. [<http://www.ces.clemson.edu/stb>], January 1997.
- [3] Christopher M. Bishop. *Patter Recognition and Machine Learning*. Springer Science + Business Media, LLC, 2006.
- [4] V. Blanz, C. Basso, T. Poggio, and T. Vetter. Reanimating faces in images and video. *EUROGRAPHICS*, 22(3), 2003.
- [5] V. Blanz, K. Scherbaum, T. Vetter, and H.P Seidel. Exchanging faces in images. *EUROGRAPHICS*, 23(3), 2004.
- [6] Jean-Yves Bouguet. Pyramidal implementation of the lucas kanade feature tracker. The paper is included into OpenCV distribution.
- [7] Gary Bradski and Adrian Kaehler. *Learning OpenCV*. O'Reilly Media, Inc., 2008.
- [8] Jinxiang Chai. Csce 641 - computer graphics: The geometry of perspective projection. Department of Computer Science and Engineering, Dwight Look College of Engineering, Texas A&M University. [http://faculty.cs.tamu.edu/jchai/cpsc641\\_spring10/PerspectiveProjection.pdf](http://faculty.cs.tamu.edu/jchai/cpsc641_spring10/PerspectiveProjection.pdf).
- [9] Donghui Chen and Rober J. Plemmons. Nonnegativity constraints in numerical analysis. *Conference Proceedings of the Symposium on the Birth of Numerical Analysis*, October 2007.
- [10] T.F. Cootes and C.J. Taylor. Statistical Models of Appearance for Medical Image Analysis and Computer Vision. *Proc. SPIE Medical Imaging*, 2001.
- [11] T.F. Cootes and C.J. Taylor. Statistical Models of Appearance for Computer Vision. mar 2004.
- [12] Daniel F. DeMenthon and Larry S. Davis. Model-based object pose in 25 lines of code. *Proceedings of the European Conference on Computer Vision*, pages 335–343, 1992.
- [13] Paul L. Fackler. Notes on matrix calculus. North Carolina State University, September 2005.
- [14] Carlos Felippa. Introduction to finite element methods: Appendix d. Department of Aerospace Engineering Sciences, University of Colorado at Boulder, 2010. <http://www.colorado.edu/engineering/cas/courses.d/IFEM.d/>.
- [15] Vojtech Franc, Vaclav Hlavac, and Mirko Navara. Sequential coordinate-wise algorithm for non-negative least squares problem. *Research Report CTU-CMP-2005-06*, February 2005.
- [16] D.F. Gillies. Intelligent data and probabalistic inference lecture notes. *Imperial College London*, 2009.
- [17] Duncan F. Gillies. Graphics lecture notes 1. Imperial College London, 2010.

- [18] Gene H. Golub and Charles F. Van Loan. *Matrix Computations: Third Edition*. The Johns Hopkins University Press, 1996.
- [19] L. De Lathauwer. *Signal Processing based on Multilinear Algebra*. Phd dissertation, Katholieke Universiteit Leuven, Belgium, 1997.
- [20] Tommer Leyvand. Advanced topics in computer graphics: Poisson image editing. Blavatnik School of Computer Science, Tel Aviv University. <http://leyvand.com/research/adv-graphics/ex1.htm>.
- [21] Bruce D. Lucas and Takeo Kanade. An iterative image registration technique with an application to stereo vision. *International Joint Conference on Artificial Intelligence*, pages 674–679, 1981.
- [22] Dimitri Metaxas and Demetri Terzopoulos. Shape and nonrigid motion estimation through physics-based synthesis. *IEEE Transactions on Pattern Analysis and Machine Intelligence*, 15(6):580–591, 1993.
- [23] Jacey-Lynn Minoi. *Geometric Expression Invariant 3D Face Recognition using Statistical Discriminant Models*. Phd dissertation, Imperial College London.
- [24] J.L. Minoi and D.F. Gillies. 3d face and facial expression recognition using tensor-based discriminant analysis methods.
- [25] Alex Pentland and Stan Sclaroff. Closed-form solutions for physically based shape modelling and recognition. *IEEE Transactions on Pattern Analysis and Machine Intelligence*, 13(7):715–726, 1991.
- [26] P. Perez, M. Ganget, and A. Blake. Poisson image editing. *ACM Transactions on Graphics*, 22(3):313–318, July.
- [27] W.H. Press, S.A. Teukolsky, W.T. Vetterlin, and B.P. Flannery. *Numerical Receipes in C: The Art of Scientific Computing 2nd Edition*. Cambridge University Press, 1992.
- [28] M. Reiter. Neural computation ws 2006/2007 lecture notes. *Vienna University of Technology*, 2006.
- [29] Szymon Rusinkiewicz and Marc Levoy. Efficient Variants of the ICP Algorithm. In *Third International Conference on 3-D Digital Imaging and Modeling*, 2001.
- [30] J. Nelder S. Singer. Nelder-Mead algorithm. 2009. [[http://www.scholarpedia.org/article/Nelder-Mead\\_algorithm](http://www.scholarpedia.org/article/Nelder-Mead_algorithm)].
- [31] Dave Shreiner, Mason Woo, Jackie Neider, and Tom Davis. *OpenGL Programming Guide: The Official Guide to Learning OpenGL*. <http://www.glprogramming.com/red/>.
- [32] W.-H. Steeb. *Matrix Calculus and Kronecker Product with Applications and C++ Programs*. World Scientific Publishing Co. Pte. Ltd., 1997.
- [33] Robert W. Sumner and Jovan Popovic. Deformation Transfer for Triangle Meshes. *SIGGRAPH*, 2004.
- [34] Carlo Tomasi and Takeo Kanade. Detection and tracking of point features. *Carnegie Mellon University Technical Report CMU-CS-91-131*, April 1991.
- [35] M. Turk and A. Pentland. Eigenfaces for Recognition. *Journal of Cognitive Neuroscience*, 3(1):71–86, 1991.
- [36] M. Alex O. Vasilescu and Demetri Terzopoulos. Multilinear analysis of image ensambles: Tensorfaces. In *Proc. European Conf. on Computer Vision*, pages 447–460, May 2002.

- [37] M. Alex O. Vasilescu and Demetri Terzopoulos. Multilinear independent components analysis. In *IEEE Computer Vision and Pattern Recognition Conference*, San Diego, CA, June 2005.
- [38] M. Alex O. Vasilescu and Demetri Terzopoulos. Multilinear projection for appearance-based recognition in the tensor framework. pages 1–8, October 2007.
- [39] Paul Viola and Michael Jones. Robust real-time object detection. *Second International Workshop on Statistical and Computational Theories of Vision – Modeling, Learning, Computing and Sampling*, July 2001.
- [40] D. Vlasic, M. Brand, H. Pfister, and J. Popovic. Face Transfer with Multilinear Models. *ACM Transactions on Graphics*, 24(3), 2005.
- [41] Lijun Yin, Xiaozhou Wei, Yi Sun, Jun Wang, and Matthew J. Rosato. A 3d facial expression database for facial behavior research.
- [42] Z. Zhang. A flexible new technique for camera calibration. *IEEE Transactions on Pattern Analysis and Machine Intelligence*, November 2000.